The Hong Kong Polytechnic University

Department of Civil and Environmental Engineering

DEGRADATION OF ANTIBIOTIC NORFLOXACIN BY SOLAR LIGHT/VISIBLE LIGHT-ASSISTED OXIDATION PROCESSES IN AQUEOUS PHASE

CHEN Meijuan

A Thesis Submitted in Partial Fulfillment of the Requirements for the

Degree of Doctor of Philosophy

Oct 2013

CERTIFICATE OF ORIGINALITY

I hereby declare that this thesis is my own work and that, to the best of my knowledge and belief, it reproduces no material previously published or written, nor material that has been accepted for the award of any other degree or diploma, except where due acknowledgement has been made in the text.

_____(Signed)

CHEN Meijuan_____(Name of Student)

ABSTRACT

In recent years, the contamination of water sources by antibiotics is one of the most concerned environmental issues worldwide due to the widespread application of antibiotics in both human and animals health care. Among the existing antibiotics, norfloxacin contributes to a significant portion of the water environment and thus has to be removed prior to the discharge of the treated water. The presence of norfloxacin in aquatic environment has been reported to interfere with bacterial DNA replication, be toxic to aquatic plants and organisms, and contribute to bacterial geno-toxicity. Therefore, the development of treatment technologies operating in low cost and with high efficiency becomes an important and attractive issue for the removal of antibiotics from aqueous medium. Till now, little is known about the degradability and reaction products of norfloxacin by solar light or visible light excited photocatalysis. The knowledge regarding the norfloxacin decomposition by UV, ozonation, and ClO_2 oxidation processes is limited although these processes have shown good performance in terms of norfloxacin decay in some studies. The objectives of this dissertation are to explore and evaluate three processes including simulated solar light mediated bismuth tungstate process (SSL/Bi_2WO_6), SSL/Bi_2WO_6 with the assistance of hydrogen peroxide (SSL/Bi_2WO_6/H_2O_2), and visible light mediated carbon doped titanium dioxide process (Vis/C-TiO_2) for the elimination of norfloxacin in water and waste waters.

For the degradation of norfloxacin via SSL/Bi_2WO_6 process, the effects of environmental parameters including catalyst dosage, probe concentration, and solution pH on the process performance were investigated systematically. At weak alkaline, an optimal decay performance was obtained which can be attributed to the beneficial effect of hydroxyl ions. The reaction rationale and related constants were determined by Langmuir-Hinshelwood (LH) model combined with the experimental results. Our results showed that the adsorption of norfloxacin onto Bi_2WO_6 benefited the SSL/Bi_2WO_6 process, and the Bi_2WO_6 maximum adsorption capacity was determined to be 3.20×10^{-3} mmol/g. In the SSL/Bi_2WO_6 process, the degradation of norfloxacin was accompanied by the decomposition of germicidal group and benzene ring, as well as gradually generation of inorganic ions of NH_4^+ and F^-. Furthermore, the toxicity of initial norfloxacin solution was efficiently eliminated by the SSL/Bi_2WO_6 process.

The practical oxidative species in the SSL/Bi_2WO_6 process for the removal of antibiotic norfloxacin was investigated in details. The norfloxacin decay performance under the influence of different radicals scavengers were carried out to determine the effective oxidative species and the hydroxyl radical was confirmed to be the key oxidative species. The effect of inorganic salts on the decay performance was also investigated. The overall norfloxacin decay can be characterized into photolysis, photocatalysis-via hydroxyl radical, and photocatalysis-via direct hole oxidation; it was calculated that their contribution will be 29.7, 65.5, and 4.8% respectively for norfloxacin removal. The

degradation mechanism of norfloxacin through the SSL/Bi_2WO_6 process was further proposed based on the LC/MS analysis.

The SSL/Bi_2WO_6 process was effective at a pH range from 5.0 to 9.0 for norfloxacin decay. To further broaden the sensitive/workable pH range of SSL/Bi_2WO_6 process, a buffer system and Fe^{3+} salt was introduced at extreme basic and acidic pH, respectively. The buffer system continuously supplies higher dosage of hydroxyl ion for active radical generation and prevents the acidification of the solution, resulting in a better norfloxacin and TOC removal at alkaline condition. The Fe^{3+} salt on the other hand, offered an additional homogeneous photo-sensitization pathway and altered the surface property of heterogeneous Bi_2WO_6. The former will assist the norfloxacin decay and the latter can increase the collision between the photo-generated hole and hydroxyl ions. The combination of both will significantly improve the decay of norfloxacin at acidic pH range.

To improve the decay of norfloxacin, the SSL/Bi_2WO_6/H_2O_2 process was carried out for the removal of antibiotic norfloxacin in aqueous solution. The degradation kinetics can be characterized by a two-stage pseudo first-order reaction kinetics under various reaction conditions. In general, a fast first-stage was observed and followed by a slower second-stage. The effects of the norfloxacin initial concentration (0.05 - 0.30 mM), catalyst dosage (0.5 - 3.0 g/L), and hydrogen peroxide dosage (0.2 - 20.0 mM) were

investigated, and the process was optimized at 2g/L Bi_2WO_6 and 10 mM hydrogen peroxide. The kinetic model derived for the SSL/Bi_2WO_6/H_2O_2 process can predict the removal of norfloxacin successfully. In addition, the degradation mechanism of norfloxacinin during the process was also proposed based on the identified six aromatic intermediates, in which the reaction is initiated by the attack of ·OH on either the piperazine or quinolone moieties as discussed in detail in this study.

Finally, a Vis/C-TiO_2 process was used for the degradation of norfloxacin. An original model for deciphering the surface property of the catalyst was proposed and confirmed by various tests. The decay rates fit a pseudo first-order kinetics and can be described by the LH model. The effects of C-TiO_2 dosage, norfloxacin initial concentration, and pH levels were investigated and optimized. The optimal pH level was found to be located at weak basic condition; out of this range, the decay rate will be reduced. This is due to the change of charges on C-TiO_2/norfloxacin interface, effective particle size and surface property of C-TiO_2. To get a deep insight of the process, the norfloxacin decay performance was investigated with the addition of hydroxyl radical scavenger and electron acceptor. Hydroxyl radicals were verified to play a major role in the decomposition of norfloxacin by applying methanol as scavenger. In the presence of electron acceptor (IO_3^-), the norfloxacin decay was improved at low [IO_3^-], but the effect was attenuated at higher concentrations. Moreover, the effect of various inorganic ions was also studied: the hole scavenger of ammonium did not show negative influence,

whereas the fluoride presented a unique restriction in the norfloxacin decay. The reuse and sedimentation properties of C-TiO_2 was evaluated for practically application as well.

LIST OF PUBLICATIONS

1. **CHEN Meijuan**, Chu W., Efficient Degradation of an Antibiotic Norfloxacin in aqueous Solution via a Simulated Solar-light-Mediated Bi_2WO_6 process, *Industrial & Engineering Chemistry Research,* 51(13), 4887-4893, 2012.

2. **CHEN Meijuan**, Chu W., Degradation of Antibiotic Norfloxacin in Aqueous Solution by Visible-light-mediated C-TiO_2 photocatalysis, *Journal of Hazardous Materials*, 219-220, 183-189, 2012.

3. **CHEN Meijuan**, Chu W., The Role of Oxidative Species and Reaction Mechanism Study of SSL/Bi_2WO_6 Process for Norfloxacin Decay. Submitted

4. **CHEN Meijuan**, Chu W., Exploring a Broadened pH Range for Bi_2WO_6 Photocatalysis in Norfloxacin Decay. Submitted

5. **CHEN Meijuan**, Chu W., Hydrogen Peroxide Assisted Degradation of Antibiotic Norfloxacin by Simulated Solar-light-mediated Bi_2WO_6 Process: Modeling and Reaction Mechanism. Submitted

ACKNOWLEDGEMENTS

I would like to express my deepest gratitude to my supervisor, Prof. Wei Chu, for his unwavering support throughout the project. Without his guidance and advice, the completion of this thesis is unattainable. I also wish to extend my thanks to the technicians in the Water and Wastewater Laboratory, especially Mr. Wai Shung Lam for his invaluable assistance and also Mr. Chi Wai Lau for his technical support.

Special thanks are given to Dr. Yongfang Rao and Dr. Yuru Wang for their valuable advice on this research work. Their suggestions on experimental design, data analysis and paper preparation are highly appreciated. Thanks also go to my colleages, especially Dr. Fei Qi, Dr. Hao Xu, Ms. K. Y. Lin, Ms. Lijie Xu whose moral support and encouragement are greatly appreciated.

I am deeply grateful to my beloved parents and family for their understanding, patience and unwavering support.

Last but not least, the financial support from the Hong Kong Polytechnic University is highly appreciated.

LIST OF CONTENTS

LIST OF FIGURES

LIST OF TABLES

LIST OF SCHEMES

LIST OF ABBREVIATION

Abbreviation	Full name
$[Bi_2WO_6]_0$	Initial dosge of Bi_2WO_6
$[H_2O_2]_0$	Initial dosage of H_2O_2
$[Norfloxacin]_0$	Initial concentrations of norfloxacin
AOPs	Advanced oxidation processes
CB	Conduction band
cfu	Colony-forming units
E.coli	Escherichieae coli
FQs	Fluoroquinolones
HPLC	High performance liquid chromatography
IC	Ion chromatography
k	Rate constant
LC/MS	HPLC equipment with mass spectrometer system
LH	Langmuir-Hinshelwood
MSA	Methane sulphonic acid
pzc	Point of zero charge
SEM	Scan electron microscope
SSL	Direct simulated solar light photolysis
SSL/Bi_2WO_6	Simulated-solar-light mediated Bi_2WO_6 heterogeneous photocatalysis
$SSL/Bi_2WO_6/H_2O_2$	SSL/Bi_2WO_6 with the assistance of H_2O_2
SSL/H_2O_2	H_2O_2 irradiated by simulated solar light
STP	Sewage Treatment Plant
TOC	Total organic carbon
UV/Bi_2WO_6	UV light irradiated Bi_2WO_6 photocatalysis
VB	Valence band
Vis/Bi_2WO_6	Visible light irradiated Bi_2WO_6 photocatalysis
$Vis/C\text{-}TiO_2$	Visible light mediated carbon-doped TiO_2 photocatalysis
WWTP	Wastewater Treatment Plant
XRD	X-ray Diffraction
λ	Light wavelength

Chapter 1 Introduction

1.1 Background

The shortage and increasing demand of clean water have become an urgent issue worldwide due to population growth and the rapid development of industry. It is estimated that millions of people died of severe waterborne diseases annually, and about 4 billion people in the world experience of no or little access to clean water (Malato et al. 2009). In order to restrain the deterioration of clean water shortage, the recycling of wasterwater through the low cost and high efficiency water treatment technologies has attracted more and more attentions. Recycling wastewaters are usually associated with the presence of health-threat refractory organic compounds; and thereby their removal performance is critical to evaluate the feasibility of the water treatment technology. Currently available water treatment technologies, such as adsorption, coagulation filtration, sedimentation and membrane technology, have been utilized on the removal of those refractory organic compounds from water environment. However, these conventional water treatment methods only transfer the pollutants, but the pollutants still remain without completely elimination. Therefore, the application of these conventional methods is suppressed due to the generation of toxic secondary pollutants and high operation cost. The advanced oxidation processes (AOPs) have been intensively explored and developed as the innovative water treatment technologies due to their low-cost and high efficiency through in-situ generation of highly reactive radical

for mineralization of organic pollutants. Among these AOPs, heterogeneous photocatalysis employing semiconductor catalysts has been confirmed of effective in degrading a wide range of organic pollutants into readily biodegradable compounds, and eventually mineralized them into innocuous carbon dioxide and water.

Heterogeneous photocatalysis employing TiO_2 catalyst have demonstrated fair performance in terms of decomposing norfloxacin (An et al. 2010a). However, the application of TiO_2 photocatalysis is usually restrained by the employ of high energy of UV light with wavelength less than 380 nm, requiring extra supply of UV light and thereby high operating costs. In the view of energy saving, one attractive option is to design a photoreaction system which can utilize the abundance of solar light. Herein, the major objective of this study is to design solar light (and visible light)-activated photocatalytic treatment process for the degradation and mineralization of norfloxacin.

1.2 Aims and Objectives

In this study, the heterogeneous photocatalytic technologies employing solar light and/or visible light as the energy resources are studied to evaluate their probability in the degradation and mineralization of norfloxacin. The specific objectives of this study are as following:

(1) To investigate the feasibility of degrading norfloxacin by different types of treatment processes including sole SSL photolysis, SSL/Bi_2WO_6, SSL/Bi_2WO_6/H_2O_2, and Vis/C-TiO_2 photocatalysis;

(2) To identify the effect parameters governing the degradation performance of norfloxacin, such as probe concentration, catalyst dosage, oxidant dosage, initial pH level, and inorganic salts; and to optimize effect parameters for achieving the best norfloxacin decay performance;

(3) To explore and compare the reaction mechanisms and decay pathways of norfloxacin by the SSL, SSL/Bi_2WO_6 and SSL/Bi_2WO_6/H_2O_2 through examining the evolution of aromatic intermediates by LC/MS analysis;

(4) To establish kinetic models on the prediction of norfloxacin removal efficiency in the process of SSL/Bi_2WO_6/H_2O_2;

(5) To evaluate the efficiency of mineralization of each process.

1.3 Scope of Study

This thesis comprises 9 chapters. The present chapter (Chapter 1) consists of the

background, objectives, and organization of the thesis.

The literature review of this study is given in Chapter 2, where the theory of AOPs, especially heterogeneous photocatalysis is discussed. A brief review of the efforts involved in shifting the optical response of TiO_2 from UV to visible light is present. Furthermore, the background information referring to norfloxcin is described in detail, including the toxicological effects, environmental fate, and previous studies on norfloxacin removal in this chapter.

Chapter 3 describes the material and technologies used in this study.

Chapter 4 discusses the possibility of application of the Bi_2WO_6 catalyst in norfloxacin degradation under the irradiation of solar light. The effect of environmental parameters including catalyst dosage, probe concentration, and solution pH on the process performance were investigated systematically. The reaction rationale and related constants was determined by LH model combined with the experimental results. To evaluate the practical application potential of the proposed process, toxicity examination in vitro bioassays was conducted on the treated samples.

Chapter 5 presents in-depth investigation on the degradation mechanism of norfloxcain via the SSL/Bi_2WO_6 process by examining the practical oxidative species and

determining the degradation pathway of norfloxacin. For practical oxidative species determining, the effect of quenchers and selected inorganic salts were investigated; and for mechanism study, the intermediates were identified by LC/MS analysis and the norfloxacin decay pathway was thereby proposed.

Based on the findings derived from Chapter 4 and 5, the solution pH level is critical to the SSL/Bi_2WO_6 process. Chapter 6 reports that only a narrow pH range from 5.0 to 9.0 is of effective in the SSL/Bi_2WO_6 process. To broaden the operating pH range of SSL/Bi_2WO_6 process, a buffer system and Fe^{3+} salt was introduced at extreme basic and acidic pH conditions, respectively, aiming to achieve better norfloxacin and TOC removal at extreme pH conditions. Furthermore, two deciphering models were derived to describe the Bi2WO6 surface property at basic and acidic pH conditions.

To improve the norfloxacin degradation, Chapter 7 carries out another approach of SSL/Bi_2WO_6/H_2O_2 through combining the advantages of SSL/Bi_2WO_6 photocatalysis and H_2O_2 photolysis. The degradation kinetics was characterized in term of various reaction conditions, such as Bi_2WO_6 dosage, norfloxacin concentration and H_2O_2 dosage. Kinetic model was derived first and then used in prediction of the norfloxacin decay in the SSL/Bi_2WO_6/H_2O_2 process. The degradation pathway of norfloxacin via the SSL/Bi_2WO_6/H_2O_2 process was proposed according to the aromatic intermediates observed by LC/MS analysis.

Chapter 8 addresses the investigation on the decay of norfloxacin by Vis/C-TiO_2 process. The effects of C-TiO_2 dosage, norfloxacin initial concentration, pH levels, and inorganic ions were investigated and optimized in this chapter. The reaction rational and radicals generation in the Vis/C-TiO_2 process were examined by a series of experiments. An original model for deciphering the surface property of C-TiO_2 was derived and further confirmed by various tests. The reuse and sedimentation properties of C-TiO_2 were evaluated for practically application.

The conclusions are presented in Chapter 9.

Chapter 2 Literature Review

2.1 Advanced Oxidation Processes in Wastewater Treatment

In decades, advanced oxidation processes (AOPs) have attracted more and more attentions, especially the processes with combination of oxidants, radiation and catalyst (e.g. UV/H_2O_2, UV/TiO_2, Fe^{2+}/H_2O_2, UV/Fe^{2+}/H_2O_2, O_3/H_2O_2, and UV/O_3), which have been developed for the removal of organic pollutants (Chang et al. 2009; Chang et al. 2012; Hu et al. 2011; Lanao et al. 2008; Ruppert et al. 1994; Wu 2009; Xu et al. 2009). AOPs involve the generation of highly reactive radicals, especially the hydroxyl radical (·OH), and provide the opportunity of organic pollutants to gain complete oxidation or mineralization at ambient temperature and pressure (Matilainen and Sillanpää 2010). The ·OH radical is known to be one of the most powerful oxidant possessing a redox potential of 2.8 V. The reaction of organic pollutants with ·OH radical is fast with a reaction rate constant in the range of 10^8–10^{10} M^{-1} s^{-1}, which is usually several orders of magnitude higher than other active species (e.g. O_3) under identical conditions (Matilainen and Sillanpää 2010).

The non-selective property of ·OH radical guarantees a series of simple reactions with organics once radical generation is initiated by photolysis, ozone, hydrogen peroxide, heat, etc. In general, the reaction of ·OH radical with organic pollutants proceeds by three different ways: (1) by the addition of ·OH radical onto the double bonds in the

organic pollutants, (2) by reactions where ·OH radicals get electron from organic substituent and leave carbon centred radicals, and (3) by H-atom abstraction which yields carbon centred radicals. The carbon centred radicals will react rapidly with oxygen to form organic peroxyl radicals, which further undergoes self-reaction and gives birth to ketones or aldehydes and/or carbon dioxide (Kleiser and Frimmel 2000). In this section, background information in regarding to the development of AOPs such as UV/H_2O_2, Fenton and photocatalytic processes will be summarized.

2.1.1 UV photolysis and UV/H_2O_2

UV photolysis is widely used for disinfection purpose. For the oxidation of organic pollutants (R-X), the electron transfers from the excited-state C* (Eq. 2-1) to ground-state molecular oxygen (Eq. 2-2), with subsequent recombination of the radical ions or hydrolysis of the radical cation, or homolysis to form radicals (Eq. 2-3) which then react with oxygen (Eq. 2-4) (Legrini et al. 1993).

$$C \xrightarrow{h\nu} C^* \quad (2\text{-}1)$$

$$C^* + O_2 \xrightarrow{h\nu} C^{*+} + O_2^{\cdot -} \quad (2\text{-}2)$$

$$R - X \xrightarrow{h\nu} R^{\cdot} + X^{\cdot} \quad (2\text{-}3)$$

$$R^{\cdot} + O_2 \rightarrow RO_2 \quad (2\text{-}4)$$

Although UV photolysis alone has been proved to change the chemical and biological properties of organic pollutants (Frimmel 1998), the oxidation reactions only occur with rather high UV doses (Goslan et al. 2006; Huang et al. 2008a). The process combining UV irradiation with H_2O_2 oxidant (UV/H_2O_2) has been observed to enhance the organic pollutants oxidation ability and promote the ·OH radical formation (Goslan et al. 2006). Previous studies demonstrated that the degradation of target organic compounds in UV/H_2O_2 process is eight times more effective than that with direct UV photolysis (Bond et al. 2009; Dobrović et al. 2007). With the involvement of H_2O_2, irradiation by light with wavelength (λ) lower than 400 nm is able to photo-excite H_2O_2 molecule. The widely accepted mechanism for the photolysis of H_2O_2 is that the cleavage of the molecule into hydroxyl radicals with a quantum yield of two OH· radicals from per quantum of radiation absorbed, which can be described by the following reaction (Eq. 2-5):

$$H_2O_2 \xrightarrow{h\nu} 2 \cdot OH \ (\lambda < 400nm) \qquad (2\text{-}5)$$

Upon UV/H_2O_2 treatment, organic pollutants can be oxidized to by-products with smaller molecular size (Sarathy and Mohseni 2009), less hydrophobicity (Sarathy and Mohseni 2010; 2009), and better biodegradability (Thomson et al. 2004; Toor and Mohseni 2007).

2.1.2 Fenton reaction

Fenton process for the treatment of wastewater is a well known and effective method to remove various hazardous organic pollutants (Neyens and Baeyens 2003). Complete destruction of organic pollutants can be achieved by Fenton reaction to produce harmless compounds, i.e. CO_2, water and inorganic salts. The Fenton's reagents are a mixture of H_2O_2 and ferrous iron (Fe^{2+}), where Fe^{2+} initiates the decomposition of H_2O_2 and results in the generation of hydroxyl radicals (Eq. 2-6):

$$Fe^{2+} + H_2O_2 \rightarrow Fe^{3+} + \cdot OH + OH^- \quad (2\text{-}6)$$

Moreover, the newly formed ferric ions (Fe^{3+}) can also lead to the decomposition of hydrogen peroxide, and produce ferrous ions and radicals, as demonstrated in the Eqs. 2-7 to 2-11.

$$Fe^{3+} + H_2O_2 \leftrightarrow Fe - OOH^{2+} + H^+ \quad (2\text{-}7)$$

$$Fe - OOH^{2+} \rightarrow Fe^{2+} + HO_2. \quad (2\text{-}8)$$

$$Fe^{2+} + HO_2. \rightarrow Fe^{3+} + HO_2^- \quad (2\text{-}9)$$

$$Fe^{3+} + HO_2^- \rightarrow Fe^{2+} + O_2 + H^+ \quad (2\text{-}10)$$

$$\cdot OH + H_2O_2 \rightarrow H_2O + HO_2. \quad (2\text{-}11)$$

As compared with other AOPs, one of the advantages of the Fenton process is that no energy input is required to decompose hydrogen peroxide because the reaction can occur at ambient pressure and room temperature. Furthermore, the Fenton process takes a relatively short time period and uses easy-to-handle reagents. The main disadvantages

are the high cost of hydrogen peroxide and that the homogeneous catalyst, added as iron salt, cannot be retained in the process which needs further separation to prevent additional water pollution. Furthermore, in the Fenton process, the consumption of ferrous ions Fe^{2+} is more rapid than the regeneration, resulting in the formation of large amount of ferric hydroxide sludge. This phenomenon can cause additional separation and disposal problems (Babuponnusami and Muthukumar 2012).

To overcome the shortcomings of conventional Fenton's reagents, a combination of photolysis and Fenton process, namely photo-Fenton method, has been developed to improve the organic pollutants oxidation reaction. Under optimal pH level (acidic), $Fe^{III}(OH)^{2+}$ complex becomes the dominant component of Fe (III) cations. Irradiation plays a positive role in the improvement of Fenton oxidation process, which should be mainly ascribed to the photo-reduction of ferric ions (in the form of $Fe^{III}(OH)^{2+}$) to ferrous ions. This photo-reduction process can generate additional hydroxyl radicals and is an essential step to promise the further reaction of hydrogen peroxide with photo-generated ferrous ions. The photo-reduction of ferric ions follows Eq. 2-12 :

$$Fe^{III}(OH)^{2+} \xrightarrow{h\nu} Fe^{2+} + \cdot OH \qquad (2\text{-}12)$$

The above reaction introduces a continuous generation of Fe(II), which results in the enhancement of the catalytic cycle of Fe(III)/Fe(II) and thereby minimizes the required catalyst concentration. It was reported that the $Fe^{III}(OH)^{2+}$ species has an absorption

spectrum between 290 and 400 nm in wavelength. Therefore, the irradiation employed in the process involves the utilization of UVA (λ = 315-400 nm), UVB (λ = 285-315 nm), and UVC (λ < 285 nm) as energy source. Furthermore, the UV light supplied in the photo-Fenton method can excite the direct photolysis of H_2O_2, which also contributes to the production of hydroxyl radicals according to Eq. 2-5. As a result, the photo-Fenton process has gained increasing attention as a very promising water treatment method for the degradation of various organic pollutants, including penicillin G (Arslan-Alaton and Gurses 2004), alizarin red S (Devi et al. 2013), and dyes (Lam and Hu 2013). Despite the photo-Fenton shows significant advantages over traditional Fenton process, there still is room for much improvement. The demanding of strict acidic condition limits the operating pH levels and restrains the field application of the photo-Fenton process (Zheng et al. 2007).

2.1.3 Photocatalysis

Photocatalysis is defined as a catalytic reaction involving light absorption by a catalyst or a substrate by International Union of Pure and Applied Chemistry (IUPAC). Compared with other conventional chemical oxidation methods, photocatalysis is more effective in water treatment because of its important features, including (1) ambient operating temperature and pressure, (2) complete mineralization of parents and their intermediate compounds without secondary pollution, and (3) low operating cost.

To elaborate the fundamental principles of heterogeneous photocatalysis, semiconductor TiO_2 is taken as an example. When TiO_2 is irradiated by light with photon energy (*hv*) greater than or equal to its band gap energy (3.2 eV), the lone electron will be photo-excited and subsequently jumps to the conduction band. This excitation leaves behind an empty unfilled valence band, where the electron-hole pair is created and expressed as electron conduction band (CB) and hole valence band (VB), as depicted in Figure 2-1. A series of reactions that occur on the photon activated TiO_2 surface are described as follows (Chong et al. 2010):

$$\text{Photoexcitation: } TiO_2 \xrightarrow{hv} e^- + h^+ \quad (2\text{-}13)$$

$$\text{Photoexcited } e^- \text{scavenging: } O_2 + e^- \rightarrow O_2^{\cdot -} \quad (2\text{-}14)$$

$$\text{Oxidation of hydroxyls: } OH^- + h^+ \rightarrow \cdot OH \quad (2\text{-}15)$$

$$\text{Organic compounds degradation by } \cdot OH\text{: } R + \cdot OH \rightarrow \text{Intermediate(s)} \quad (2\text{-}16)$$

$$\text{Organic compounds decay by photoholes: } R + h^+ \rightarrow \text{Intermediate(s)} \quad (2\text{-}17)$$

$$\text{Protonation of superoxides: } O_2^{\cdot -} + \cdot OH \rightarrow \cdot OOH \quad (2\text{-}18)$$

$$\text{Co} - \text{scavenging of electron: } \cdot OOH + e^- \rightarrow HO_2^- \quad (2\text{-}19)$$

$$\text{Formation of } H_2O_2\text{: } HO_2^- + H^+ \rightarrow H_2O_2 \quad (2\text{-}20)$$

$$\text{Electron} - \text{hole recombination: } e^- + h^+ \rightarrow \text{heat} \quad (2\text{-}21)$$

In the absence of electron scavengers, the TiO_2 photocatalysis will be of low efficiency because the photogenrated holes recombine with electrons immediately. The

recombination reactions transfer the luminous energy to heat energy directly, and no radicals will be produced (Eq. 2-21). Therefore, the presence of electron scavengers (e.g. O_2) is critical for restraining the recombination. As shown in Eq. 2-14, oxygen prevents the recombination of electron-hole pairs, and produces superoxide radical ($O_2^{\bullet-}$). The $O_2^{\bullet-}$ radical will be further protonated to produce •OOH (hydroperoxyl radical) and peroxide hydrogen (H_2O_2) with high oxidation capacity subsequently (Eqs. 2-18 to 2-20).

TiO_2 photocatalysis has been extensively applied on the decay of organic contaminates, including dye (Jiang et al. 2004), triclosan (Son et al. 2009), and 4-nitrophenol (Dieckmann and Gray 1996). The overall reaction of TiO_2 photocatalysis with organic contaminates can be divided into five independent steps (Herrmann 1999): (1) mass transfer of the organic contaminants from solution to TiO_2 surface; (2) adsorption of the organic contaminants onto the activated TiO_2 surface; (3) photocatalytic reaction for the adsorbed contaminants on the TiO_2 surface; (4) desorption of the intermediates from the TiO_2 surface; and (5) mass transfer of the intermediates from the interface region to the bulk fluid.

However, the application of TiO_2 photocatalysis is restrained by its high band gap energy that can only be excited by UV light with wavelength less than 380 nm, resulting in the request of extra supply of UV light and thereby high operating cost. In view of

energy saving, one attractive option is to design a photoreaction system which can utilize the abundance of solar light. Therefore, researchers became interested in modifying the photocatalysts so that they can be activated by visible light. Various approaches have been adopted to extend the optical absorption spectrum of TiO_2 to visible light region. More recently, the non-metal doped TiO_2 have been widely studied because of its simple fabrication and highly photoactivity (Chen et al. 2005; Gombac et al. 2007; Liu et al. 2009; Nah et al. 2010). Asahi published a paper about nitrogen doped titanium dioxide materials with effective UV and visible light activity (Asahi et al. 2001). The N-doped TiO_2 was shown to have a much greater optical absorbance in the visible region through extending from a sharp cut off at about 380 nm to a broad cut off at above 500 nm, which subsequently increased the amount of visible light that the material could absorb, and hence the visible light-mediated photocatalyst was achievable.

The mechanism on enhancement of nitrogen doping TiO_2 was proposed by Nakoto (Nakamura et al. 2004), where the N-doping narrowed the gap between the valence band and conduction band of TiO_2. As shown in Figure 2-2, the N-doping introduced a new occupied orbital, named N-2p orbital, between the valence band and conduction band, which is comprised primarily of O-2p orbital and Ti-3d orbital, respectively. These N-2p orbital acted as a mid-step up for the electrons in the O-2p orbital. Once this process proceeds, on the one hand, electrons from the original valence band can

immigrate into the N-2p orbital, leaving a hole in the valence band; on the other hand, the electrons on the N-2p orbital can jumped into the conductive band easily by providing small jump energy (i.e. irradiation with larger wavelength). As a result, the electron-hole pairs are generated in the N-doped TiO_2 photocatalysis, which will further produce radicals by similar reactions as described in the traditional TiO_2 photocatalysis. Recent experimental studies have shown that the desired band gap narrowing of TiO_2 can be achieved through main group dopants (i.e. B, C, N, O, F, Al, Si, S, Cl and Br) to enhance photocatalytic activity in the visible light range (Yu et al. 2005; Yu et al. 2002; Yu et al. 2003a; Yu et al. 2003b).

Besides narrowing the band gap energy of TiO_2, researchers have made a lot of effort to increase the visible light activity via facilitating charge separation. One way of doing this is to incorporate noble metal (e.g. Ag and Au) into TiO_2 (Chen et al. 2009). Taking the incorporation of silver into TiO_2 (Ag/TiO_2) as an example, the photocatalytic performance was increased significantly as the amount of silver ranged from 1% to 5% (Kim et al. 2013). That is because the silver has a Fermi level with the energy just below the conduction band. The recombination of electron-hole pairs was restrained because the electron in the conduction band can be trapped by Ag efficiently once the electron-hole pairs have been produced by the irradiation of light. As a result, the amount of separated hole on the valance band will be increased, and thereby •OH radicals and photocatalytic acitivity. Various investigations have demonstrated that the

dosage of silver onto the TiO_2 catalyst is critical to the performance (Daniel et al. 2013; Kuo et al. 2007; Lin and Lee 2010). At the optimal dosage, a rapid electron trap will be achieved because the silver is well dispersed through TiO_2 catalyst. However, if the silver is overdosed, the silver will cover the surface of TiO_2 and prevent light absorption. Moreover, the excess silver will act as the recombination center for electron and hole (Chen et al. 2005). The mechanism of Ag/TiO_2 photocatalysis is present in Figure 2-3. Although noble metals incorporation is efficient in promoting the photocatalytic performance, the high price of novel metals restrains the industrial application of cooperated TiO_2. Therefore, it is usually replaced by more economical transition or non-metals doping.

Nowadays, another intensive research activity in this field focuses on the development of novel alternative materials with non-TiO_2 base to use sunlight as the green energy source (Kubacka et al. 2012). Among these novel photocatalysts, WO_3 offers several advantages of simple, cheap and relatively high stable, and presents a promising ability in waste treatment (Szilagyi et al. 2012). But WO_3 still demonstrates relatively low photocatalytic activity in visible light region (Chen et al. 2013). Fortunately, bismuth (Bi) is a kind of p-block metal with a d^{10} configuration, and the Bi 6s can hybridize O 2p levels to form a preferable hybridized valence band (VB), which favors the mobility of photogenerated holes in the VB and benefits the enhancement of the photocatalytic performance of the Bi^{3+}-based oxides (Tang et al. 2004). Previous studies have

demonstrated that Bi_6WO_{12} possesses significantly higher optical absorption in the wavelength region above 440 nm than either bismuth oxide (Bi_2O_3) or WO_3, increasing the possibility of enhanced photocatalytic activity under solar illumination (Finlayson et al. 2006). A variety of intermediate oxides exhibiting different but related crystal structures exist in the Bi_2O_3-WO_3 phase system such as $Bi_2W_2O_9$, Bi_2WO_6, Bi_4WO_9, Bi_6WO_{12} and $Bi_{14}WO_{24}$. More importantly, it has been found that Bi_2WO_6 exhibits the highest photocatalytic activity among the above Bi^{3+}-based oxides under visible light irradiation (Finlayson et al. 2006; Li et al. 2010).

2.2 Description of Norfloxacin

2.2.1 Background

Fluoroquinolones (FQs) are an important class of antibiotics currently used in human and veterinary medicine due to their broad activity spectrum against gram-positive and gram-negative bacteria. It is reported that FQs are only partially metabolized in body after administration and are largely excreted in their pharmacologically active forms, which results in environmental contamination (Sturini et al. 2012). Norfloxacin is a second generation of FQs, which demonstrates excellent activity in treating common as well as complicated urinary tract infections and achieves high concentration in the urinary tract. It functions by inhibiting DNA gyrase, a type II topoisomerase and topoisomerase IV enzymes necessary to separate bacterial DNA, thereby inhibiting cell

division. The physiochemical characteristics of norfloxacin are summarized in Table 2-1.

2.2.2 Toxicological effects

The toxicological effects of FQs on human health have been reported by Santos in medical literature (Santos et al. 2010). The most commonly adverse effects of FQs are gastrointestinal upset including nausea, vomiting, diarrhea, constipation and abdominal pain, which amounts nearly 7% of the total adverse effects. The less common effects may contribute to the central nervous system events, blood disorders, renal disturbances, and skin hypersensitivity and photosensitivity effects (Childs 2000; Stahlmann and Lode 2010) as indicated in Table 2-2. Rare occurrences of convulsions, psychosis and tendinitis have also been reported (Childs 2000). Some of these adverse effects, such as additional drug therapy unrelated to the antimicrobial, may contribute to side effects. Furthermore, phototoxicity, which is often reported in lomefloxacin (Wadworth and Goa 1991), sparfloxacin (Tokura et al. 1996) and clinafloxacin therapy (Koker et al. 2010), is a dose-dependent phenomenon that requires exposure to direct or indirect ultraviolet A (UVA) light (Paton and Reeves 1991). The presence of FQs in aquatic environment has reported to interfere with bacterial DNA replication, be toxic to aquatic plants and organisms, and contribute to bacterial geno-toxicity (Niu et al. 2012b).

2.2.3 Environmental fate

It is reported that the FQs excreted in urine or feces after administration either as metabolites or unchanged species (Thiele-Bruhn 2003). Moreover, the excreted amount in unchanged species reaches up to 90% of an administered dose of antibiotics (Drillia et al. 2005), which subsequently enters the aqueous environment (e.g. sewage treatment system) and imposes potentially hazardous effects on other organisms living in aqueous environment. FQs antibiotics are frequently detected at various conventional water environments, such as domestic wastewater, municipal wastewaters, WWTP effluents, surface waters and effluents from drug manufactures, and shows relatively high concentrations in the range of ng L^{-1} to several μg L^{-1} (Golet et al. 2001; Gros et al. 2010; Larsson et al. 2007; Renew and Huang 2004; Watkinson et al. 2007; Watkinson et al. 2009). The highest concentrations of FQs over 100 μg L^{-1} were found in hospital wastewaters (Verlicchi et al. 2010). Moreover, the opportunity for FQs antibiotics to be introduced into drinking water systems has increased due to the reuse of treatment wastewater, which leads to the increment of human exposure to these FQs antibiotics (Kim and Aga 2007; Li and Zhang 2013). The widespread FQ antibiotics and their high concentrations in water might result in an increased probability for the development and spread of antibiotic resistant bacteria and resistance genes, which is regarded as one of the three greatest threats to human health by the World Health Organization (Kümmerer 2009; Oberlé et al. 2012).

The problem of FQs pollution becomes much more serious especially when the pathogens possess antibiotic resistance which leads to an increase of the morbidity and mortality (Andersson and Hughes 2010; Levy 2001). Currently, people are becoming more and more concerned about the potential toxic effects of antibiotics. Thus the antibiotic erythromycin has been added into the Drinking Water Contaminant Candidate List established by the U.S. Environmental Protection Agency (Li and Zhang 2013).

The FQs of norfloxacin has been widely detected in the aqueous environment worldwide. Vieno et al. reported that the elimination of norfloxacin has been observed in twelve sewage treatment plants (STPs) in Finland (Vieno et al. 2007). In Canada, norfloxacin has been frequently detected in the final effluents of in wastewater treatment plants (WWTPs) (Miao et al. 2004). In the Pearl River of China, the concentration of norfloxacin has been reported to be up to 108 ng/L. In Hong Kong, norfloxacin is the most common one among those detected FQs because the prescribed heavily for medical application. Furthermore, its concentration in the aqueous systems in Hong Kong is relative high, especially in the Sewage Treatment Plant, which reaches 460 ng/L and 320 ng/L in the influent and effluent, respectively (Gulkowska et al. 2008). Besides, the norfloxacin has been identified even in the Victoria harbor at the concentration of 28.1ng/L due to it serves as main venues for WWTP effluent outfalls in Hong Kong (Xu et al. 2007).

2.2.4 Previous work in norfloxacin degradation

Considering the widespread appearance and the potential risks to human and ecological health, the removal of norfloxacin residue in aquatic environments is therefore becoming an important and attractive issue. Different available technologies, including sewage treatment plants (STPs), biological degradation adsorption and AOPs, have been developed for this purpose as show in below.

STPs are the most important residue places of antibiotics in aquatic environment. Commonly, the concentration of antibiotics in the influent of the STPs is the highest ranging from several hundred ng L^{-1} to several μg L^{-1}. It has been demonstrated that the application of STPs can achieve partially elimination of norfloxacin. In Italy, the mean and maximum elimination efficiency of norfloxacin via STPs reach 66% and 81%, respectively (Castiglioni et al. 2006), while the mean elimination efficiency of norfloxacin in the largest STP in Switzerland is 88% (Golet et al. 2002). In Lindberg's work, the mean degrees of norfloxacin elimination in Sweden was estimated to be 87% in terms of five different STPs (Lindberg et al. 2004). Despite the elimination efficiency of norfloxacin through the STPs is not bad, it is impossible for complete removal of norfloxain from water body due to the limitation of absorption capacity of sludge.

Yang and coworkers (Yang et al. 2012a) have suggested that the biodegradation plays a major role in the norfloxacin degradation by using the non-sterile soil. In the presence

of biodegradation, the removal constant and half-live of norfloxacin has been significantly improved, especially the removal constant, which shows 3.22 times higher than that in the absence of biodegradation. The biodegradation of norfloxacin is found to be affected by the environmental factors such as soil moisture, manure amendment, where the soil moisture affects the microbial activity and redox potential of the soil (Heberer et al. 2008), and the manure affects the microbial activity by supplying nutrients required by microbes (Kotzerke et al. 2008).

Adsorption is considered as a simple and effective method to remove norfloxacin from water and wastewater. Generally, the adsorption mechanisms of FQs onto model sorbent phases have been proposed to be cation exchange, cation bridging, surface complexation, hydrophobic effect, electrostatic interaction, and electron-donor–acceptor (EDA) interactions (Yang et al. 2012b). Previous studies have utilized various adsorbents were utilized in the norfloxaicn removal, such as soil, clay minerals, activated carbon, carbon nanotubes, porous resins, and alumina (Liu et al. 2011a; Pei et al. 2011; Peng et al. 2012a; Peng et al. 2012b; Sui et al. 2012; Wang et al. 2010d; Yang et al. 2012c; Zhang and Dong 2007). Among these adsorbents, the clay mineral has an impressive advantage of low operational cost because it is solid waste derived from industry production. However, these low cost adsorbents always exhibit ineffective removal performance of pollutants because of the intrinsic shortage of relative small surface area in solid waste.

The carbon nanotubes, activated carbons, alumina and porous resins were reported to be of efficient in norfoxacin decay because they possess large surface area and controllable pore size distribution (Liu et al. 2011a). Furthermore, the "removed" norfloxacin mainly resides in the absorbents through the adsorption treatment, which may still own underserved opportunity to be released into aquatic environment. Therefore, it is essential to develop effective technologies to decompose the norfloxacin into harmfulness products.

Several AOPs, including photocatalysis, ozonation, chlorination, and Fenton-like reaction have been selected for the degradation and mineralization of norfloxacin in previous studies. The details of these investigations are demonstrated as below.

As reported by Niu et al., the heterogeneous Fenton system employing Fe_3O_4@ALG/Fe MNPs (Alginate-Fe^{2+}/Fe^{3+} polymer coated Fe_3O_4 magnetic nanoparticles) was used to degrade norfloxacin from aqueous media in the presence of H_2O_2 (Niu et al. 2012a). The system showed high efficiency on norfloxacin degradation with 100% of norlfoxacin and 90% of TOC removed within 60 min, and fluorine changing into F^- ions within 1 min. But the operation at a narrow pH range (pH 3.5) suppresses the practical application of this Fe_3O_4@AlG/Feli$_2O_2$ system.

Chlorine dioxide (ClO_2) is a powerful disinfectant which has the advantages of high biocidal efficiency, less pH dependence and few disinfection by-products formation (Neta et al. 1988). Wang et al. investigated degradation of norfloxacin by ClO_2 oxidation (Wang et al. 2010b). It was reported that norfloxacin can be decayed to certain degree by using ClO_2 but the effective functional group of antibiotics remains intact due to the low redox potential of ClO_2 (0.95 V). The reaction mechanism demonstrated that piperazine ring of norfloxacin is the primary reactive center toward ClO_2. The ClO_2 is likely to attack piperazine N4 atom followed by concerted fragmentation involving piperazine N1 atom, which results in hydroxylation, dealkylation and intramolecular ring closure at the piperazine moiety.

Ozonation is another route for norfloxacin removal. A study from Liu (Liu et al. 2012) addressed the degradation of norfloxacin via ozonation in the secondary wastewater effluent. Unfortunately, the ozonation process could not decompose the functional group of norfloxacin effectively because of its lower redox potential of 2.07 V. The degradation mechanism was proposed to be derived from the attack of either molecular ozone on both the piperazine and quinolone moieties.

In addition, photolysis is an attractive method for norfloxacin decay. Hubicka's work has demonstrated that antibiotic norfloxacin (in solid phase) can be decomposed under the irradiation of UVA (320-400 nm) with maximum emission at 365 nm, showing a

10.8% removal of norfloxacin after 113 days of exposure (Hubicka et al. 2013). In Babic' study, the norfloxacin also underwent decomposition by the irradiation of simulated solar irradiation (Babic et al. 2013). The photodecay of norfloxacin follows a stepwise sequence of piperazine > benzene ring > pyridone ring according to the oxidability of these functional group. A competitive defluorination reaction involved in the fluorine atom in 6 position of the quinolone ring was also occurred in the photolysis process. The study also showed that the norfloxacin decay was influenced by the environmental parameters, such as component, pH and temperature of the designed solution.

To improve the norfloxacin removal efficiency, the strategy of integration of multi processes into one provides a new approach to deal with the norfloxacin pollution. For example, Zhang's work illuminates that the norfloxacin photodecay performance through UV photolysis has been extremely improved by dosing Fe (III) salts and/or supply of ultrasound (Zhang et al. 2012a). The combination of UV photolysis and O_3 oxidation (O_3/UV) results in the best decay of norfloxacin over sole UV photolysis and O_3 oxidation as assessed by Rivas and coworkers (Rivas et al. 2011). However, the combination technologies will not be always beneficial to norfloxacin decay. For example, the addition of TiO_2 to the O_3/UV system showed an adverse effect on norfloxacin removal because the TiO_2 can reduce the hydroxyl radical generation in O_3/UV system due to the light obstruction by TiO_2, despite it improves the formation of

hydroxyl radicals via the generation of electron-hole pairs in a certain extent (Rivas et al. 2011). Due to the same reason of light obstruction, the combination of activated carbon with O_3/UV system completely inhibited the TOC elimination of norfloxacin. Therefore, the selection of appropriate technologies for combination is critical to improve the norfloxacin degradation.

The heterogeneous photocatalysis, incorporating the photo irradiation with semiconductor catalyst, has attracted much more concern since the technology supplies a new basic platform for norfloxacin degradation. In An's research (An et al. 2010a), with the irradiation of a high-pressure mercury lamp (λ_{max} = 365 nm), the heterogeneous photocatalysis using TiO_2 is approved to be an attractive treatment technologies for norfloxacin decay, where most of produced intermediates was finally mineralized into CO_2, water, and mineral species. This study also demonstrated that the major active species generated in heterogeneous TiO_2 photocatalysis is •OH radicals. Moreover, the decay reaction between norfloxacin and •OH radicals is extremely rapid presenting a rate constants of $(6.18 \pm 0.18) \times 10^9\ M^{-1}\ s^{-1}$. The hydroxyl radical of non-selective and high redox potential results in the excellent performance in pollutants removal comparing to other process such as ClO_2 and O_3. It was reported that the elimination of piperazine ring in FQs, addition of hydroxyl radical to quinolone ring, and attack at the F atoms on the aromatic ring by hydroxyl radicals occurred (An et al. 2010a).

Heterogeneous TiO_2 photocatalysis was also reported to be an effective method in norfloxacin decay. In previous studies, the decay performance is closely related to the conditions of aquatic environment, such as norfloxacin concentration, pH level, co-existence of contaminations (Javier Rivas et al. 2012; Li et al. 2012b). However, it still has a room for the performance improvement via TiO_2 photocatalysis. The hybrid system by combining selected substances (e.g. graphene) was thereby proposed to enhance the norfloxacin degradation efficiency. In Li's study, the graphene/TiO_2 composites were successfully utilized in norfloxacin decomposition. Compared with pure TiO_2 photocatalysis, the photocatalytic activity of the graphene/TiO_2 composite was enhanced 32.7% towards aqueous norfloxacin degradation. The significant improvement is ascribed to the excellent charge carrier mobility of graphene (i.e 200000 $cm^2V^{-1}S^{-1}$ at room temperature) (Wang et al. 2012), which will consequently enhance the quantum efficiency and decrease the band gap of TiO_2 photocatalyst (Li et al. 2011). Another composite of mesoporous graphene and tourmaline co-doped TiO_2 was also reported to exhibit considerably high photocatalytic activities in terms of norfloxacin degradation under simulated sunlight irradiation (Li et al. 2012a). The high photocatalytic activities can be attributed to: (1) the enhanced quantum efficiency: graphene serves as the transporter of photogenerated electrons from TiO_2, whereas tourmaline serves as the acceptor. Both electron transporting and electron accepting roles effectively suppress the recombination of electron−hole pairs, leaving more photogenerated holes to form reactive species and facilitating the photodegradation of

the aqueous norfloxacin and (2) the perfect physical and chemical properties of the composite surface: the large surface area of this composites improve the degradation performance by increasing the number of active sites, and providing efficient transport for active species in the process.

Despite above TiO_2 based photocatalysis (including UV/TiO_2 and TiO_2 hybrid system) has been extensively studied and shows good performance on norfloxacin decay. It still deserved to note that only the ultraviolet (UV) light with energy matches or exceeds the band gap energy (TiO_2 = 3.2 eV, $\lambda < 380$ nm) can excite the TiO_2 photocatalyst to generate active radicals. In order to abate the gap, photocatalysts exited by both UV and visible lights are proposed in organics removal in many literatures, such as Bi_2WO_6 (Saison et al. 2011), $BiVO_4$ (Jiang et al. 2011), C-TiO_2 (Goldstein et al. 2008)，N-TiO_2 (Senthilnathan and Philip 2010) and $InVO_4$ (Yao et al. 2009).

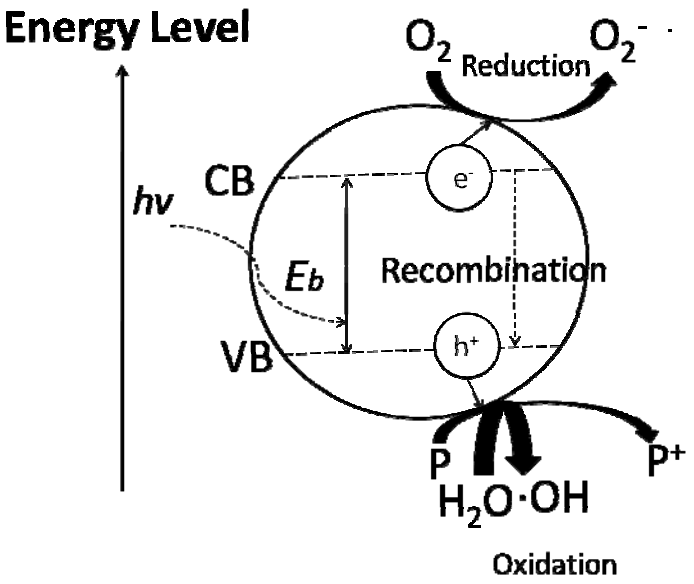

Figure 2-1. The mechanisms of photo-generated electron-hole pairs for TiO_2 photocatalysis in the presence of water pollutant (P).

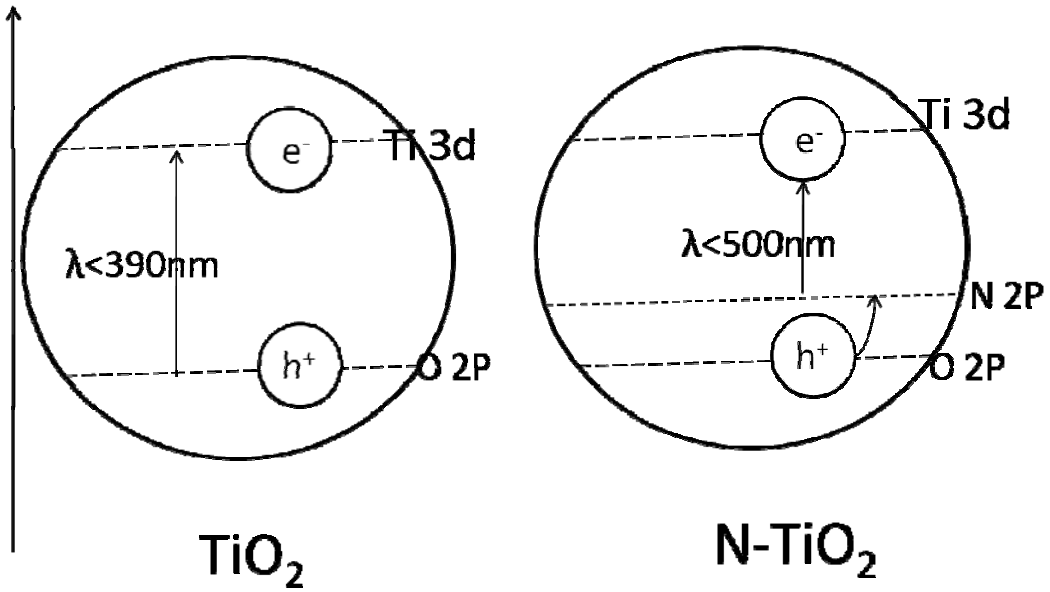

Figure 2-2. Doping with nitrogen results in the reduction of band gap in TiO_2 photocatalysis.

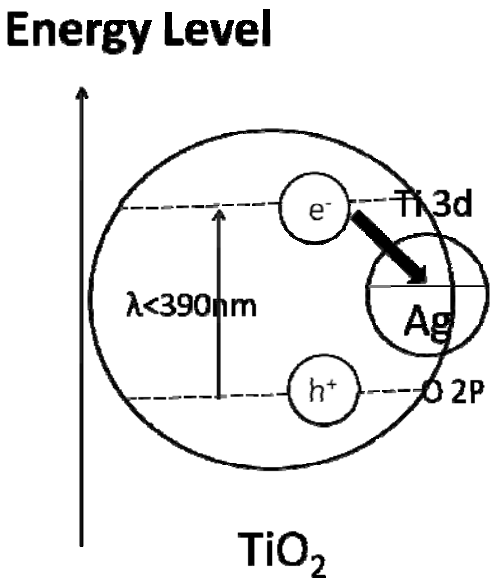

Figure 2-3. Incorporation of silver facilitates longer charge separation by trapping photogenerated electrons.

Table 2-1 Summary of physiochemical characteristics of norfloxacin.

Parameter	Information
Chemical structure	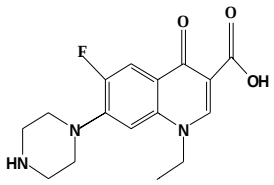
IUPAC name	1-ethyl-6-fluoro-4-oxo-7-piperazin-1-yl-1H-quinoline-3-carboxylic acid
Molecular formula	$C_{16}H_{18}FN_3O_3$
Mol.mass	319.331 g/mol
pKa_1	6.42
pKa_2	8.75

Table 2-2. Adverse effect associated with FQs.

Adverse effect	Range of incidence %
Gastrointestinal (diarrhea, vomiting)	0.8-6.8
Central nervous system (dizziness, headache)	0.9-11
Skin (rashes)	0.4-2.1
Blood disorders	0.5-5.3
Cardiovascular(palpitations)	0.5-2.0
Phototoxicity or photoallergy	0.5-2.1
Serious reactions, eg, hemolytic uremic syndrome, Stevens Johnson syndrome	<0.5

Note: cited from reference (Stahlmann and Lode 2010)

Chapter 3 Materials and Methodology

3.1 Introduction

In this chapter, the methodology regarding to the whole study is described, where the detailed descriptions of experimental setup and reactors for the wastewater treatment processes are given. Some important chemicals and reagents employed in this study are listed. The sampling and analytical methods of probe compounds can also be obtained in this chapter. In addition, some other instruments used to determine the solution parameters (e.g. TOC, pH and ferrous ions) are also provided. The systematic flowchart for is shown in Scheme 3-1.

3.2 Materials

All chemicals are of analytic reagent grade and all solvents are of HPLC grade and used as received without further purification. All the chemical and solvents used in this study were summarized in Table 3-1. The stock solutions were prepared in deionized and distilled water with a resistivity of 18.2 MΩ from a Bamstead NANOpure water treatment system (Thermo Fisher Scientific Inc., USA).

3.3 Catalyst Preparation

3.3.1 Bi_2WO_6

Bismuth tungstate was synthesized by a low cost and simple method using hydrolysis followed by calcining, where equal mole of H_2WO_4 and $C_6H_5BiO_7$ was dispersed into 32% v/v ammonia to form a homogenous solution. Then the solution was mixed with 4 times of distilled water, dried at 100°C, and calcined at 600 °C for 1 hour to obtain the target product. The synthesized product was washed several times by deionized water, and then dried for further use.

3.3.2 C-TiO_2

The C-TiO_2 photocatalyst was synthesized by a solution phase carbonization method. First, 10 mmol of titanium tetrachloride was added dropwise into 30 mL of ethanol with continuous stirring to form a transparent yellowish solution. Then 4 ml of diethanolamine was added into the above solution and continuously stirred for 24 h at ambient temperature. The mixture was dried at 100^{o}C, and followed by raising the temperature to 500 ^{o}C with a heating rate of 1^{o}C/min and maintained for 5 h. After calcination, the obtained powder was washed by DI water for several times. For comparison, pure TiO_2 was synthesized in the same procedure in parallel with the absence of diethanolamine.

3.4. Experiment Setup

3.4.1 SSL/Bi_2WO_6 and SSL/Bi_2WO_6/H_2O_2 processes

The degradation of norfloxacin was mainly conducted in a simulated solar light photochemical reactor equipped by a 300 W Xenon lamp (Beijing Changtuo Company), where a Perkin Elmer 300 W xenon lamp was used to produce a collimated beam and the light passed through a filter to remove infrared radiation. The experiment setup was shown in Figure 3-1. The irradiation spectrum was shown in Figure 3-2. To get a visible light irradiation ($\lambda > 400$ nm), a UV cut-off filter was inset into the light path to remove UV light. Prior to each batch reaction, 100 mL of suspension (a mixture of norfloxacin and Bi_2WO_6 in SSL/Bi_2WO_6 process; or a mixture of norfloxacin, Bi_2WO_6, and H_2O_2 in SSL/Bi_2WO_6/H_2O_2 process) was stirred in darkness to achieve adsorption equilibrium. After the equilibrium, the degradation was started by turning on the pre-heated light source. At preset intervals, exact 1mL of sample was withdrawn and filtered through a 0.2 μm PTFE membrane for further analysis. All experiments were carried out in duplicate at room temperature (air-conditioned) at 23±1°C.

3.4.2 Vis/C-TiO_2 process

The photocatalytic reaction via Vis/C-TiO_2 process was conducted in a computerized Luzchem CCP-4V photochemical reactor containing twelve low-pressure mercury lamps as shown in Figure 3-3. The irradiation wavelength of these lamps is mainly

located at 420 nm as stated previously. The emission spectra of 420 nm lamp are shown in Figure 3-4. Prior to the reaction, a predetermined amount of C-TiO_2 was added into 100 mL of norfloxacin solution in a quartz beaker/cylinder, and stirred in darkness for 1 h to achieve adsorption equilibrium. After equilibrium, the degradation was started by exposing to the pre-heated light source. Exact 1 mL of sample was withdrawn from the reactor at a preset time interval and then filtered through a 0.2 μm PTFE membrane to ensure a solid free solution for further analysis. All experiments were carried out at room temperature (air-conditioned) at $23 \pm 1^{o}C$ in duplicate and the error is less than 5.0 %.

It deserved to note that, the term of "visible light" appears in both Bi_2WO_6 and C-TiO_2 photocatalysis; however, they falls into different light source. The visible light in Bi_2WO_6 photocatalysis was a continuous spectrum with (λ > 400 nm) supplied by Xenon lamp. In the Vis/C-TiO_2 process, the visible light was mainly located at 420 nm.

3.5. Analysis

3.5.1 Analysis by HPLC

The concentration of probe was determined by high performance liquid chromatography (HPLC). The HPLC is comprised with a Waters 515 pump, a Waters 2489 Dual λ (UV and Visible) absorbance detector and a Waters 717 plus autosampler. The

chromatographic separations were performed on a Pinnacle DB C18 reversed phase column (250 mm × 4.6 mm with i.d. of 5 μm) from RESTEK. For the quantification of norfloxacin, the mobile phase was composed of 50% acetonitrile and 50% water (V/V), and the pH level was adjust to 3 by adding H_3PO_4. Before using, the mobile phase was filtrated through 0.2 μm PTFE filters (Whatman) and degassed for more than 30 min. The flow rate was 0.8 $mLmin^{-1}$ and injection volumes were 10 μL. The UV/Visible Detector was set at 280 nm, which was the maximum absorbance wavelength of norfloxacin solution and determined by scanning the spectra of the tested samples from 200 nm to 900 nm using a spectrophotometer Spectronic (Figure 3-5).

3.5.2 Analysis by LC-ESI/MS

The identification of aromatic intermediates was carried out by a Thermo Quest Finnigen LCQ Duo Mass spectrometer system, which was equipped with Thermo P4000 pumps, Thermo AS3000 autosampler with a 20 μL injection loop, UV6000LP photodiode array UV detector and an electrospray ionization with an ion-trap mass spectrometer operating at a positive mode (LC-ESI/MS, $[M+H]^+$ ions) at a capillary temperature of 225^oC. The chromatographic separations were performed on a Pursuit XRs C18 reversed phase column (150 mm× 2.0mm, 3.0 μm) from Varian. The mobile phase was comprised with two solutions: (A) 5 mM CH_3COONH_4 aqueous solution, adjust the pH to 4.6 by CH_3COOH, and (B) acetonitrile. The composition of the mobile

phase was changed according to the following gradient: 100% of A was kept during the first 2 min; from 2 to 50 min, B was linearly increased from 0 to 50%; from 50 to 60 min, B was continuous linearly increased to 100%. The flow rate of mobile phase was kept at 0.4 mL/min.

3.5.3 TOC, pH and adsorption spectrum

TOC (Total Organic Carbon) was measured by a Shimadzu TOC-5000A analyzer equipped with an ASI-5000A autosampler to identify the mineralization of the organic contaminants. The solution pH level was determined by a digital pH meter (HANNA instrument, B417). The adsorption spectrum of compounds was performed by Biochrom Libra S35 UV-Visible spectrophotometer.

3.5.4 Ion chromatography

The generated inorganic ions in the process were quantified by ion chromatography (Dionex Series 4500i) composed of a Dionex CD25 Conductivity Detector and Dionex AS 40 Autosampler. For anion analysis, the ion chromatography was equipped with an anion column (Dionex IonPac® AS14 (4 mm × 250 mm) and eluted by a mixture of 1 mM of $NaHCO_3$ and 3.5 mM of Na_2CO_3 at a flow of 1 mL/min. For cation analysis, a Dionex Ionpac® CS 12 (4 mm × 250 mm) was adopted as column and 0.022 M methane sulphonic acid (MSA) was used as mobile phase eluting at 1 mL/min.

3.5.5 Emission spectra of lamps and antibacterial activity tests

The emission spectra of 420 nm lamp and Xe lamp were recorded by ILT900 Wideband Rapid Portable Spectroradiometer (International Light TECHNOLOGIES). To study the remaining antibacterial activity of the decayed norfloxacin, a toxicity test was performed on stationary phase of E.coli (Escherichieae coli) K-12 ATCC 15153 by spread plate method. The cell density was diluted to 4200 colony-forming units (cfu)/mL for further test. The prepared plates were incubated at 35°C for 16 h. The experiment was repeated by three times, and the difference of each sample is less than 15%. The average result was used for further calculation.

3.5.6 Turbidity and effective diameters

The turbidity of suspension was continuously monitored by a Hach 2100 Series Laboratory Turbidimeter. The effective diameters of suspension at different pH levels were measured by Zeta Plus/Zeta Potential Analyzer (Brookhaven Instruments Corporation).

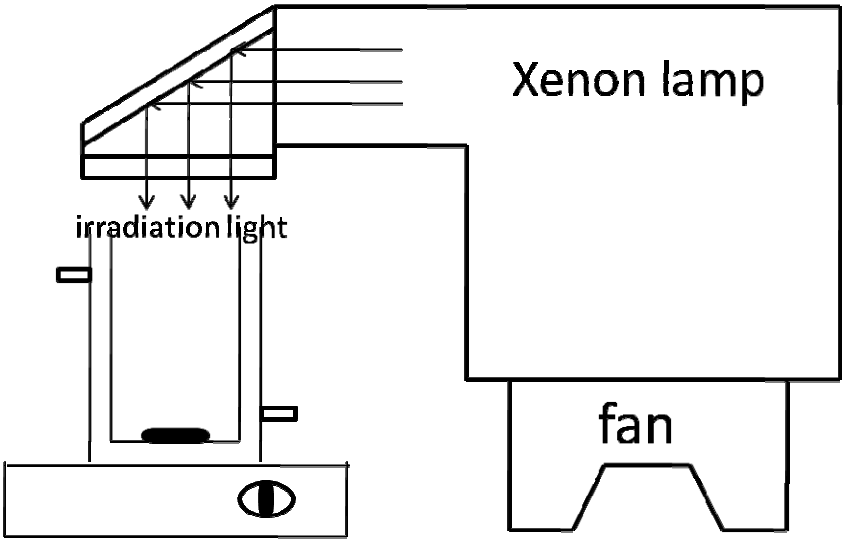

Figure 3-1. The experiment setup of simulated solar light mediated reaction.

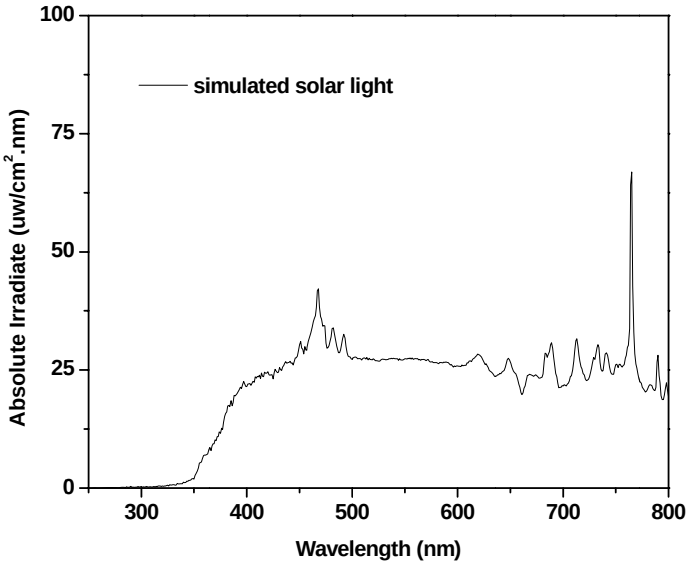

Figure 3-2. The irradiation spectrum of simulated solar light.

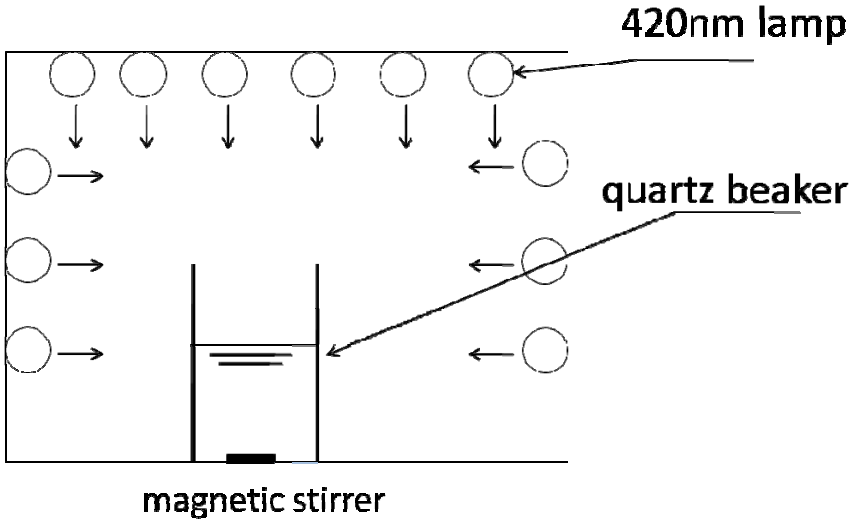

Figure 3-3. Schematic diagrams of the photoreactor Luzchem CCP-4V.

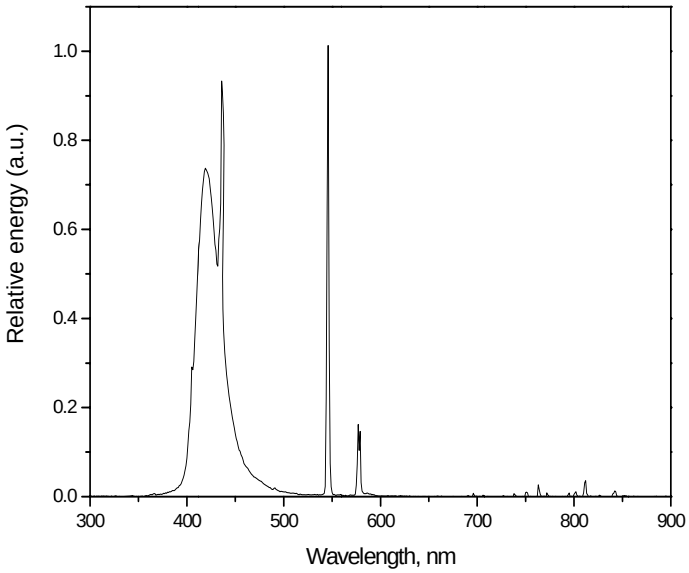

Figure 3-4. The irradiation spectrum of 420 nm lamp.

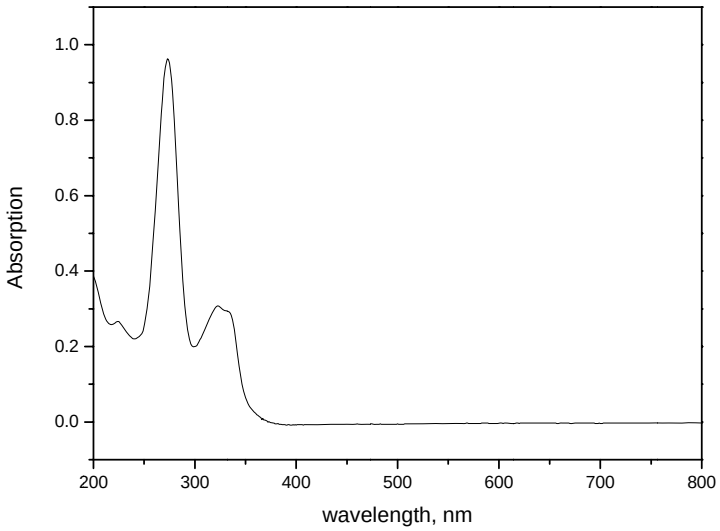

Figure 3-5. The absorption spectrum of norfloxacin solution.

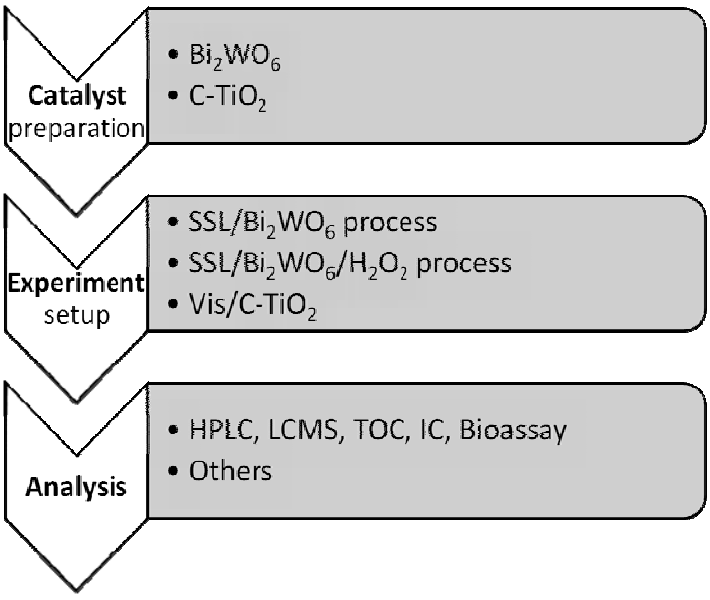

Scheme 3-1. The systematic research flowchart of Material and Methodology section

Table 3-1. List of chemicals used in this study.

Chemicals	MW, g mol^{-1}	Formula	Purchased from
Target Compounds			
Norfloxacin	319.33	$C_{16}H_{18}FN_3O_3$	Wako Pure Chemical Industries, Ltd.
Chemicals for Bi_2WO_6 synthesis			
Tungsten acid	249.85	H_2WO_4	Sigma Aldrich
Citric bismuth	398.08	$C_6H_5BiO_7$	Sigma Aldrich
Ammonia	35.05	$NH_3 \cdot H_2O$	Sigma Aldrich
Chemicals for C-TiO_2 synthesis			
Titanium tetrachloride	189.679	$TiCl_4$	Sigma Aldrich
Diethanolamine	105.14	$C_4H_{11}NO_2$	Sigma Aldrich
Solvents			
Acetonitrile (HPLC grade)	41.05	C_2H_3N	Tedia
Methanol (HPLC grade)	32.04	CH_4O	Tedia
Others			
Hydrochloric acid	36.46	HCl	Sigma Aldrich
Orthophosphoric acid	98	H_3PO_4	Sigma Aldrich
Sodium hydroxide	40	NaOH	Sigma Aldrich
Sodium bicarbonate	84.01	$NaHCO_3$	BDH, England
Sodium carbonate	105.99	Na_2CO_3	BDH, England
Methanesulphonic acid	96.11	CH_4O_3S	Sigma Aldrich

Cont'd Table 3-1

Sodium nitrate	84.99	$NaNO_3$	Sigma Aldrich
Ammonium nitrate	80.04	NH_4NO_3	Sigma Aldrich
Sodium chloride	58.44	NaCl	Sigma Aldrich
Sodium fluoride	41.99	NaF	Sigma Aldrich
Potassium iodide	166	KI	Sigma Aldrich
Sodium sulfate	142.04	Na_2SO_4	Sigma Aldrich
Magnesium chloride	95.21	$MgCl_2$	Sigma Aldrich
Calcium chloride	110.98	$CaCl_2$	Sigma Aldrich
Ferric chloride	162.2	$FeCl_3$	Sigma Aldrich
Ferrous chloride	126.75	$FeCl_2$	Sigma Aldrich
Ammonium acetate	77.08	CH_3COONH_4	BDH, England
Acetic acid	60.05	CH_3COOH	Sigma Aldrich
Potassium dihydrogen phosphate	136.09	KH_2PO_4	BDH, England
Potassium hydrogen phosphate	174.18	K_2HPO_4	BDH, England
Hydrogen peroxide	34.01	H_2O_2	Riedel-deHaën
Potassium iodate	214	KIO_3	Sigma Aldrich

Chapter 4 An Effective Approach of Using Simulated Solar Light Mediated Bi_2WO_6 Process for Nofloxacin Degradation

4.1 Introduction

Fluoroquinolones (FQs) are a class of synthetic antibiotics that have broad-spectrum antibacterial properties by inhibiting DNA replication and transcription (Albini and Monti 2003). The high effectiveness has made them widely used both in human medicine and veterinary practice (Chang et al. 2010). However, most of the FQs are not fully metabolized in the body and are partially excreted in its pharmaceutically active form (> 50%) (Rigos et al. 2004). Because of the limited biodegradability and widespread use of these antibiotics, an incomplete removal is attained in conventional wastewater treatment plants and relative large quantities are released into the environment. As a result, numerous antibiotics can be found in surface waters causing adverse effects on aquatic organisms (Duong et al. 2008). Norfloxacin is a second generation of synthetic FQs used to treat urinary tract infections. It is widely used in prescription in Hong Kong, consequently, the norfloxacin was frequently detected in the aquatic systems, including sewage, surface water and the Victoria Harbor (Xu et al. 2007). Furthermore, the detected norfloxacin presents a higher concentration, which

reaches to 460 ng/L and 320 ng/L in the influent and effluent of Sewage Treatment Plant in Hong Kong, respectively (Gulkowska et al. 2008).

Currently, scientists have increasing interests in developing technologies to remove norfloxcacin from aquatic environment. The previous works showed that norfloxacin can be absorbed or biodegraded via the activated sludge process, but it cannot be completely removed (Li and Zhang 2010). Advanced oxidation processes (AOPs) have been proven to be an effective alternative for drug elimination. The common AOPs, including ozonation, UV, ClO_2, $KMnO_4$, UV/O_3 and UV/TiO_2 has been used to treat norfloxacin (An et al. 2010b; Naik et al. 2009; Rivas et al. 2011; Wang et al. 2010c). The use of TiO_2 as a catalyst for environmental cleanup of organic pollutants through the activation of the UV light has been widely studied due to its low cost, photo-stability, easy separation from water body (Molinari et al. 2006). However, TiO_2 can only be excited by UV light with an irradiation wavelength less than 380 nm, leading to an compulsory extra UV light source for initializing the process (Xu 2001). Concern about energy saving, solar light as a source of abundance and free of charge has been taken into consideration. But, in the solar light, UV light occupies only 4%, whereas visible light composes 43%. In order to abate the gap, photocatalytic reaction using the catalyst responded to both UV and visible light has received more and more attention. Bi_2WO_6 has been determined to have excellent performance in the solar light mediated systems (Huang et al. 2010; Wang et al. 2011). To our best knowledge, there

are limited studies on photocatalytic degradation of antibiotic norfloxacin using solar light mediated Bi_2WO_6 process. Furthermore, very few data are available concerning the effect of environmental parameters and reaction rationale of the SSL/Bi_2WO_6 system.

In this chapter, solar light mediated Bi_2WO_6 process was investigated in depth by evaluating the degradation of the antibiotic norfloxacin in aqueous solution. The effects of environmental parameters including catalyst dosage, probe concentration, and solution pH on the process performance were investigated systematically. The reaction rationale and related constants were determined using the Langmuir-Hinshelwood (LH) model, combined with the experimental results. To evaluate the practical application potential of the proposed process, in vitro examination of the toxicity of bioassays was conducted on the treated samples.

4.2 Results and Discussion

4.2.1 Norfloxacin decay in different processes

Figure 4-1 displays the decay curves of norfloxacin with or without the presence of Bi_2WO_6. It was observed that Bi_2WO_6 significantly benefits the norfloxacin decay. More than 90% of norfloxacin was decomposed in 30 min under SSL irradiation in the presence of Bi_2WO_6 (SSL/Bi_2WO_6), compared to that of 39% by sole-SSL. After

removal of UV light, no degradation was observed under sole-visible light irradiation, while in the presence of Bi_2WO_6 however 73% of norfloxacin was decomposed (Vis/Bi_2WO_6). It suggests that the process in the presence of Bi_2WO_6 is much superior. The difference of degradation performance between reactions with and without the involvement of Bi_2WO_6 is apparently a result of the photocatalytic ability of Bi_2WO_6.

Since UV and visible light are both involved in the photocatalytic process, it is important to distinguish their contribution to the degradation. All the reactions are found to follow pseudo-first-order kinetics, and the rate constant (k, expressed in units of min^{-1}) of SSL/Bi_2WO_6 (0.076 min^{-1}) is higher than the sum of Vis/Bi_2WO_6 (0.042 min^{-1}) and sole-SSL (0.016 min^{-1}). The difference in rate constant should be ascribed to the Bi_2WO_6 photocatalysis at UV range ($\lambda < 400$ nm). Therefore, the contribution of the sole-SSL, UV/Bi_2WO_6, and Vis/Bi_2WO_6 to the norfloxacin decay can be quantified as 21%, 24%, and 55%, respectively.

4.2.2 Effect of Bi_2WO_6 dosage

The influence of Bi_2WO_6 dosage was investigated and the result was shown in Figure 4-2. It can be seen that the decay rate increases with the increment of Bi_2WO_6 dosage. It is interesting to find that the trend of the pseudo-first-order decay rates can be divided into two stages, in which the rate increases linearly at lower catalyst dosages, then levels

off after a breakpoint dosage of 2 g/L. The linear increase of the rate constant is a result of the proportional increment of the total amount of Bi_2WO_6, which concurrently increases the number of reaction sites for norfloxacin. However, as the catalyst was overdosed, the increase in the opacity of the suspension leads to a blockage of the light penetration (Bansal et al. 2010), thus the shadowed Bi_2WO_6 particles become inert in generating radicals. In another word, the process is gradually transformed from an optical-dilute system into an optical-dense system due to light deficiency as the Bi_2WO_6 dosage increased.

4.2.3 Effect of initial concentration of norfloxacin

The decay of norfloxacin at different norfloxacin intial concentrations ($[Norfloxain]_0$) was studied. As observed in Figure 4-3, The pseudo-first-order rate constant continuously decrease as $[Norfloxacin]_0$ increased from 0.0313 to 0.1565 mM. Almost 90% of norfloxacin is removed at $[Norfloxacin]_0$ = 0.0313 mM after 20 min of reaction, whereas less than 30% is decomposed at $[Norfloxacin]_0$ = 0.1563 mM.

To further analyze the reaction kinetics, a LH kinetics model was employed to examine the heterogeneous photocatalysis reaction. The LH model assumes that the reaction rationale is a rapid Langmiur adsorption achieving equilibrium, and followed by a slower surface reaction on the catalyst surface, which is the rate determining step.

$$\mathbf{A(liquid)} \underset{\mathbf{k_{-1}}}{\overset{\mathbf{k_1}}{\rightleftharpoons}} \mathbf{A(ads)} \xrightarrow[\mathbf{slow}]{\mathbf{k_{LH}}} \mathbf{Products} \quad (4\text{-}1)$$

The concentration of the adsorbed probe on the catalyst surface, A(ads), can be stipulated by a reactant equilibrium coverage (Θ_A) and is calculable when the adsorption/desorption reaching equilibrium (Emeline et al. 2005):

$$_A = \frac{\left(\frac{k_1}{k_{-1}}\right)C_A}{1+\left(\frac{k_1}{k_{-1}}\right)C_A} \quad (4\text{-}2)$$

where C_A is the initial concentration of norfloxacin ([Nrofloxacin]$_0$, mM), and k_1 and k_{-1} are the adsorption and desorption rate constants of norfloxacin on Bi_2WO_6 surface, respectively.

In this study, if the rate limiting step is on the surface, it should approximate the observed pseudo first-order decay rate, so

$$\text{Rate} = k_{LH}\theta_A = kC_A \quad (4\text{-}3)$$

where k_{LH} is the apparent LH rate constant of the slow reaction on the catalyst surface (mM min^{-1}), and k is the observed pseudo first-order rate constant (min^{-1}). The original LH model can therefore be reformulated by incorporating Eqs. 4-2 and 4-3 as Eq. 4-4:

$$k = \frac{k_{LH}K_L}{1+K_LC_A} \quad (4\text{-}4)$$

or in a linearized expression of

$$\frac{1}{k} = \frac{1}{k_{LH}}C_A + \frac{1}{k_{LH}K_L} \quad (4\text{-}5)$$

where K_L (i.e. k_1/k_{-1}) is the equilibrium adsorption constant of norfloxacin on Bi_2WO_6 surface (mM^{-1}) in aqueous system. After plotting 1/k vs. C_A (i.e. [Norfloxacin]$_0$), an

excellent linear correlation with a r^2 of 0.995 was obtained (Figure 4-3, inset), and the K_L and k_{LH} were determined to be 3490 mM^{-1} and 0.0023 mM min^{-1}, respectively. This excellent linear relationship reveals that the LH models fits the SSL/Bi_2WO_6 process well, which suggests that the adsorption is of importance as a prerequisite and the heterogeneous reaction occurs on the Bi_2WO_6 surface is the dominant mechanism. This also agrees with our previous estimation that Bi_2WO_6 photcatalysis (including UV/ Bi_2WO_6 and Vis/ Bi_2WO_6) is major, which contributed 79% of removal efficiency in total.

Plotting K_LC_A vs. 1+ K_LC_A (from Eq. 4-2), a correlation K_LC_A = 0.997 (1+ K_LC_A) was obtained with a r^2 of 0.996 (Figure 4), indicating that at different C_A, the reactant equilibrium coverage (Θ_A, or $K_LC_A/(1+ K_LC_A)$) kept at a constant of 0.997.

Despite the adsorption amount of norfloxacin onto Bi_2WO_6 is negligible (less than 10% of the initial amount from experiment results) compared to the large amount of photocatalytic reaction. The exact adsorbed amounts ($C_{adsorption}$ = adsorbed norfloxacin/suspension volume) at different [Bi_2WO_6] were also recorded in Figure 4-4 as $[Norfloxacin]_0$ = 0.0313 mM. It was founded that the adsorption amount of norfloxacin is linear related to Bi_2WO_6 dosage, presenting an adsorption concentration of 3.17×10^{-3} mmol norfloxacin molecule per gram of Bi_2WO_6. By incorporating with

its Θ_A of 0.997, the maximum adsorption capacity of Bi_2WO_6 (when Θ_A=1) is determined to be 3.20×10^{-3} mmol/g.

In addition, it was interesting to note that after incorporating the resulted K_L and k_{LH} to Eq. 4-5, the first term ($(1/k_{LH})\ C_A$) on the right hand side is found 2 to 3 logs higher than the second term ($1/k_{LH}K_L$), so the Eq. 4-5 can be further simplified by ignoring the second term:

$$kC_A = k_{LH} \quad (4\text{-}6)$$

This finding was verified by comparing the observed initial decay rate of norfloxacin (i.e. kC_A) at different C_A to the k_{LH} of 0.0023 mM min^{-1}, suggesting the assumption of Eq. 4-3 was valid as the Θ_A was close to 1.

4.2.4 Effect of initial pH level

Figure 4-5 demonstrates the influence of the initial pH of probe solution, where the decay rate increased with the increment of pH, and reached an optimal at pH of 10.5, and then it decreased again at extreme basic conditions. The surface charges of norfloxacin and Bi_2WO_6 catalyst are responsible for this observation. Norfloxacin has two relevant ionizable functional groups, the 3-carboxyl group and 4'-amine of the piperazine substituent. The two ionizable groups lead to two ionization constant pK_{a1} (pH = 6.34) and pK_{a2} (pH = 8.75), which corresponds to a proton of dissociation from

the carboxyl group and of combination to 4'-amine in the piperazinyl group, respectively (Hyoung-Ryun Park 2000). As a result, the norfloxacin can be positively charged, negatively charged, and zwitterionic charged as shown in the following Scheme 4-1. In view of the Bi_2WO_6 pH_{pzc} of 5 (Kim et al. 2009), the Bi_2WO_6 is either positively or negatively charged as the solution pH is lower or higher than the pH_{pzc}, respectively.

Under an acidic condition (pH = 3.8), norfloxacin and Bi_2WO_6 are both dominated by positive charge. The electrostatic repulsive effect on like charge restrains the approaching of norfloxacin to Bi_2WO_6 surface, thus the degradation of norfloxacin is retarded. At pH level between pKa_1 and pKa_2 (pH = 6.7), the main species of norfloxacin is the zwitterions (D'Andrea and Di Nicolantonio 2002), which containing a positive and a negative charge concurrently, whereas Bi_2WO_6 is negative charged. The attraction force between positively charged 4'- amine in norfloxacin (Scheme 4-1) and negatively charged Bi_2WO_6 promotes the norfloxacin decay. As the pH level slightly beyond pKa_2 (10.5), optimal norfloxacin decay was observed. That might be due to a higher concentration of hydroxyl anion. It is suggested that hydroxyl anions in photocatalytic reaction is a source of hydroxyl radicals (Mahmoodi et al. 2006). More hydroxyl radicals could be generated at the higher $[OH^-]$. Above the optimal pH, the decay rate was decreased likely due to the repellent effect between negatively charged norfloxacin and Bi_2WO_6.

4.2.5 Determination of inorganic ions and UV-vis absorption spectrum

Figure 4-6 shows the temporal evolution of norfloxacin and inorganic products at predetermined time intervals. To match the detection limits of ion chromatography and increase the profile resolution, $[norfloxacin]_0$ and $[Bi_2WO_6]$ was set at 0.313 mM and 2 g/L, respectively. It was founded that fluoride (F^-) and ammonium (NH_4^+) were gradually accumulated in the process. The F^- apparently comes from the defluoridation at benzene ring. However, the NH_4^+ is not further oxidized to nitrite or nitrate (no NO_2^- or NO_3^- was detected in the ion chromatograph test). This is likely due to lower probability of ammonium in competing with norfloxacin and its daughter intermediates. Another interesting observation resulted from the mass balance is that, at the beginning of reaction (e.g. 2 h), 0.022 mmol of norfloxacin was decomposed, while the accumulated F^- and NH_4^+ were 0.016 mmol only. This difference suggests that most of the F and N atoms are still remained on the molecule of intermediates. At the later stage of the reaction (i.e. 8 h), however, most of the norfloxacin was decomposed and more than 1/3 of the stoichiometric quantity of F^- and NH_4^+ was released to the solution. Because the F^- and NH_4^+ stand for good indicators of mineralization as end products, it suggests that the subsequent decay of intermediates will lead to mineralization of norfloxacin.

UV-vis absorption spectrum is investigated as shown in Figure 4-7, and two peaks around 272 and 330 nm are observed. The shorter wavelength is mainly due to the

aromatic ring absorption, while the longer one is caused by quinolones nitrogen atom with n→π* (HOMO-LUMO) electronic transition (Neugebauer et al. 2005). After degradation, the absorption intensity reduced at 330 nm indicating that the decomposition of germicidal quinoline occurred, while the decreased absorbance at 272 nm suggests the opening of aromatic ring (Chen et al. 2007).

4.2.6 Antibacterial activity assays

Toxicity examination in vitro bioassays has been performed on the treated samples to determine the changes of antibacterial activity via the SSL/Bi_2WO_6 process. E.coli was used as the model microorganism. The original norfloxacin solution presents a great bactericidal performance on E.coli by inhibiting its growth, where the E.coli strains were all killed. At the earlier stage of the treatment process (2 h), the remaining compounds in solution retain a measurable degree of antibacterial activity, in which 60% of E.Coli was survived. Then, the antibacterial ability became insignificant with the E.coli almost intact after 4, 6, and 8 h of treatment. This observation is consistent with the experiment result of UV-Vis absorption spectrum where the decomposition of germicidal quinoline occurred during the process. By integrating the removal efficiency of E.Coli and norfloxacin into Figure 4-8 (Notes: removal efficiency of norfloxacin = 1 - C/Co, and removal efficiency of E.Coli = 1 - [survived E.Coli]/ [initial E.Coli]), it was noticed that a retardation occurs on E.Coli removal at 2 h, where the removal

efficiency of E.Coli is 40% compared to norfloxacin of 75%. It indicates that the primary intermediates formed at earlier stage still retain a measurable degree of antibacterial activity. Then, a quicker drop of E.Coli was observed due to the co-decomposition of norfloxacin and intermediates. After 4 h of reaction, almost all E.Coli were survived because the norfloxacin and germicidal intermediates were degraded to an ineffective level.

4.3 Summary

In the present chapter, the SSL/Bi_2WO_6 photocatalytic process showed an excellent performance in antibiotic norfloxacin decay. The main contribution was ascribed to visible light irradiation, which takes a portion of 55% in norfloxacin decay. The effect of various parameters such as [Bi_2WO_6], $[Norfloxacin]_0$, and initial solution pH on the norfloxacin decay were investigated. The results showed that the decay rate constant linearly increased with the increment of Bi_2WO_6 dosage, then leveled off after a breakpoint. The initial pH level of norfloxacin solution significantly affected the norfloxacin decay, in general, the higher the pH, the faster the decay. At an extreme alkaline condition, the decay was slightly abased. The reaction rationale of the SSL/Bi_2WO_6 was proposed to be a rapid Langmiur adsorption achieving equilibrium, and followed by a slower surface reaction on the catalyst surface. Moreover, the adsorption was verified to promote the reaction and the maximum adsorption capacity

of Bi_2WO_6 was determined to be 3.20×10^{-3} mmol/g. During the reaction, the inorganic ions of NH_4^+ and F^- were gradually accumulated, whereas the germicidal group and benzene ring decomposed simultaneously. In addition, the antibiotic activity of norfloxacin was efficiently removed via the SSL/Bi_2WO_6 process, which was consistent with the decomposition of germicidal group. It was also suggested that the primary intermediates retain a measurable degree of antibacterial activity and these primary intermediates were formed at earlier stage and followed by decomposition.

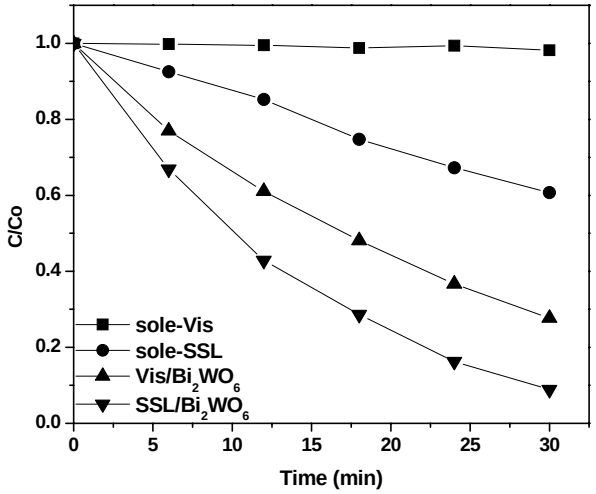

Figure 4-1. Degradation performance at different processes

Experiment conditions: $[Norfloxacin]_0$ = 0.0313 mM, $[Bi_2WO_6]$ = 1 g/L

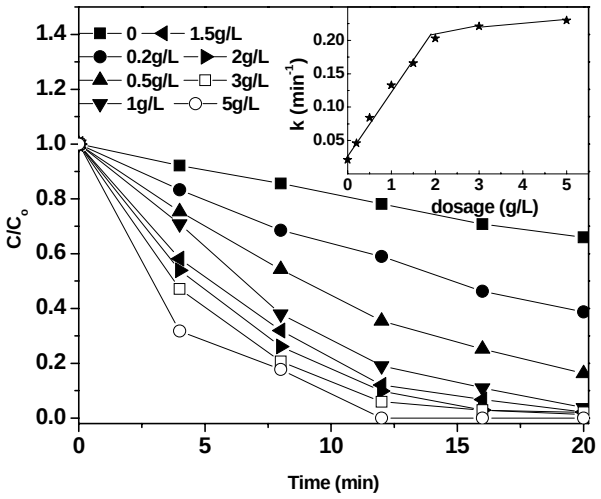

Figure 4-2. Effect of Bi_2WO_6 dosage.

Experiment conditions: $[Norfloxacin]_0$ = 0.0313 mM

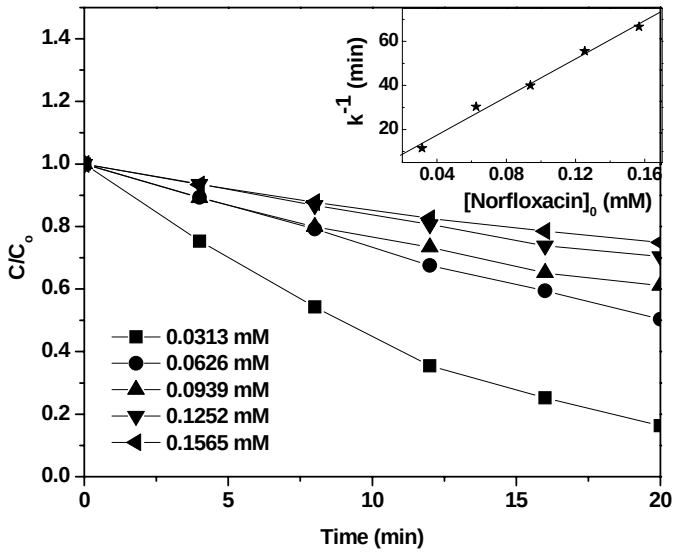

Figure 4-3. Effect of the initial concentration of norfloxacin.

Experiment conditions: [Bi_2WO_6] = 0.5 g/L

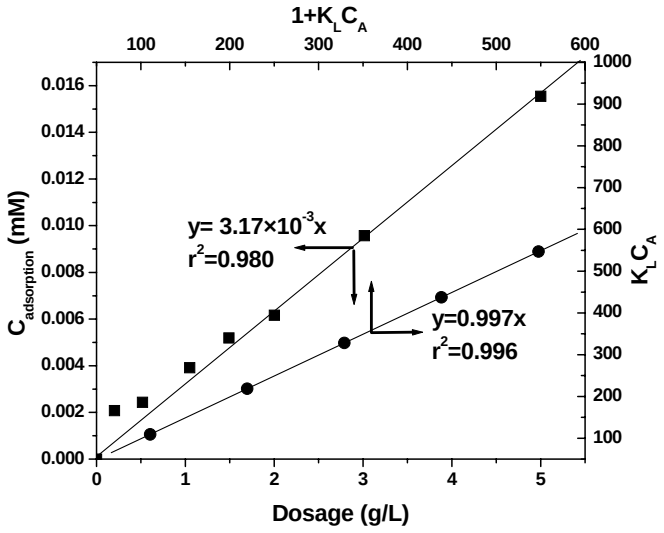

Figure 4-4. $C_{adsorption}$ at different Bi_2WO_6 dosage, and the plot of K_LC_A versus 1+ K_LC_A

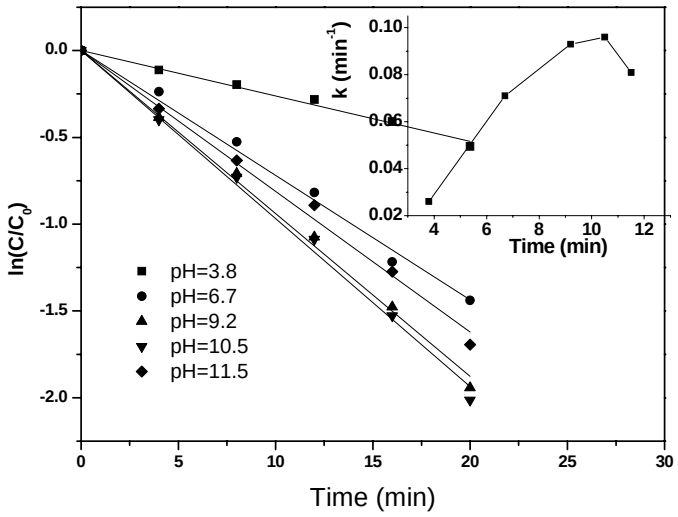

Figure 4-5. Effect of initial pH level.

Experiment conditions: [Norfloxacin]0 = 0.0313 mM, [Bi2WO6] = 0.5 g/L

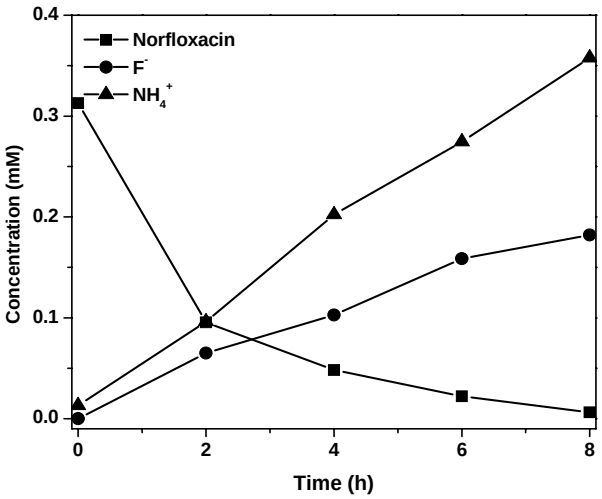

Figure 4-6. Temporal evolution of norfloxacin and inorganic products.

Experiment conditions: $[Norfloxacin]_0$ = 0. 3130 mM, $[Bi_2WO_6]$ = 2 g/L

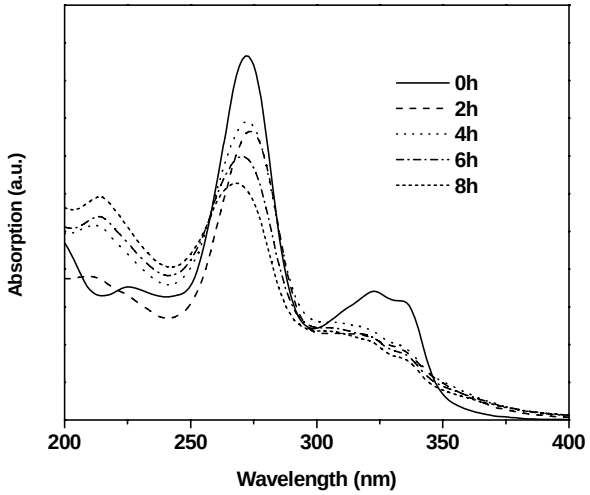

Figure 4-7. UV-vis absorption spectrum.

Experiment conditions: $[Norfloxacin]_0$ = 0. 3130 mM, $[Bi_2WO_6]$ = 2 g/L

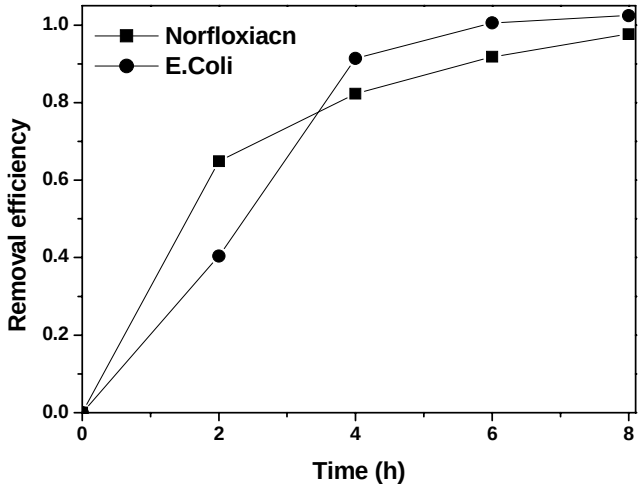

Figure 4-8. Removal efficiency of E.Coli and norfloxacin.

Experiment conditions: $[Norfloxacin]_0$ = 0. 3130 mM, $[Bi_2WO_6]$ = 2 g/L

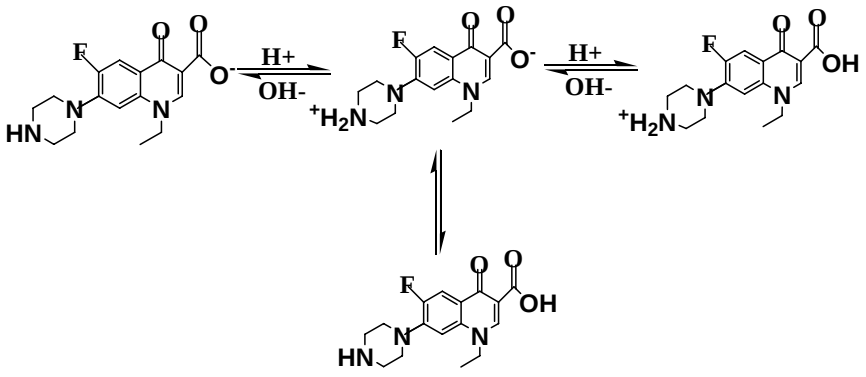

Scheme 4-1. The positively charged, negatively charged, and zwitterionic charged of norfloxacin.

Chapter 5 The Role of Oxidative Species and Reaction Mechanism Study of SSL/Bi_2WO_6 Process for Norfloxacin Decay

5.1 Introduction

Heterogeneous photocatalysis is one of the most studied advanced oxidation processes, and its capability at room temperature and pressure has been widely demonstrated (Chen and Chu 2012a; Linsebigler et al. 1995; Pelaez et al. 2010; Zhang et al. 2012b). In the past decades, the use of TiO_2 as a catalyst for the clean up of environmental organic pollutants through the activation of the UV light has been widely studied. However, TiO_2 can only be excited by UV light with an irradiation wavelength less than 380 nm, leading to a compulsory artificial UV light source for initializing the process (Bamwenda et al. 2001). Concerning about energy conservation, solar light has been considered as a free and abundant source of great potential for new technology. Many researchers have reported non-TiO_2 based photocatalyst with good performance under the solar light irradiation (Ai et al. 2011). Thereinto, Bi_2WO_6 was known as an excellent photocatalyst with higher removal efficiency on organic pollutants, such as dyes (Shang et al. 2008) and bisphenol A (Wang et al. 2010a). Our previous study (Chen and Chu 2012b) has also demonstrated that the SSL/Bi_2WO_6 process is a competitive process for the destruction of antibiotic norfloxacin, as well as its drug property. However, the information regarding the role of oxidative species and reaction mechanism in SSL/Bi_2WO_6 process is still limited, especially in lacking of the degradation route and

the identification of intermediate products, which is critical in achieving effective operational parameters and features for further industrial optimization.

It was well known that the heterogeneous photocatalysis involves a series of chemical reactions, following the initiation step of electron-hole formation. The photoinduced valence band hole could react with adsorbed water or OH^- to produce hydroxyl radical. In the presence of dissolved oxygen, the conduction band electron could be transferred to dioxygen, leading to the generation of other reactive oxygen species such as superoxide radical ($O_2{\cdot}^-$), hydrogen peroxide (H_2O_2) and singlet oxygen ($^1O_2$) in the subsequent reactions. However, the acting oxidative species in heterogeneous photocatalysis may still exist a continuous controversy. For example, most studies agree, in the TiO_2 photocatalysis, hydroxyl radicals are likely the dominant radicals for organic pollutant's degradation (Sun and Bolton 1996); while for the catalyst of Bi_2WO_6, the hydroxyl radicals (Zhu et al. 2007), photogenerated holes (Wang et al. 2010a), and superoxide radicals (Chen et al. 2012) are all been proposed as the key oxidative species in different studies.

In this chapter, the degradation of antibiotic norfloxacin by the SSL/Bi_2WO_6 photocatalysis process was investigated, and the roles of reactive oxidative species in the SSL/Bi_2WO_6 process were evaluated by using appropriate radical scavengers. Based on the speculated oxidative species in the process, the potential influential inorganic

salts that commonly exist in water were further examined. For the study of the reaction mechanism of SSL/Bi_2WO_6 process, the products from norfloxacin degradation were identified and the decay pathways of norfloxacin were thereby proposed.

5.2 Results and Discussion

5.2.1 Effect of radical, hole and electron scavengers

The degradation of norfloxacin in Bi_2WO_6 suspension was illustrated in Figure 5-1. It was noted that 83.7% of norfloxacin was decomposed in 20 min. To clarify the role of oxidative species in this process, the influence of scavengers to hydroxyl radicals, electron, and hole by using methanol (Cho et al. 2004), oxygen (Schwitzgebel et al. 1995), and KI (Palominos et al. 2008), respectively on the norfloxacin decay performance were investigated. As indicated in Figure 5-1, the presence of methanol significant retarded the degradation of norfloxacin, indicating hydroxyl radicals (·OH) play a major role in the decomposition of norfloxacin (from Eq. 5-2), because methanol selectively quenches hydroxyl radicals (Chin et al. 2004). It is also interesting to note that the norfloxacin decay was inhibited in the absent of oxygen (by purging N_2 gas) and by adding KI. Under the oxygen-free condition, photogenerated electrons (e^-) cannot be transferred efficiently (from Eq. 5-3), leading to a higher electron-hole recombination and a lower transformation efficiency of oxidative species. While in the presence of KI, photogenerated holes (h^+) are likely depleted by I^- ions via Eq. 5-4,

thereby the subsequent production of hydroxyl radicals (from Eq. 5-3) was retarded.

$$Bi_2WO_6 \xrightarrow{\text{SSL irradiation}} e^- + h^+ \quad (5\text{-}1)$$

$$H_2O + h^+ \rightarrow \cdot OH + H^+ \quad (5\text{-}2)$$

$$O_2 + e^- \rightarrow O_2^{\cdot -} \quad (5\text{-}3)$$

$$2h^+ + 2I^- \rightarrow I_2 \quad (5\text{-}4)$$

Figure 5-2 showed the norfloxacin decay performance at various [CH_3OH], where higher the [CH_3OH] greater the reduction of the degradation rate. It was interesting to find that the decay performance was level off when [CH_3OH] exceeded 4.8 mM, which indicated the ·OH radicals had been completely exhausted by overdosing methanol. It was noted that the norlfoxacin removal efficiency was decreased from 83.7% to 32.4% after ·OH radicals were completely exhausted. Undoubtedly, the reduction (51.3%) was entirely contributed to the hydroxyl radicals.

It was also deserved to note that the norfloxacin removal efficiency was decreased to 24.8% after I^- was introduced into the SSL/ Bi_2WO_6 system, where the removal efficiency was almost the same to that of direct SSL (24.5%). This phenomenon indicated that the photocatalytic reaction of Bi_2WO_6 was completely inhibited and the Bi_2WO_6 catalyst became talentless as photogenerated h^+ was absent. It also suggested that the superoxide radicals ($O_2^{\cdot -}$) originated from photogenerated electrons as shown in Eq. 5-2 should be a useless oxidant in norfloxacin decay, its role is mainly an electron

carrier to reduce the electron-hole recombination. Furthermore, the decay rate reduction involving hole scavenger I^- was calculated to accounts for 58.9% of norfloxacin removal. In view of the removal efficiency of 51.7% responding to ·OH radicals, it can be deduced that 87.8% photogenerated h^+ have been translated into ·OH radicals for norfloxacin decay via Eq. 5-2. Meanwhile, the left holes should participate in the norfloxacin decay directly. The overall norfloxacin decay therefore can be characterized into photolysis, photocatalysis-via hydroxyl radical, and photocatalysis-via direct hole oxidation, it was calculated that their contribution will be 29.7, 65.5, and 4.8%, respectively. This finding demonstrated that the ·OH radicals played a major role in the SSL/Bi_2WO_6 process for norfloxacin decay.

5.2.2 Effect of inorganic salts

Many studies have reported that the inorganic salts existing in water results in significant influence on the efficiency of pollutants treatment (Guillard et al. 2003; Sökmen and Özkan 2002). Here, the effect of inorganic salts, including selected anions and cations were investigated. Figure 5-3 showed the decay performance of norfloxacin in the presence of anions NO_3^-, HCO_3^-, and SO_4^{2-}, and the results showed that a mild retardation occurred in the presence of SO_4^{2-}, while the anions of NO_3^- and HCO_3^- were inert to the SSL/Bi_2WO_6 process. The sulfate ion was reported to react with hydroxyl radicals (·OH) via Eq. 5-5 (Wang et al. 2000) :

$$SO_4^{2-} + \cdot OH + H^+ \rightarrow \cdot SO_4^- + H_2O \qquad (5\text{-}5)$$

In this reaction, another oxidizing agent sulfate radicals ($\cdot SO_4^-$) are formed as the consumption of ·OH radicals. Sulfate radical is a selective radical and it has a larger molecular structure (than ·OH), which might hinder its chance to react with the probe. In addition, the formation of sulfate radicals and then react with the probe is a two-step process, which in theory will kinetically require longer time to react with the probe than that of hydroxyl radical. Above two mechanisms both result in a mild retardation of norfloxacin decay in the presence of SO_4^{2-}.

The NO_3^- apparently is inert in the process, but the HCO_3^- ion was reported as a ·OH radical scavenger (Eq. 5-6) and frequently restrain photocatalytic reaction in previous literatures (Buxton and Elliot 1986).

$$HCO_3^- + \cdot OH \rightarrow CO_3^{\cdot -} + H_2O \quad (5\text{-}6)$$

However, an imperceptible influence in norfloxacin decay was observed. It was found that the pH level of reaction solution was increased from neutral (6.7) to weak alkaline (9.2) after dosing 10 mM HCO_3^- salt. It has been demonstrated that weak basic pH accelerated the norfloxacin decay in SSL/Bi_2WO_6 process in chapter 4, because the higher [OH^-] improves the formation of ·OH radicals through Eq. 5-2. Therefore, the imperceptible variation in norfloxacin removal is likely due to the joint result of scavenger retardation and raised pH level. In addition, the norfloxacin decay performance in the presence of SO_4^{2-} and HCO_3^- reconfirms the important role of ·OH radicals in the SSL/Bi_2WO_6 process.

The performances of norfloxacin decay in the presence of cations Fe^{3+} and Fe^{2+}) were also evaluated, and the result was shown in Figure 5-4. It can be noted that a dramatic promotion with 95% of norfloxacin removal was achieved in 5 min in the presence of Fe^{3+}, while the process was almost totally terminated in the first 15 min in the presence of Fe^{2+}. It was known that Fe^{3+} is an efficient electron acceptor (Bamwenda et al. 2001), which effectively separate photo-generated electron-hole pairs and increase the yield of photogenerated oxidant species. Besides, it was noted that the solution pH level was changed from neutral to acidic (pH = 3.5) after Fe^{3+} salt was dosed. At acidic condition, $Fe(OH)^{2+}$ is the dominant photoreactive species, which could produce hydroxyl radicals via its photolysis according to the following reaction (Mestankova et al. 2009);

$$Fe(OH)^{2+} \xrightarrow{hv} Fe^{2+} + \cdot OH \qquad (5\text{-}7)$$

Thereby, the hydroxyl radicals generated from the ferric ions photolysis also accelerate the norfloxacin decay.

For the ferrous ions, the retardation in the first 15 min suggests that the Bi_2WO_6 photocatalysis is completely inhibited by the Fe^{2+} ions. This is because the Fe^{2+} is an effective hole scavenger (Eq. 5-8),

$$Fe^{2+} + h^{+} \rightarrow Fe^{3+} \qquad (5\text{-}8)$$

After 15 min, however the norfloxacin started to decompose slowly, it is a good evidence to justify both the proposed Fe^{3+} and Fe^{2+} mechanisms, where the accumulation of enough [Fe^{3+}] in the solution is capable of initiating the accelerated

norfloxacin decay as previously discussed. The almost zero norfloxacin removal in the first 15 min also demonstrated that even the direct photolysis via SSL was null after dosing Fe^{2+} salts, which might be ascribed to the solution pH change to acidic level of 4.2 in such circumstances. Under this pH level, the direct photolysis (via SSL) was found ineffective (data not shown).

5.2.3 Proposed mechanism of norfloxacin decay in SSL/Bi_2WO_6 process

The transformation and/or degradation mechanism of norfloxacin in the proposed SSL/Bi_2WO_6 and SSL processes were investigated. The intermediates were identified on the basis of molecular ions and mass fragment ions detected by MS spectrum. The information of the intermediates including the protonated ion ([M+ H^+]), the proposed molecular structure is summarized in Table 5-1**.** From the structure of intermediates, it was found that the decay of norfloxacin via two process both involves defluorination (Compound 5), decarboxyl acid (Compound 10), and piperazine ring transformation (Compounds 2, 3, 4, 7, 9, 13 and 14). These three routes are consistence with previous studies on fluoroquinolines degradation via direct photolysis (Budai et al. 2008; Sturini et al. 2010) and heterogeneous photocatalysis (An et al. 2010a). 14 intermediates were identified in SSL/Bi_2WO_6 process, while 9 of them were detected in SSL process. To the SSL/Bi_2WO_6 process, the norfloxacin degradation can theoretically be divided into two sub-processes of direct photolysis and Bi_2WO_6 photocatalysis. Consequently, the 5

additional intermediates in SSL/Bi_2WO_6 process could be ascribed to the Bi_2WO_6 photocatalysis, especially the attraction of hydroxyl radicals, since hydroxyl radical was verified to be the main oxidative species in Bi_2WO_6 photocatalysis. This estimation can be verified by the intermediates' structure i.e. compound 2 with m/z of 336 corresponded to the attack of OH to the parent compound, which is obviously resulted from the attraction of hydroxyl radicals. Besides, the 5 intermediates produced from Bi_2WO_6 photocatalysis were also found in An's (An et al. 2010a) previous study in norfloxacin decay by the attack of hydroxyl radicals.

The evolution profiles of intermediates of SSL and SSL/Bi_2WO_6 processes were summarized in Figure 5-5. In the first two hour of SSL process, 34.9, 17.3 and 0.8% of norfloxacin removal was ascribed to piperazine ring transformation, defluorination, and decarboxyl acid, respectively. Meanwhile, a corresponding contribution via SSL/Bi_2WO_6 process was 53.3, 18.1, and 0.9%, respectively. It can be concluded that piperazine ring transformation in both processes is the dominate reaction mechanism. It was also interesting to find that, the Bi_2WO_6 photocatalysis observably promote the piperazine ring transformation, where the transformation efficiency of SSL/Bi_2WO_6 process is 1.53 times higher than that of SSL process, when the promotion impact via defluorination, and decarboxyl acid is minor. This observation demonstrated that the dominate reaction site attracted by hydroxyl radicals is the piperazine of norfloxacin. Furthmore, the norfloxacin removal via piperazine ring transformation was increased by

the reaction time extended, showing a 53.3, 68.8, 77.7 and 89.0% removal efficiency at 2, 4, 6, and 8 hours' reaction through the SSL/Bi_2WO_6 process, respectively, suggesting the hydroxyl radicals continuously react with the piperzine ring during the process. It is also deserved to note that, compound 7 is a major intermediates in both SSL/Bi_2WO_6 and SSL process, and it present a fast increase in the early stage, following by a continuously decrease. However, its concentration in SSL process is much higher than that of SSL/Bi_2WO_6 process. This noticeable accumulation is likely due to the faster decay efficiency of intermediates in SSL/Bi_2WO_6 process. This can also explain the higher accumulation yields of compounds 3, 5, 6, 8 and 11 in the sole SSL process.

Based on the evolution profiles of intermediates and their corresponding chemical structures, the degradation pathways of norfloxaicn by SSL/Bi_2WO_6 process was proposed as illustrated in Figure 5-6. The decomposition of norfloxacin was mainly initiated by the attack of hydroxyl radicals on the piperazinyl substitution leading to the generation of compound 2. Organic product analysis suggests that piperazine ring transformations generally proceed firstly by ring cleavage (compounds 3, 4), followed by loss of the 4'- amine nitrogen (compound 9 and 13), then the 1'- amine nitrogen (compound 14). Besides, defluorination also accompanied with hydroxyl radicals substitution (compounds 5 and 8) or simple direct reduction (compounds 6, 11, 12, 15) through photodehalogenation (Chu et al. 1998; Wang and Chu 2012). In addition, the intermediates compounds also occurs reaction of decarboxyl acid and defluorination.

Mineralization of norfloxacin by SSL/Bi_2WO_6 and SSL processes were quantified by measuring the TOC contents of the solutions. For the SSL/Bi_2WO_6 process, 0.4, 7, 11.9 and 15.5% of TOC was reduced in 2, 4, 6, and 8 h, respectively. In contrast, No TOC reduction was apperceived during the sole-SSL process.

The differences in TOC and aromatic compounds in the presence (SSL/Bi_2WO_6) and absence (sole-SSL) of Bi_2WO_6, suggesting the hydroxyl radical in the SSL/Bi_2WO_6 process is essential to the TOC removal and the cleavage of benzene ring. Besides, the inorganic ions of fluoride and nitrogen were also detected in the SSL/Bi_2WO_6 process, which was reported in our previous literature (Ling et al. 2012). This observation is also confirmed with the decay pathways of defluorination and de-nitrogen in the process. The pH level continuously decreased from 6.8 to 4.5 during the reaction, likely due to the formation of low molecular organic acids and the release of protons (e.g. Eq. 3).

As shown in Figure 4-8, the decay curve of antibacterial activity indicates that the primary intermediates formed at earlier stage (2h) still retain a measurable degree of antibacterial activity. Then, a quicker drop of antibacterial activity (4h) demonstrates the co-decomposition of norfloxacin and intermediates. This trend is fits the development of Compound 7 (Mw 294), suggesting the compound 7 is a toxic intermediate. After 4 h treatment, all the E.coli were survived which demonstrates that the toxicity of norfloxacin and its intermediates has been removed efficiently. This

phenomenon also illuminated that other intermediates (except for compound 7) in the SSL/Bi_2WO_6 process are nontoxic.

5.3 Summary

Hydroxyl radicals are believed to play a major role in the decomposition of norfloxacin in SSL/Bi_2WO_6 process, judging from the norfloxacin decay in the involvement of different scavengers. It was further confirmed by the norfloxaicin decay performance in the present of inorganic ions of SO_4^-, HCO_3^-, Fe^{3+} and Fe^{2+}, and the chemical structure of degradation products as well. It was calculated that the hydroxyl radical responses for 65.5% of norfloxacin removal and the hydroxyl radicals is mainly react on the piperazine of norfloxacin. In the SSL/Bi_2WO_6 process, the norfloxacin decay involves reactions of defluorination, decarboxyl acid, and piperazine ring transformation, where the piperazine ring transformation was processed first by ring cleavage, followed by loss of the 4'- amine nitrogen, then the 1'- amine nitrogen. TOC reduction and the cleavage of aromatic ring were also found in the SSL/Bi_2WO_6 process.

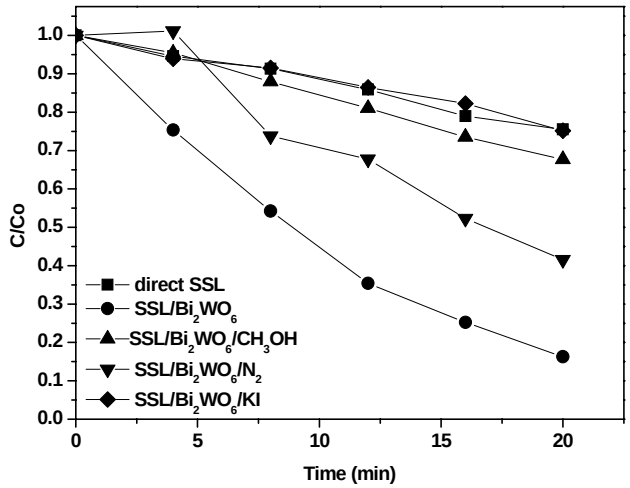

Figure 5-1. Effect of hydroxyl radical, hole and electron scavengers.

Experiment conditions: $[Norfloxacin]_0$ = 0.0313 mM, $[Bi_2WO_6]$ = 0.5 g/L, $[CH_3OH]$ = 4.8 mM, [KI] = 0.1 M

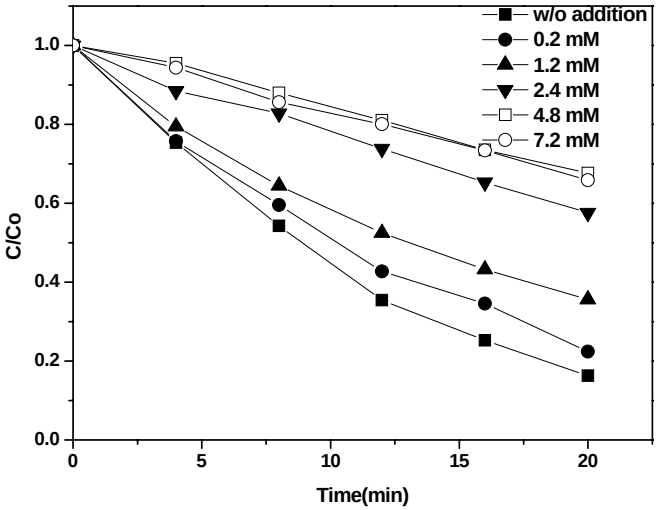

Figure 5-2. Effect of methanol dosage.

Experiment conditions: $[Norfloxacin]_0$ = 0.0313mM, $[Bi_2WO_6]$ = 0.5 g/L

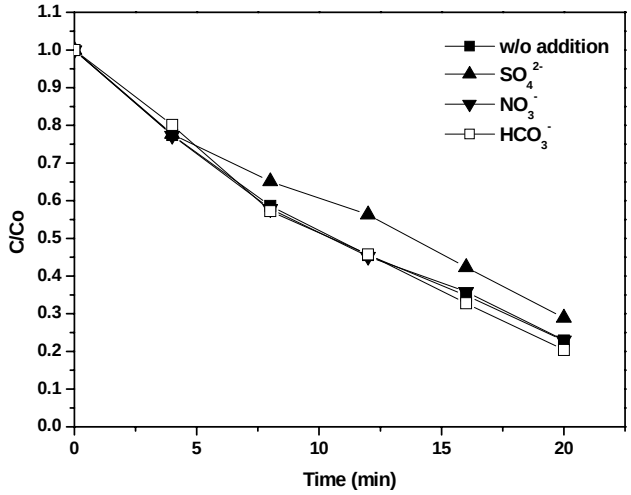

Figure 5-3. Effect of anions.

Experiment conditions: $[Norfloxcin]_0$ = 0.0313 mM, $[Bi_2WO_6]$ = 0.5 g/L. The cations are supplied by sodium salts, and all concentrations are of 10 mM

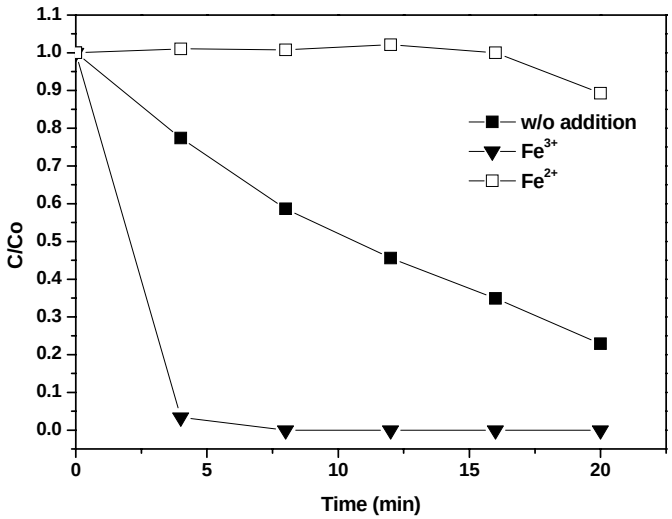

Figure 5-4. Effect of cations.

Experiment conditions: $[Norfloxcin]_0$ = 0.0313 mM, $[Bi_2WO_6]$ = 0.5 g/L.

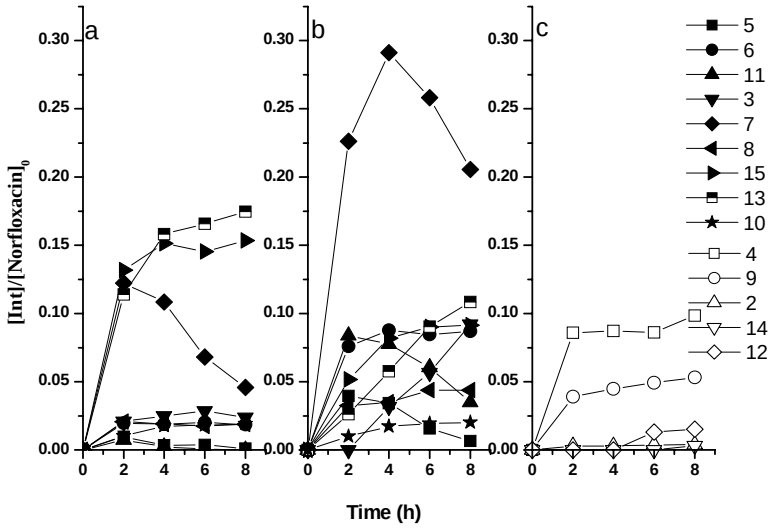

Figure 5-5. Evaluate profiles of processes of SSL/Bi_2WO_6 (a and c) and direct SSL (b).

Experiment conditions: $[Norfloxcin]_0$ = 0. 3130 mM, $[Bi_2WO_6]$ = 2 g/L

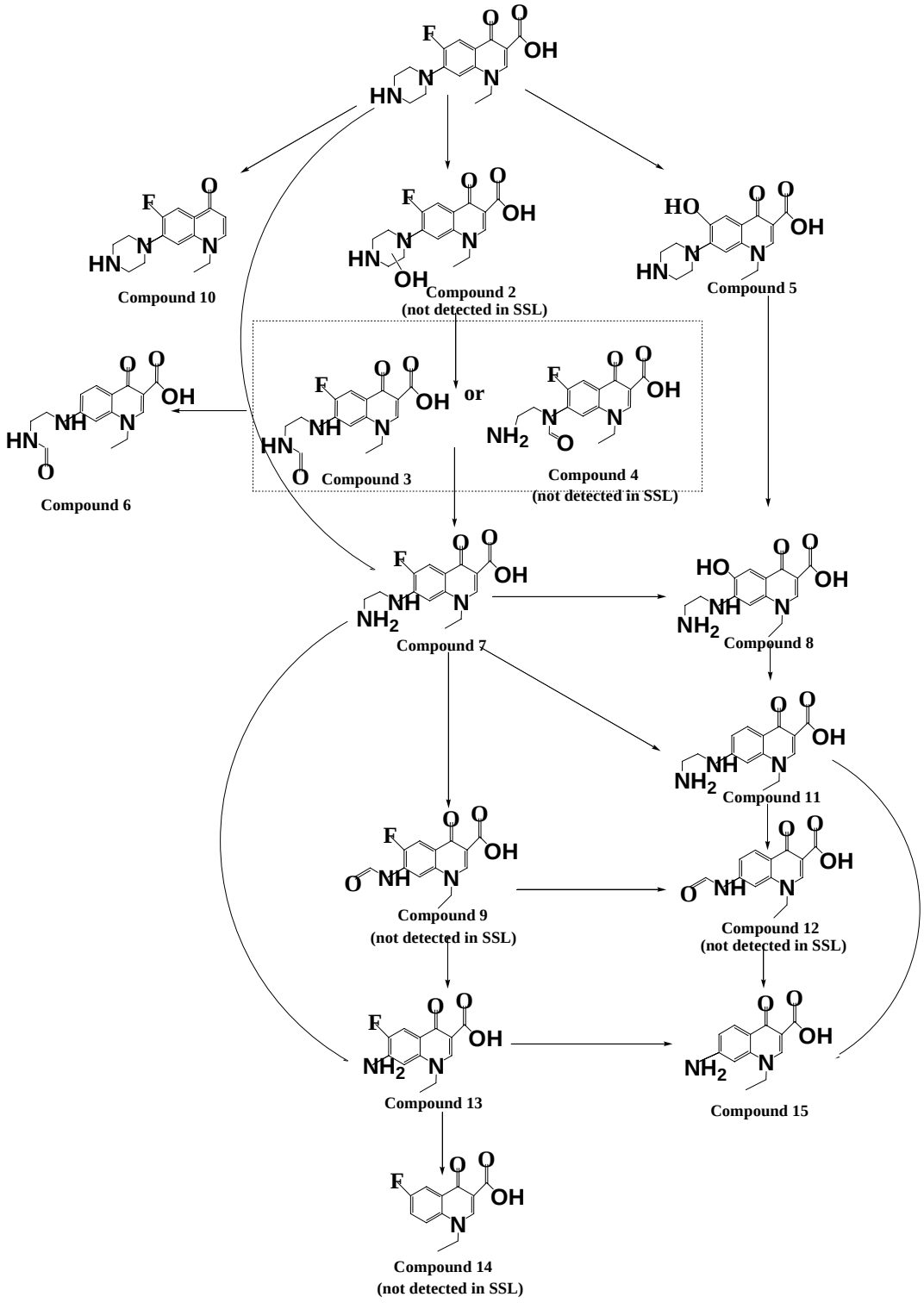

Figure 5-6. Degradation pathway of norfloxacin in SSL/Bi_2WO_6 process.

Table 5-1. Intermediates in the SSL/Bi_2WO_6 process.

Product ID	Molecular ion, [M+ H+]	Proposed Structure	Product ID	Molecular ion, [M+ H+]	Proposed Structure
1	320	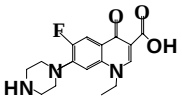	8	292	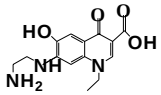
2	336	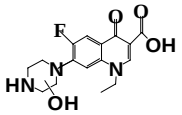	9	279	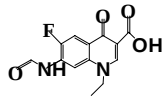
3	322	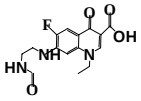	10	276	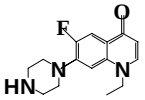
4	322	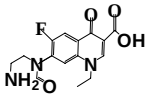	11	261	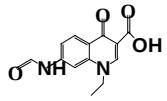
5	318	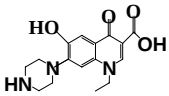	12	251	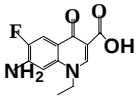
6	304	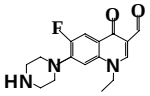	13	236	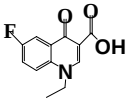
7	294	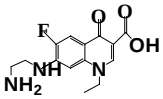	14	233	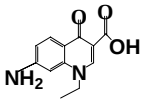

Chapter 6 Exploring a Broadened Operating pH Range for Bi_2WO_6 Photocatalysis

6.1 Introduction

Organic pollutants such as pesticides (Hao et al. 2011), pharmaceuticals (de Jongh et al. 2012), phenols (Zhong et al. 2012), hydrocarbons (Cao et al. 2012), and dyes (Vedrenne et al. 2012) were widely detected in water environment due to their continuing increase of usage and production. Various approaches including biodegradation, adsorption and advanced oxidation processes (AOPs) have been adopted in removing these organic pollutants and minimizing their damage in aquatic environment (Liu and Li 2010; Liu et al. 2013; Namasivayam and Sangreetha 2006; Pophali et al. 2011; Scialdone et al. 2012; Zhu et al. 2008). Among these emerging treatment approaches, AOPs are considered very effective and currently gaining significant attention in water industries (Deng and Ezyske 2011).

In practice, the suitable operating pH levels for most AOPs are normally confined within a narrow pH range. In Dewulf's study (De Witte et al. 2010), the ozonation oxidation performed well at basic pH condition because the ozone can decompose and yield a highly oxidizing species of hydroxyl radicals (·OH) at basic pH level. For the TiO_2 photcatalysis process, the optimum operating pH is reported to be 9.0, where a high level of hydroxyl ions will induce the generation of more ·OH radicals (Chu et al.

2007). It is well known that the photo-Fenton process demands strict acidic pH condition, which limits the operating pH level and restrains the filed application of the photo-Fenton process (Zhao et al. 2012).

To obtain the optimum operating pH level, additional acid or alkali was often used in industry to promote the organic removal (Burbano et al. 2005). However, it is necessary to note that the pH level cannot keep constant throughout the process by considering the formation of low molecule organic acids and carbon dioxide during most of the AOPs. It has been reported in previous literatures that the pH level will continuously decrease during the reaction and eventually the solution pH level will depart from the optimal pH level (Cai et al. 2011; Cao et al. 2005; Rao and Chu 2009). Therefore, the approach with the aim of widening pH sensitivity range for AOP processes will be very useful for promoting the organic pollutants removal, however, such studies are very limited.

Bismuth tanstate (Bi_2WO_6) is known as a promising photocatalyst with higher removal efficiency on organic pollutants and has been utilized in water treatment (Shang et al. 2008; Wang et al. 2010a). One of the advantages of Bi_2WO_6 photocatalysis is its utilization of solar light of a free and abundant source of energy. However, similar to other AOPs, the Bi_2WO_6 still has the problem of limited operating pH range. In Fu's study, the Bi_2WO_6 catalyst showed an optimal performance at neutral pH of 7.0. In addition, the performance dramatically decreased when pH shifted to acidic or basic pH

conditions (Fu et al. 2013b). Our previous work demonstrated that the optimum pH for simulated solar light mediated Bi_2WO_6 photocatalysis is located in the pH range from neutral to slight basic.

In this study, innovative approaches were proposed to expand the operating pH range of Bi_2WO_6 photocatalysis. Norfloxacin was selected as the probe compound and simulated solar light was chosen as light source. The performances of norfloxacin degradation at different pH levels were studied in the proposed SSL/Bi_2WO_6 process in details. To broaden the sensitive pH range, efforts have been carried out to achieve high removal efficiency in wide pH range, including at extreme basic and acidic conditions. At extreme basic pH condition, a buffer system was introduced by using buffer salt; at the extremely acidic pH condition, the SSL/Bi_2WO_6 was improved by dosing ferric salts.

6.2 Result and Discussion

6.2.1 Degradation performance at different pH

The norfloxacin degradation was carried out in different pH levels ranged from 3.0 to 13.0. Unless otherwise specified, the pH levels were all measured from the solution of ready for reaction. The decay curves of norfloxacin were presented in Figure 6-1. It was found that the decay was significantly restrained under extremely acidic (pH 3.0) and alkaline (pH 13.0) conditions. This is due to the electrostatic repulsion between

norfloxacin molecular and Bi_2WO_6 particle surface in view of pKa of norfloxacin (pKa_1 = 6.34, pKa_2 =8.75) and point of zero charge of Bi_2WO_6 (pH = 5.0). As shown in Scheme 6-1, there are three species of norfloxacin (cationic, zwitterionic and anionic) and two phases of Bi_2WO_6 (cationic and anionic divided by pH of 5.0). The moderate pH level (i.e. pH 5.0 to 10.0) is favorable to the norfloxacin decay, showing 90% to 98% removal in 150 min, respectively. In particular, the optimal performance was obtained at the pH of 8.6, which matches the pKa_2 of norfloxacin. In the range of pH 5.0 to 8.6, the norfloxacin removal efficiency was gradually increased from 46% to 93% in 60 min, indicating the higher pH improve the norfloxacin decomposition as long as the surface charges of catalyst and the probe are electrostatic attractive. For the pH level slightly over pKa_2 (i.e. pH at 9.0 and 10.8), a retardation was observed on the norfloxacin decay ascribing to the repulsive force between norfloxacin and Bi_2WO_6, which restricts the approaching of probe to the catalyst surface. Despite the existence of repulsive force is a shortage for norfloxacin removal, it was interesting to find that the removal efficiency at pH of 9.0 is superior to that of 7.5, suggesting the pH level itself has a significant effect on the norfloxacin decay, and it's even more critical than the electrostatic effect in some instances.

6.2.2 pH variation during norfloxacin decay

The pH variations during the pre-adsorption step and the reaction step were monitored

in three different inital pH levels, and the results were shown in Figure 6-2. It was observed that all three runs presented a continuous pH decrease from alkaline (before the adsorption) to weak basic (reaction start), and then to acidic (end of reaction). During the pre-adsorption stage, the pH quickly dropped from 10.0, 9.3 and 8.1 to 8.6, 7.8 and 7.5, respectively. The obvious pH decrease in the pre-adsorption step indicated that the hydroxyl ions in the solution were adsorb (or at least attracted) onto the surface of Bi_2WO_6. This could be critical for the SSL/Bi_2WO_6 process by offering a reservoir of precursors for the formation of hydroxyl radicals in the next (reaction) step. A OH^- enriched model was proposed to describe this property of Bi_2WO_6 at this stage as shown in Scheme 6-1, where the hydroxyl ions is inclined to adhere and concentrate onto the surrounding of Bi_2WO_6 surface. After the reaction begin (by turning on the light source), the pH level continuously reduced at a lower rate, suggesting the hydroxyl ions in the solution were gradually consumed in the degradation process likely due to the formation of low molecule organic acids and carbon dioxide.

Considering the pH decrease during the SSL/Bi_2WO_6 process, it can also be deduced that the norfloxacin decay rate might be gradually hindered if the pH level is shifted to an unfavorable range. It was known that only the hydroxyl ions closing to the Bi_2WO_6 surface can be the source of active hydroxyl radicals due to the limited lifetime of photo-generated hole (Fox and Dulay 1993). Therefore, to maintain a higher concentration of hydroxyl ions nearby or on the Bi_2WO_6 surface should be a critical

approach to improve or maintain a faster probe decomposition.

6.2.3 Effect of magnesium and calcium ions

To verify the proposed OH^- enriched model, the norfloxacin decay in the presence of calcium and magnesium salts were investigated in view of their similar chemical property and the big difference in the ability of capturing hydroxyl ions. The K_{sp} (solubility product constant) of $Mg(OH)_2$ and $Ca(OH)_2$ are 1.5×10^{-11} and 0.166, respectively. Thereby, it can be deduced that the magnesium ions have the priority to deplete the hydroxyl ions and generate magnesium hydroxide at a lower $[OH^-]$. A presumption is that once the metal salt dosages are designed properly, the hydroxyl ions originally concentrated on the Bi_2WO_6 surface (see the OH^- enriched model) could be grabbed away by the magnesium ion, and resulted in a deficiency of the hydroxyl ions (on catalyst surface) for hydroxyl radical generation; but the same procedure would not work for the calcium salt due to its lower K_{sp}. The detailed investigations were carried out by varying the $[Ca^{2+}]$ and $[Mg^{2+}]$ from 0 to 40 mM, and the results were shown in Figure 6-3. The calcium ions displayed no correlation with the norfloxacin degradation even when the $[Ca^{2+}]$ increased to 40 mM. However, the magnesium showed a significant retardation in norfloxacin decay. It was found that a higher $[Mg^{2+}]$ leads to a slower the norfloxacin decay. The remaining norfloxcin after 20 min of degradation was determined to be 22.9, 29.0, 31.9, 38.3, and 42.1% in the $[Mg^{2+}]$ of 0, 10, 20, 30 and 40

mM, respectively. The experimental results are quite encouraging and support the assumption that the concentration of hydroxyl ions surrounding Bi_2WO_6 is at an equivalent level to produce $Mg(OH)_2$ but not enough for the formation of $Ca(OH)_2$. This evidence justifies the inhibition effect of norfloxaicn decay in the presence of magnesium salt but inert to the calcium salt; and also validates the proposed OH^- enriched model in Scheme 6-1. As described in the OH^- enriched model, the hydroxyl ions are adsorbed on the Bi_2WO_6 surface to form a thin layer of concentrated [OH^-], which is high enough to form $Mg(OH)_2$ but too low to form $Ca(OH)_2$. It can therefore be calculated that the hydroxyl ions concentration in the thin layer surrounding Bi_2WO_6 should be between 3.87×10^{-4} M and 2.03 M in the tests based on the K_{sp} at 10 mM magnesium and 40 mM calcium salts, respectively.

In addition, it was observed that the pre-adsorption capacity of norfloxacin was interfered in the presence of Mg^{2+}, and the pre-adsorbed norfloxacin level decreased with the increase of [Mg^{2+}]; where the pre-adsorption efficiency of norfloxacin was 7.1, 6.2, 4.8, and 2.7% at [Mg^{2+}] of 0, 10, 20, 30 and 40 mM, respectively. The variation on the pre-adsorption efficiency should also be ascribed to the formation of magnesium hydroxides nearby the Bi_2WO_6 surface, which left fewer adsorption sites available for the adsorption of norfloxacin and blocked the pathway for the diffusion of norfloxacin to the catalyst surface. In the presence of Ca^{2+} ions, however, no pre-adsorption variation was observed at all the tested, because the surface property of Bi_2WO_6 surface

as shown in the OH^- enriched model was not changed even when the [Ca^{2+}] increased from 0 to 40 mM. The pre-adsorption variation phenomena in the presence of Mg^{2+} but not Ca^{2+} can further justify the proposed OH^- enriched model.

6.2.4 Explore norfloxacin decay at extremely basic pH level (pH > 9.0)

The norfloxacin decay at extreme basic pH condition was seriously retarded as shown in Figure 6-4. At pH 13.0, only 22.0% of norfloxacin was removal after 150 min. Considering the hydroxyl ion is the source of the active radical ·OH, the NH_4Cl salt was gradually added into the reaction solution to decrease the pH to 9.0 by forming a buffer system. Different to the pH adjustment by adding acid, the buffer system has a higher capacity of hydroxyl ions. Under this circumstance, the norfloxacin decay was significantly improved with over 97.0% of norfloxacin removal in 60 min, revealing the pH adjustment by preparing buffer system at extremely basic condition is a practicable method for the SSL/Bi_2WO_6 process.

A comparison experiment was also carried out at pH 9.0 by pH adjustment with HCl (non-buffer system). As shown in Figure 6-4, the norfloxacin decay in this non-buffer system is different to buffer system despite they possessed the same intial pH level. The non-buffer system showed a 93.2% of norfloxacin removal in 150 min, which is 3.8% less than that of buffer system. The comparison of two processes can be divided into

three stages: (1) the first stage (0−10 min), where the decay curves of the two processes were completely overlapped; (2) the second stage (10-20 min), where the norfloxacin removal in the buffer system was slightly slower than that in the non-buffer system; (3) the third stage (20 - 150 min), where the buffer system showed a faster decomposition rate throughout this stage. In the first stage, the same initial pH level resulted in the same removal efficiency. The differences in the later two stages should be ascribed to the different pH variation trends in the two processes. It was noted that the pH level was gradually decreased to 8.8, 8.3 and 7.0 in the non-buffer system at the reaction time of 10, 20 and 150 min, respectively; while the pH was kept at a constant in the buffer system. As mentioned previously, the optimal pH for norfloxacin decay was pH 8.6, which is embedded in the second stage of non-buffer system, leading to better norfloxacin removal efficiency. In the third stage, however, the pH level of the non-buffer process gradually decrease and away from the optimum range.

In addition, the TOC removal was also investigated in the two processes as illuminated in Figure 6-5. Both buffer and non-buffer system showed obvious TOC removal while the TOC decrease at their original pH 13.0 was imperceptible. It was found that the TOC removal in buffer system was much superior, which shows a 20.8% higher than non-buffer system in 150 min. Compared to the 3.8% difference in norfloxacin removal, the bigger difference in TOC removal apparently results from more intermediates mineralization in the buffer system. Therefore, at extremely basic condition, the pH

adjustment using a buffer system is much better than that of using acid, because the former continuously supply higher dosage of hydroxyl ion and therefore benefits the intermediate decomposition and mineralization.

6.2.5 Explore norfloxacin decay at extreme acidic pH level (pH < 5.0)

The norfloxacin decay at extremely acidic condition (i.e. pH 4.0) was explored by dosing ferric salt into the SSL/Bi_2WO_6 process (SSL/Fe^{3+}/Bi_2WO_6). The decay curve was shown in Figure 6-6. As a comparison, the norfloxacin decay via the SSL/Fe^{3+} (simulated solar light irradiated ferric salt) and SSL/Bi_2WO_6 were also investigated under the same conditions. It was found that the SSL/Fe^{3+}/Bi_2WO_6 process showed a much better performance over others, showing a 75.3% of norfloxacin decay in 20 min; while the SSL/Fe^{3+} and SSL/Bi_2WO_6 process shows the decay performance of 44.2% and 42.4%, respectively. The mechanism of norfloxacin decay in the SSL/Fe^{3+} process can be rational by the property of ferric ion. The ferric ion was proven to be an oxidant reagent under the UV light irradiation (200-400 nm) at acidic condition (Měšťánková et al. 2009). In the acidic aqueous solution, Fe^{3+} undergoes spontaneous-hydrolysis with water to form a species of $Fe^{III}OH^{2+}$, which is a photosensitive species, and such a complex is capable of producing hydroxyl radicals directly through photo-sensitization reaction:

$$Fe^{III}(OH)^{2+} + \quad hv \rightarrow Fe^{2+} + \cdot OH \qquad (6\text{-}1)$$

Under the acidic pH condition, the small part of UV light in the simulated solar light ignites the photo-sensitization reaction, and thereby results in norfloxacin decay in the SSL/Fe^{3+} process. Therefore, the better performance of SSL/Fe^{3+}/Bi_2WO_6 process should be ascribed to its combining the advantages of both homogeneous SSL/Fe^{3+} and heterogeneous SSL/Bi_2WO_6. Furthermore, the electron (e^-) transfer carrier's role of Fe^{3+} should contribute to a portion of norfloxacin decay due to its effective decrease the electron-hole combination via Eq. 6-2 (Bamwenda et al. 2001):

$$Fe^{3+} + e^- \rightarrow Fe^{2+} \quad (6\text{-}2)$$

In addition, the reaction interface of the heterogeneous SSL/Bi_2WO_6 process should be changed in the presence of $Fe^{III}OH^{2+}$. Under the acidic pH condition, the positive charged $Fe^{III}OH^{2+}$ species is easily approachable to the Bi_2WO_6 surface and form a $Fe^{III}OH^{2+}$ enriched model as illuminated in Scheme 6-1. Since the hydroxyl ion in the $Fe^{III}OH^{2+}$ is very close to the Bi_2WO_6 surface in the $Fe^{III}OH^{2+}$ enriched model, the limitation of the short lifetime of photo-generated hole can be technically diminished, which is beneficial to the subsequent generation of active radical ·OH.

6.2.6 Effect of [Fe^{3+}] in the SSL/Fe^{3+}/Bi_2WO_6 process

Figure 6-7 showed the effect of the [Fe^{3+}] on the norfloxacin decay in the SSL/Fe^{3+}/Bi_2WO_6 process under pH level of 3.0. After 20 min of reaction, the removal efficiency at [Fe^{3+}] of 0.1, 0.2, 0.3 and 0.5 mM was 23.6, 71.0, 86.2, and 88.0%, respectively. As illuminated in the insert of Figure 6-7, the effect of [Fe^{3+}] was

significant in changing the decay rate of norfloxacin, where the decay rate increased with the increment of [Fe^{3+}], and then leveled off after a break point of dosage of 0.3 mM. As described previously, the $Fe^{III}OH^{2+}$ species is critical for the norfloxacin decay in the SSL/Fe^{3+}/Bi_2WO_6 process. Higher [Fe^{3+}] provide a larger amount of $Fe^{III}OH^{2+}$ for hydroxyl radical generation (see Eq. 6-2). However, if Fe^{3+} is overdosed, an excess amount of ·OH radicals will be derived from Eq. 6-2 and results in the self-reaction of ·OH radicals (Lindsey and Tarr 2000). Therefore, the unlimited increase in [Fe^{3+}] is not suggested in real operation.

6.2.7 The optimum operating pH in SSL/Fe^{3+}/Bi_2WO_6 process

To determine the best pH level for norfloxacin decay in the SSL/Fe^{3+}/Bi_2WO_6 process, the decay performance at different acid pH level was investigated. Figure 6-8 showed that about 82.0, 86.0 and 78.3% of norfloxacin was decomposed at the pH level of 2.0, 3.0 and 4.0 in 20 min, respectively. The optimum pH level for norfloxacin decay was pH 3.0. Above or below this pH level, the process performance reduced. In an aqueous solution, Fe^{3+} undergoes spontaneous-hydrolysis with water to form four species Fe(III)-hydroxo complexes of $Fe^{III}OH^{2+}$, $Fe^{III}(OH)_2^{+}$, $Fe^{III}{}_2(OH)_2^{4+}$, and $Fe^{III}(OH)_3^{0}$ (Martin et al. 1998). At the investigated pH level of 3.0, the predominant species is the monohydroxy complex, $Fe^{III}OH^{2+}$, which is the most photosensitive species of the four (Flynn 1984). The decrease of norfloxacin removal efficiency at pH 4.0 is most likely

attributed to the formation of $Fe^{III}(OH)_3^0$ (Ensing et al. 2003), which results in a decrease of [$Fe^{III}OH^{2+}$] in the solution. On the other hand, norfloxacin removal performance also dropped when the initial pH decreased to pH 2.0. This can be rationalized by two mechanisms. First, the hydrolysis of ferric ions at the pH 2.0 was restrained leading to a low generation of $Fe^{III}OH^{2+}$ (Flynn 1984). Second, the norfloxacin carried much more positive charges at lower pH level, resulting in a strong electrostatic repulsion between Bi_2WO_6 and norfloxacin molecules, which has a negative impact on the removal efficiency.

In addition, [Fe^{3+}] has a significant influence on SSL/Bi_2WO_6/Fe^{3+} process, where the removal efficiency showed a great improvement of 89.7% by varying [Fe^{3+}]. However, the pH change from 2-4 only brought 12.6% variation in removal efficiency. As a result, The [Fe^{3+}] is the key performance indicator for SSL/Bi_2WO_6/Fe^{3+} process; the small differences in norfloxacin removal efficiency demonstrated that the pH level presented a minor effect on the SSL/Fe^{3+}/Bi_2WO_6 process. Therefore, the SSL/Fe^{3+}/Bi_2WO_6 process can be used in a wide acidic pH range.

6.3 Summary

In this chapter, the SSL/Bi_2WO_6 process was employed to decay antibiotic norfloxacin. The pH level has a great influence on the performance of this process. In general, it shows a good performance at a narrow pH range from 5.0 to 9.0 in this study. An OH^-

enriched Bi_2WO_6 model (as shown in Scheme 6-1) was first proposed and verified by designed experiments by dosing of Mg^{2+} and Ca^{2+}. In order to broaden the sensitive pH range of the SSL/Bi_2WO_6 process, different modifications of the original approach were studied. At extreme basic pH condition, a buffer system was successfully introduced by using buffer salt, which demonstrated an excellent norfloxacin decomposition and TOC removal at high pH level. Furthermore, the buffer system is superior to the non-buffer system because the former continuously supplies and maintains high level of hydroxyl ion for the following radical generation. At the extremely acidic pH condition, the SSL/Bi_2WO_6 was significantly improved by dosing ferric salts (i.e. forming an alternative SSL/Fe^{3+}/Bi_2WO_6 process), in which a homogeneous photo-sensitization mechanism offered by SSL/Fe^{3+} was triggered, meanwhile the Fe^{3+} plays as an electron transfer carrier for Bi_2WO_6 photocatalysis is minor. It is believed that the interfacial property on Bi_2WO_6 surface has been changed, which can be explained by the proposed $Fe^{III}OH^{2+}$ enriched model with a positive charged surface. The best operational pH for the SSL/Fe^{3+}/Bi_2WO_6 process was 3. 0, and the decay rate increased with the increment of [Fe^{3+}] then leveled off when the ferric was overdosed.

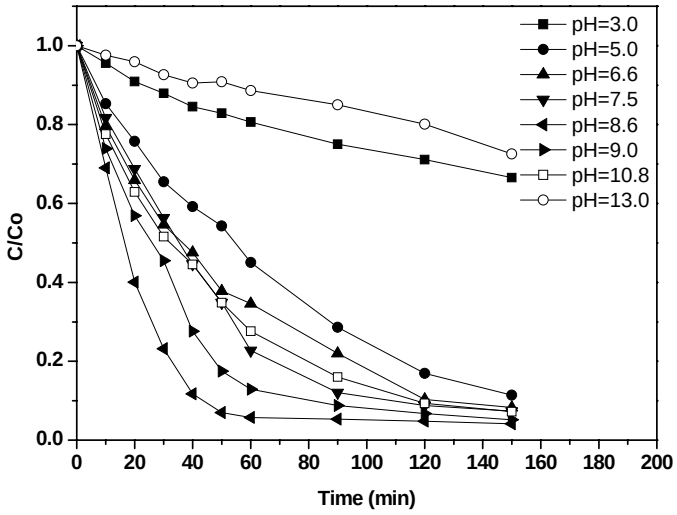

Figure 6-1. Effect of pH level.

Experiment condition: [Norfloxacin] = 0.1 mM, [Bi_2WO_6] = 1g/L

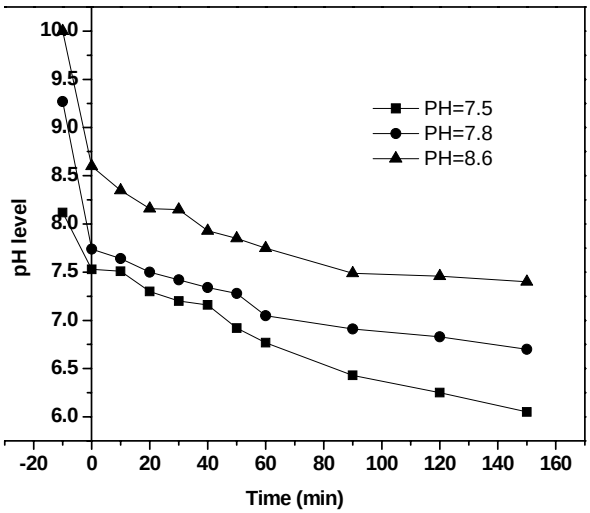

Figure 6-2. pH variation during the SSL/Bi_2WO_6 process.

Experiment condition: [Norfloxacin] = 0.1 mM, [Bi_2WO_6] = 1g/L

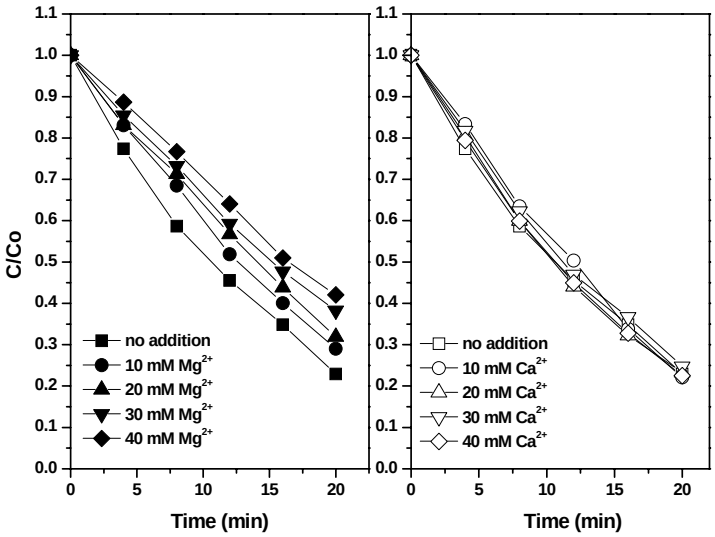

Figure 6-3. Effect of Ca^{2+} and Mg^{2+}.

Experiment conditions: [Norfloxacin] = 0.0313 mM, [Bi_2WO_6] = 0.5 g/L

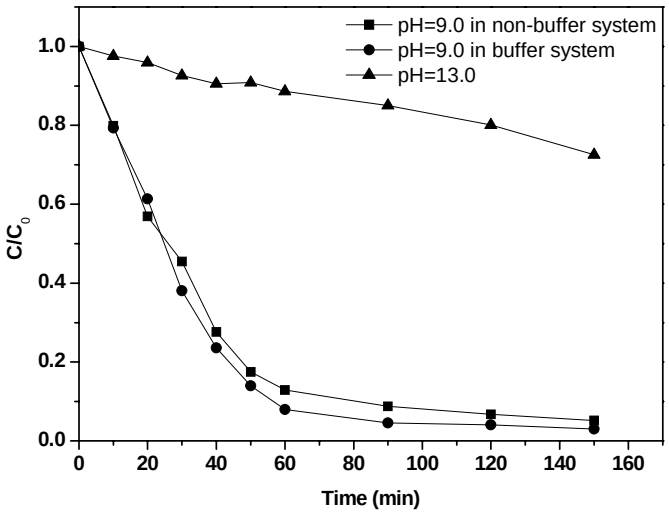

Figure 6-4. Norfloxacin decay at extreme basic conditions

Experiment condition: [Norfloxacin] = 0.1 mM, [Bi_2WO_6] = 1g/L

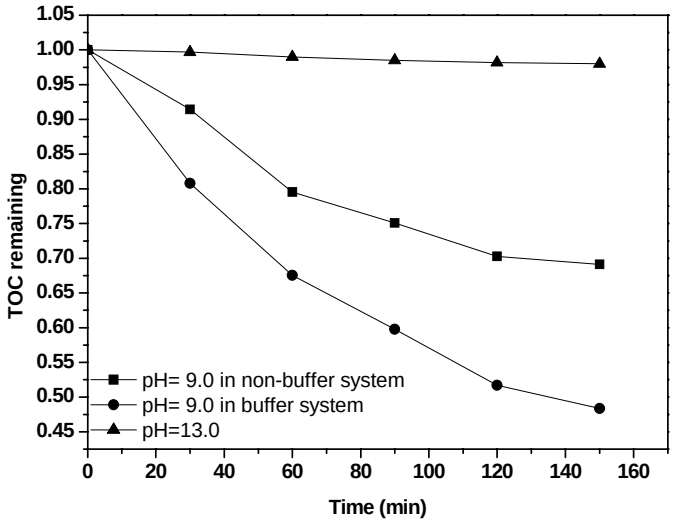

Figure 6-5. TOC removal at extreme basic conditions

Experiment condition: [Norfloxacin] = 0.1 mM, [Bi_2WO_6] = 1g/L

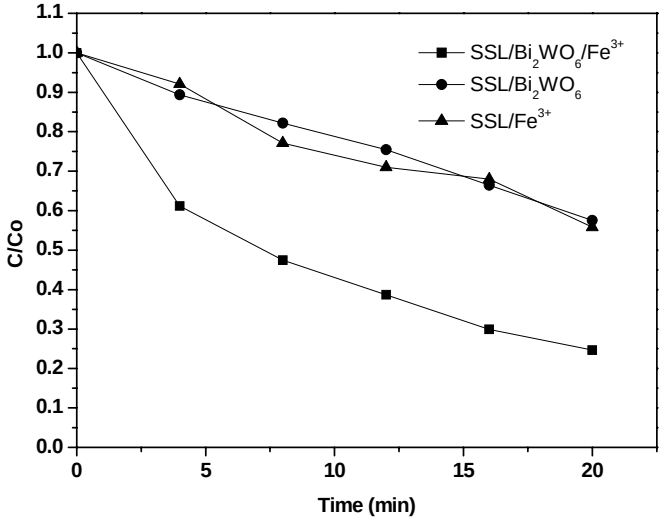

Figure 6-6. Norfloxacin decay in different processes at pH = 4.0.

Experiment conditions: [Norfloxacin] = 0.0313 mM, [Bi_2WO_6] = 0.5g/L, [Fe^{3+}] = 0.3 mM

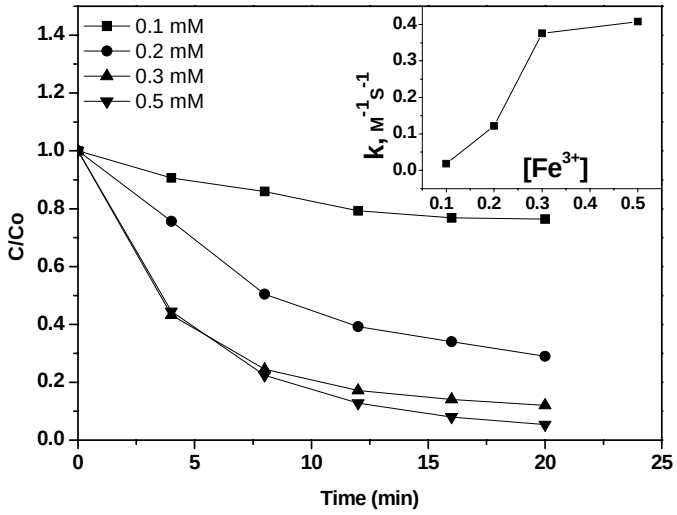

Figure 6-7. Norfloxacin decay at different $[Fe^{3+}]$ at pH =3.

Experiment conditions: [Norfloxacin] = 0.0313 mg/L, $[Bi_2WO_6]$ =0.5g/L.

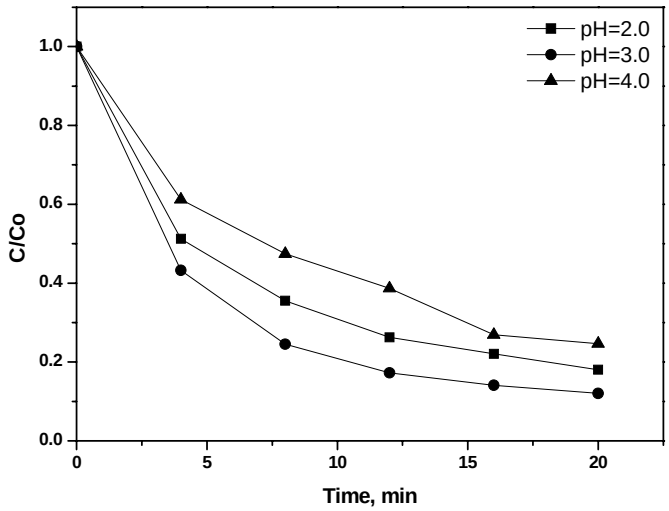

Figure 6-8. Norfloxacin decay at different acidic pH levels.

Experiment conditions: [Norfloxacin] = 0.0313 mg/L, $[Bi_2WO_6]$ = 0.5g/L, $[Fe^{3+}]$ = 0.3 mM

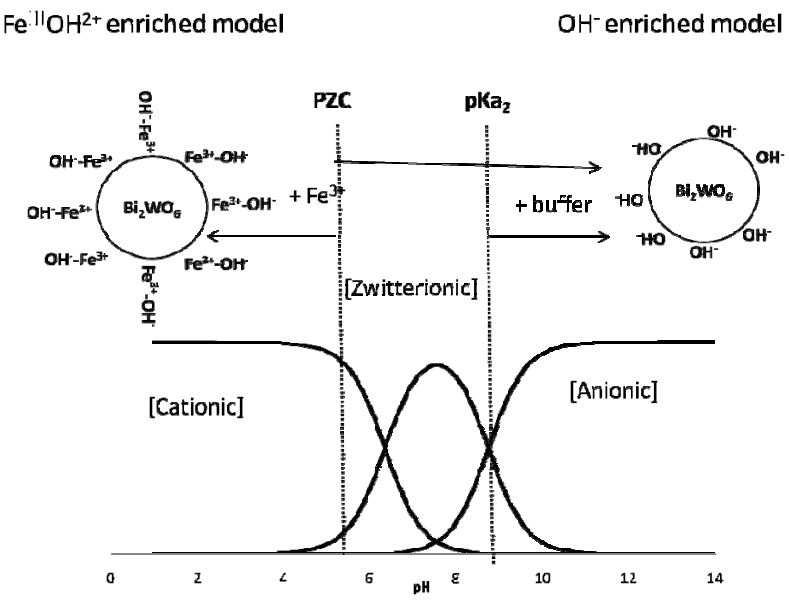

Scheme 6-1. Interface property at different pH levels.

Chapter 7 Hydrogen Peroxide Assisted Degradation of Antibiotic Norfloxacin by Simulated Solar Light Mediated Bi_2WO_6 process: Modeling and Reaction Mechanism

7.1 Introduction

In recent years, the complex oxides Bi_2WO_6 was found to display excellent photocatalytic efficiency to many contaminants with the irradiation of solar light because their catalytic activities appear in both UV and/or visible light irradiation (Zhang et al. 2011). However, its application is still imperfect due to the high electron-hole recombination rate after excitation. To improve the photoactivity of Bi_2WO_6, most studies are focused on developing different synthesis techniques to (1) produce different morphologies with high surface area, such as nest-like (Zhu et al. 2012) and flower-like (Zhang et al. 2007) Bi_2WO_6, or (2) make composite photocatalyst by doping a certain amount of metal or nonmetal elements into Bi_2WO_6 to improve the migration efficiency of photogenerated electrons and suppress the recombination of electrons and holes effectively (Fu et al. 2013a; Liu et al. 2011b).

Other than the modification of the synthetic techniques, the hybrid system in combining the inorganic oxidants and photocatalysis has provided an efficient way to promote the photo-genrated holes' reaction by decreasing electron–hole recombination (Selvam et al.

2007). Inorganic oxidants such as H_2O_2 (Zhang et al. 2013), IO_4^- (Wang and Hong 1999) and $S_2O_8^{2-}$ (Hazime et al. 2013) has been reported to have significant rate-enhancing effect on contamination removal in UV/TiO_2 process. However, the study regarding the incorporation of such oxidants to the Bi_2WO_6 photocatalysis still very limited.

Generally, small portions of antibiotics are metabolized in the human and animal bodies; most of them are excreted unchanged and end up in the wastewater. The amounts excreted can be up to 90% of an administered dose of antibiotics (Jia et al. 2012). As a result, the unutilized portion of the antibiotics enters into the municipal sewage treatment systems where they can be adsorbed to sludge. Consequently, the antibiotics ingredients, including their metabolites and conjugates, can reach the terrestrial environment when the sewage sludge and manure are used as agricultural fertilizers.

Norfloxacin is a second generation of fluoroquinolone occasionally used to treat common as well as complicated urinary tract infections. It has been widely detected in sewage treatment plant effluents (Liu et al. 2012), surface water (Peng et al. 2012a), seawater (Tan et al. 2013), groundwater (Fick et al. 2009) and drinking water (Wammer et al. 2013). The presence of norfloxacin has reported to interfere with bacterial DNA replication, be toxic to plants and aquatic organisms (Yang et al. 2008), and contribute to a large proportion of measured bacterial genotoxicity (Larsson et al. 2007). It is therefore necessary to explore effective treatment methods for removing these

contaminants before discharging them back to the environment.

In this chapter, the objective is to investigate the norfloxacin degradation by the simulated solar-light-mediated Bi_2WO_6 process with the assistant of H_2O_2 ($SSL/Bi_2WO_6/H_2O_2$). The reaction kinetics in the process under various conditions, including norfloxacin concentration, H_2O_2 and Bi_2WO_6 dosage were examined. Mathematic models were derived for the prediction of norfloxacin degradation in $SSL/Bi_2WO_6/H_2O_2$ process in view of H_2O_2 and Bi_2WO_6 dosage, as well as norfloxacin concentration. Moreover, the decomposed aromatic intermediates were detected by LC/MS and the degradation pathway of norfloxacin in the $SSL/Bi_2WO_6/H_2O_2$ process was thereby proposed.

7.2. Results and Discussion

7.2.1 Comparative study of different processes

To study the $SSL/Bi_2WO_6/H_2O_2$ process for norfloxacin degradation, a set of experiments with initial norfloxacin concentration ($[Norfloxacin]_0$) of 10 $mg \cdot L^{-1}$ were carried out, including SSL, SSL/H_2O_2 (H_2O_2 irradiated by simulated solar light), SSL/Bi_2WO_6, and $SSL/Bi_2WO_6/H_2O_2$ process. The results were shown in Figure 7-1. It can be seen that the direct SSL photolysis was weak, while the use of H_2O_2 (i.e. SSL/H_2O_2) and Bi_2WO_6(i.e. SSL/Bi_2WO_6) could significantly improve the norfloxacin

decay in the respective process. The better performance of SSL/Bi_2WO_6 process (over SSL) can be rationalized by the involvement of Bi_2WO_6 can produce hydroxyl radical under the irradiation of simulated solar light (Zhang et al. 2010). For the SSL/H_2O_2 process, its higher norfloxacin removal efficiency than SSL should be ascribed to the H_2O_2 photolysis under the irradiation of UV light (λ< 400 nm) (Matilainen and Sillanpää 2010). The mechanism accepted for the photolysis of H_2O_2 is the cleavage of the molecule into hydroxyl radicals with a quantum yield of two OH· radicals formed per quantum of radiation absorbed, according to the following reaction (Eq. 7-1):

$$H_2O_2 \overset{h\nu}{\rightarrow} 2 \cdot OH \ (\lambda < 400nm) \qquad (7\text{-}1)$$

To verify this, the visible light (i.e. SSL with a 400 nm cut filter) was used as the light source and the norfloxacin was proven inert to the Vis/H_2O_2 process (H_2O_2 photolysis under the visible light irradiation, see in Figure 7-S1). Undoubtedly, the SSL/Bi_2WO_6/H_2O_2 process leads to the highest norfloxacin efficiency among these processes through merging the advantages of H_2O_2 photo-decomposition and the Bi_2WO_6 photocatalysis together.

It was also interesting to find that the norfloxacin decay in the Vis/Bi_2WO_6 (visible light irradiated Bi_2WO_6 photocatalysis) is slightly improved by the involvement of H_2O_2 (Vis/Bi_2WO_6/H_2O_2, see in Figure 7-S1). The improvement should be completely ascribed to the electron capturer role of hydrogen peroxide because the Vis/H_2O_2 process was futile under these circumstances (Song et al. 2006). As described in Eq. 7-2,

the H_2O_2 as electron capturer is capable of arresting photogenerated electron and giving birth of hydroxyl radicals. Therefore, the number of available hydroxyl radicals is increased and it would be beneficial to the degradation of the norfloxacin. In addition, the capture of electrons by hydrogen peroxide could reduce the recombination of photo-generated electron and hole at Bi_2WO_6 surface. Therefore, the number of available hole is increased and their longer lifetime would improve the norfloxacin degradation.

$$H_2O_2 + e^- \rightarrow \cdot OH + OH^- \quad (7\text{-}2)$$

7.2.2 Effect of H_2O_2 dosage

Different dosages of H_2O_2 ($[H_2O_2]_0$) were investigated on the decay of norfloxacin in the SSL/Bi_2WO_6/H_2O_2 process. As illuminated in Figure 7-2, the decay rate increased with the increment of $[H_2O_2]_0$, and optimized at 10 mM, as higher $[H_2O_2]_0$ provides a larger pool for hydroxyl radical generation. Any dosage higher than 10 mM would retard the reaction. This is because excess H_2O_2 in the solution will compete with the norfloxacin for the ·OH radicals, generate a much weaker radical $\cdot HO_2$, and result in a negative effect (Eq. 7-3).

$$\cdot OH + H_2O_2 \rightarrow \cdot HO_2 + H_2O \quad (7\text{-}3)$$

It was found that all the decay curves followed pseudo first-order reaction kinetics and

the reaction could be clearly divided into two stages: a fast first-stage (with an initial decay rate k_1) followed by a slower second-stage (k_2). The variation of k_1, k_2, and break time (t_b, the time to separate the two stages) was demonstrated in the inert of Figure 7-2. Generally, the rate constants of both stages (k_1 and k_2) increased with the increment of $[H_2O_2]_0$ until the dosage reached the optimal 10 mM, where the maximum decay rates were observed at both stages. However, as the $[H_2O_2]_0$ was overdosed, the decay rates of both stages decreased with the increase of $[H_2O_2]_0$. In the first stage, higher initial $[H_2O_2]_0$ resulted in a faster decay (higher k_1), lower remaining [Norfloxacin], and higher level of intermediates in the solution. Under these circumstances, the k_2 of norfloxacin decay in second stage are generally lowered than k_1 because (a) the probability for remaining norfloxacin molecules to react with the hydroxyl radicals is reduced due to the lower [Norfloxacin], (b) the competition from higher level of intermediates is increased, and (c) the deficiency of H_2O_2 in the second stage makes the photocatalytic reaction of SSL/Bi_2WO_6 the major (or only) active pathway for norfloxacin decay.

7.2.3 Effect of Bi_2WO_6 dosage

To evaluate the effect of Bi_2WO_6 dosage ($[Bi_2WO_6]_0$) on the decay of norfloxacin, five different $[Bi_2WO_6]_0$ (0.5, 1, 1.5, 2 and 3 g/L) were studied with the $[Norfloxacin]_0$ and $[H_2O_2]_0$ at 0.1 and 5 mM, respectively. The decay patterns were shown in Figure 7-3 and the optimum decay performance was obtained at the Bi_2WO_6 dosage of 2 g/L. Below

the optimum dosage, the norfloxacin decay efficiency was increased with the increment of $[Bi_2WO_6]_0$, because more hydroxyl radicals were generated by the larger surface area of Bi_2WO_6, which are both suggested to be critical and positively related to the norfloxacin degradation. Over the optimum Bi_2WO_6 dosage, however, the declination of decay is likely due to the increase in the opacity of the solution with an excess amount of Bi_2WO_6 particles in the reaction, causing a reduction in the penetration of simulated solar light. As a result, an unlimited increase of photocatalyst dose not always guarantees a beneficial effect on the photoreaction. Similar to the effect of $[H_2O_2]_0$, all reactions followed two-stage pseudo first-order kinetics. The rate constants of the two stages (k_1 and k_2) and t_b at different $[Bi_2WO_6]_0$ were shown in the insert of Figure 7-3. As the Bi_2WO_6 dosage increase, similar trends of k_1 and k_2 variation were observed, which both optimized at the Bi_2WO_6 dosage of 2 g/L.

7.2.4 Effect of norfloxacin initial concentration

The effect of $[norfloxacin]_0$ on the performance of the SSL/Bi_2WO_6/H_2O_2 process was tested as well at 5 mM H_2O_2 and 1 g/L Bi_2WO_6. The $[norfloxacin]_0$ used were 0.05, 0.07, 0.10, 0.15, 0.20 and 0.30 mM. The decay curves of norfloxacin removal at different $[norfloxacin]_0$ were shown in Figure 7-4. It was found that the faster norfloxacin decay occurred at lower $[norfloxacin]_0$, which might be due to its lower competition and sufficient supply of hydroxyl radicals (i.e. higher $[H_2O_2]$/[norfloxacin] ratio) at lower

$[norfloxacin]_0$. Therefore, no second-stage decay was found if the $[norfloxacin]_0$ was lower enough. On the contrary, the degradation at higher $[norfloxacin]_0$ was significantly inhibited, which was attributed to the fast depletion of hydroxyl radicals at lower $[H_2O_2]$/[norfloxacin] ratio. The variation trend of k_1, k_2 and t_b at various $[norfloxacin]_0$ was summarized in the insert of Figure 7-4. Both k_1 and k_2 decreased with the increment of $[norfloxacin]_0$, while the t_b increased with the $[norfloxacin]_0$.

7.2.5 Development of kinetic model

From the design point of view, to select reasonable Bi_2WO_6, H_2O_2 dosage for different norfloxacin concentration, and to determine a proper retention time for the SSL/Bi_2WO_6/H_2O_2 process are necessary to ensure a cost-effective operation. Mathematic models were therefore derived for the prediction of norfloxacin degradation in SSL/Bi_2WO_6/H_2O_2 process. Various dosages of H_2O_2 and Bi_2WO_6 were used at different $[Norfloxacin]_0$ under the irradiation of simulated solar light. It was found that the values of $1/k_1$, $1/k_2$ were linearly correlated to $[H_2O_2]_0$, $[Bi_2WO_6]_0$ and $[Norfloxacin]_0$ as shown in Figure 7-5a, b and c, respectively. Thus, the value of k_1 and k_2 become predictable. Their corresponding linear equations were therefore derived and summarized in Figure 7-5.

Since the rate constants (1/k) are linearly correlated to the $[Norfloxaicn]_0$, $[Bi_2WO_6]_0$ and $[H_2O_2]_0$, theoretically, it is feasible to merge these parameters into one simple equation via multiple-regression. The general forms for $1/k_1$ and $1/k_2$ are expected as Eqs. 7-14 and 7-15.

$$\frac{1}{k_1} = a_1[\text{Norfloxacin}]_0 + a_2[Bi_2WO_6]_0 + a_3[H_2O_2]_0 + a_4 \quad (7\text{-}14)$$

$$\frac{1}{k_2} = a_5[\text{Norfloxacin}]_0 + a_6[Bi_2WO_6]_0 + a_7[H_2O_2]_0 + a_8 \quad (7\text{-}15)$$

where a_1, a_2, …, and $a_4$are process coefficients depending on the reaction condition.

In addition, the break time t_b was found to be the function of $1/k_1$, as shown in Figure 7-6. A linear relationship can be obtained as well:

$$t_b = 0.5695\left(\frac{1}{k_1}\right) + 2.905 \quad (7\text{-}16)$$

The process coefficients can be determined depending on the initial conditions selected, for example:

Case I: When $[Bi_2WO_6]_0$ and $[H_2O_2]_0$ are below the optimal condition (i.e. $[Bi_2WO_6]_0 \leq$ 2g/L and $[H_2O_2]_0 \leq 10$ mM), $1/k_1$ and $1/k_2$ can be determined as Eqs.7-17 and 7-18.

$$\frac{1}{k_1} = 209.9[\text{Norfloxacin}]_0 - 7.646[Bi_2WO_6]_0 - 1.198[H_2O_2]_0 + 15.60 \quad (7\text{-}17)$$

$$\frac{1}{k_2} = 445.4[\text{Norfloxacin}]_0 - 31.08[Bi_2WO_6]_0 - 1.796[H_2O_2]_0 + 48.72 \quad (7\text{-}18)$$

Case Ⅱ: When $[Bi_2WO_6]_0$ and $[H_2O_2]_0$ are above the optimal condition (i.e. $[Bi_2WO_6]_0$ ≥2g/L and $[H_2O_2]_0 \geq 10$ mM), $1/k_1$ and $1/k_2$ can be determined as Eqs.7-19 and 7-20.

$$\frac{1}{k_1} = 209.1[\text{Norfloxacin}]_0 - 2.940[Bi_2WO_6]_0 - 0.450[H_2O_2]_0 + 7.668 \quad (7\text{-}19)$$

$$\frac{1}{k_2} = 500.8[\text{Norfloxacin}]_0 - 8.961[Bi_2WO_6]_0 + 0.787[H_2O_2]_0 - 3.326 \quad (7\text{-}20)$$

The resulted rate constants and t_b from Eq. 16 then can be incorporated into the two-stage pseudo first-order kinetics to predict the decay of norfloxacin:

$$C = C_0 \times e^{-k_1 t} \quad \text{When } t \le t_b \quad (7\text{-}21)$$

$$C = C_0 \times \exp[-k_1 t_b - k_2 (t - t_b)] \quad \text{When } t \ge t_b \quad (7\text{-}22)$$

The norfloxacin decay data and modeled curves resulted from above equations were compared and shown in Figure 7-7, where the predicted trends fit quite well to the original data, indicating the proposed models can successfully predict the norfloxacin decay in the SSL/Bi_2WO_6/H_2O_2 process within the tested conditions.

7.2.6 Proposed mechanism of norfloxacin decay in SSL/Bi_2WO_6/H_2O_2 process

It is believed that hydroxyl radicals play a key role in the decomposition of organic compounds in SSL/Bi_2WO_6/H_2O_2 process. The investigation on the transformation products of norfloxacin produced in the process may demonstrate the norfoxacin degradation mechanism in our investigated process. Six (6) intermediates (i.e. I_A, I_B, I_C, I_D, I_E and I_F) were identified during the process on the basis of molecular ions and mass fragment ions detected by MS spectrum, and the evolution profile of relative peak areas

of all intermediates was organized in Figure 7-8. The chemical structures of intermediates can be seen in the Figure 7-9. The exact concentration of the intermediates was not determined due to the lack of authentic standards, the peak areas are therefore used (as the concentration) for the identification of the production sequence of intermediates. As indicated in Figure 7-8, most the intermediates (i.e. I_A, I_B, I_C, I_D and I_E) increased dramatically to reach the highest peak area, and followed by a continuous decreased until completely vanished. One exception was the intermediate I_F, which continuously increased and accumulated in the solution. In terms of appearance sequence, intermediates I_A and I_B were the primary and secondary intermediate, respectively; I_C, I_D and I_E appeared at the same time, and intermediate I_F was the end product, in this study.

Based on the above observations, the reaction pathways for the norfloxacin degradation in the SSL/Bi_2WO_6/H_2O_2 process were proposed in Figure 7-9. The degradation pathway can be divided into two sub-pathways, and they are initiated by the attack of ·OH on the benzene ring and piperazine ring in pathways 1 and 2, respectively. In the pathway 1, the first site of the hydroxyl radical probably takes place on the 6-position, resulting in the F atom substituted with a hydroxyl radical and giving birth to intermediate I_A. Following that, the intermediate I_B is originated from the attraction of hydroxyl radical on the most reasonable site of 2'-position of piperaine ring. In this case, both piperazine ring-opening and amide generation occurred simultaneously according

to the Scheme 7-1, in which the α-position amine I was first attacked by a hydroxyl radical, leading to the formation of a carbon centred radical II, followed by a reaction with oxygen to produce amide III (i.e. intermediates I_B). Similar reaction mechanism has been proposed by Kleiser et. al as well (Kleiser and Frimmel 2000), where ·OH radicals get electrons from the organic substituent and yields carbon centred radicals. The carbon centred radicals will react rapidly with oxygen to from organic peroxyl radicals, which further undergo self-reaction and give birth to ketones or aldehydes and/or carbon dioxide. Based on the same mechanism, it was believed that the further oxidation of intermediates I_B should generate an intermediate of Mw 348 (see Figure 7-9) with the formation of another amide functional group. However, the intermediate of Mw 348 was not detected in the MS analysis. This may be attributed to its rapid transformation of I_B to I_C, in which the amide intermediate Mw 348 was translated into amine I_C with the loss of a carbonyl group. This transformation could be described by the Scheme 7-1 from intermediate III to V, where the oxidation proceeded with a hydroxyl addition on the carbon atom of the amide groups and subsequent reaction with oxygen. Throughout the Scheme 7-1, one side chain ($-CH_2R_3$) of the initial amine at intermediate I was substituted by hydrogen atom to produce a new amine intermediate V, accompanied with the formation of stoichiometric $\cdot R_3$ and CO_2. Similar decay pathway was also observed in the following steps for the oxidation of intermediate I_C and/or I_D, which was oxidized to produce amide I_E (III) firstly and followed by the formation of amine intermediate I_F (V). The similar mechanism was also observed in the decay

pathway 2 from norfloxacin to intermediate I_D. Again, the undetected intermediates with Mw 336 and 350 were likely due to their short life time and/or fast F atom substituted with hydroxyl radical, leading to the imperceptible accumulation in the degradation progress. In addition, the formation of intermediate I_E involved defluorination and dehydroxylation on the benzene ring from intermediates I_D and I_C, respectively.

7.3 Summary

In the present chapter 7, the simulated solar light mediated Bi_2WO_6 process with the assistant of H_2O_2 (SSL/Bi_2WO_6/H_2O_2) was experimentally verified to be very effective in degrading norfloxacin. The norfloxacin decay by the SSL/Bi_2WO_6/H_2O_2 process was observed to follow a two-stage pseudo first-order reaction kinetics, which was started by a fast initial decay (k_1) then followed by a slower second-stage decay rate (k_2). The effect of various operational parameters of SSL/Bi_2WO_6/H_2O_2 process was examined to optimize the process. For the effect of H_2O_2 dosage, the test results demonstrated that 10 mM H_2O_2 exhibited the optimal norfloxacin decay performance and an uncontrolled increment of $[H_2O_2]_0$ was unfavorable to the SSL/Bi_2WO_6/H_2O_2 process. Based on the test results, the optimal $[Bi_2WO_6]_0$ was determined to be 2 g/L, where the increase of $[Bi_2WO_6]_0$ leaded to an increment of the norfloxacin decay, however, the norfloxacin decay slowed down at high $[Bi_2WO_6]_0$ due to the light attenuation. For the effect of norfloxacin concentration, the decay of norfloxacin became slower with the increase of

$[norfloxacin]_0$ in the solution. From the design point of view, the values of $1/k_1$, $1/k_2$ were observed linearly correlated to $[H_2O_2]_0$, $[Bi_2WO_6]_0$ and $[Norfloxacin]_0$, while the break time was found strongly correlated to $1/k_1$. Thereby, the values of k_1, k_2 and t_b can be estimated by using the proposed equations, then the removal of norfloxacin in SSL/Bi_2WO_6/H_2O_2 process becomes predictable. Furthermore, the decay pathway of norfloxacin by SSL/Bi_2WO_6/H_2O_2 process is proposed mainly via the defluorination and piperazine ring reaction based on the identified aromatic intermediates by LC-ESI/MS analysis.

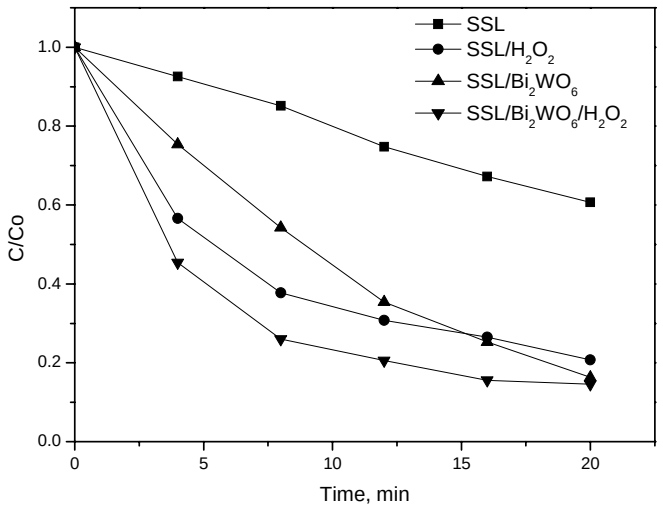

Figure 7-1. Norfloxacin decay at different processes.

Experiment conditions: Simulated solar light, $[Norfloxacin]_0$ = 0.0313 mM, $[Bi_2WO_6]_0$ = 0.5 g/L, $[H_2O_2]_0$ = 10 mM

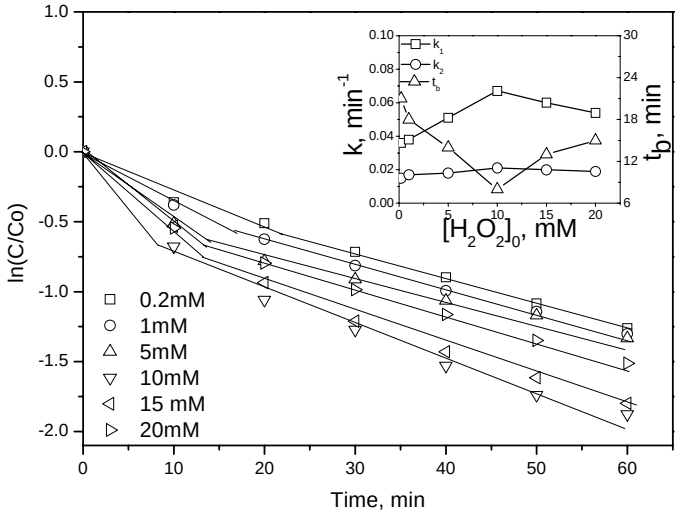

Figure 7-2. Effect of $[H_2O_2]_0$.

Experiment conditions: $[Norfloxacin]_0$ = 0.1 mM, $[Bi_2WO_6]_0$ = 1g/L

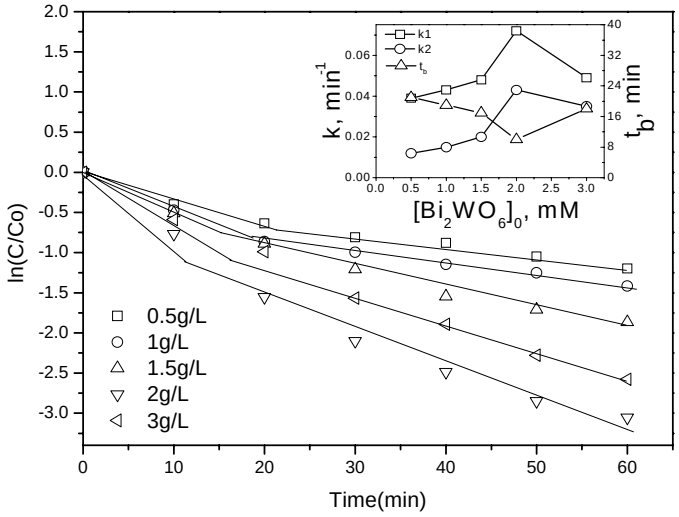

Figure 7-3. Effect of $[Bi_2WO_6]_0$.

Experiment conditions: $[Norfloxacin]_0$ = 0.1 mM, $[H_2O_2]_0$ = 5 mM

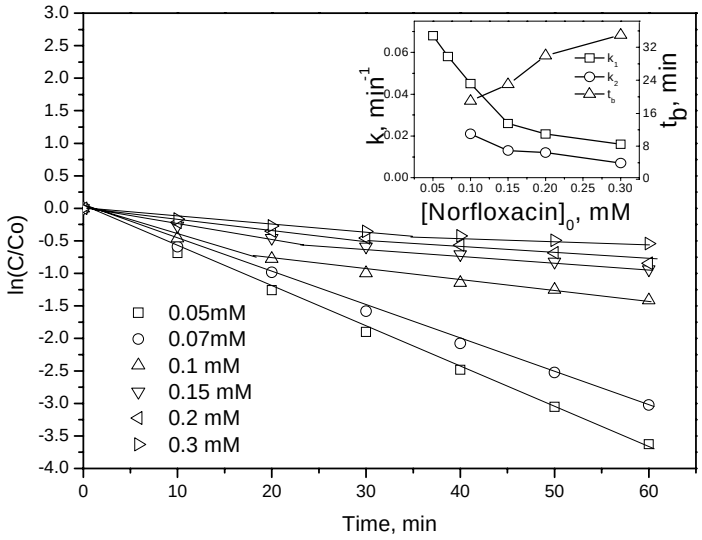

Figure 7-4. Effect of $[Norfloxacin]_0$.

Experiment conditions: Simulated solar light, $[Bi_2WO_6]_0$ = 1g/L, $[H_2O_2]_0$ = 5 mM

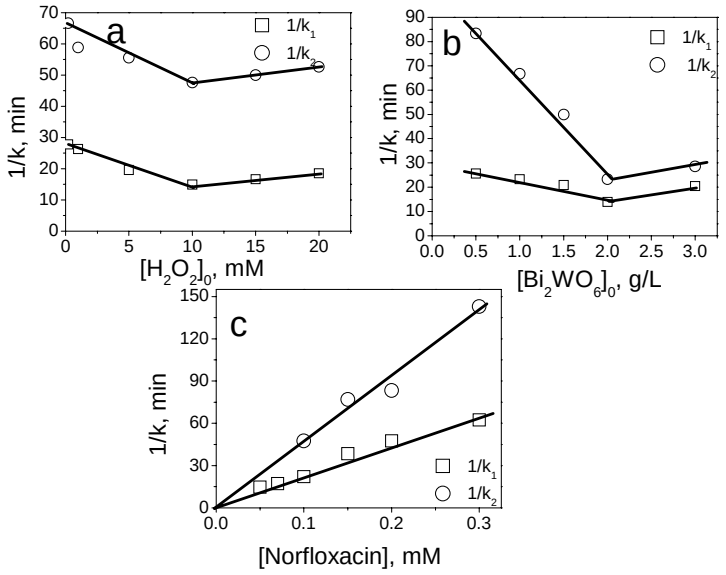

		$[H_2O_2]_0$	$[Bi_2WO_6]_0$	$[Norfloxacin]_0$
$\frac{1}{k_1}=$	≤bp	$-1.654[H_2O_2]_0 + 63.86$	$-39.38[Bi_2WO_6]_0 + 105.0$	$497.4[Norfloxacin]_0 - 7.299$
	≥bp	$0.501[H_2O_2]_0 + 42.56$	$-7.535[Bi_2WO_6]_0 + 30.32$	
$\frac{1}{k_2}=$	≤bp	$-1.320\ [H_2O_2]_0 + 27.50$	$5.315[Bi_2WO_6]_0 + 12.62$	$201.3[Norfloxacin]_0 + 4.581$
	≥bp	$0.359[H_2O_2]_0 + 11.31$	$6.519[Bi_2WO_6]_0 + 0.850$	

*bp is the abbreviation of break point

Figure 7-5. The linear relation between $1/k_1$, $1/k_2$ and H_2O_2 (a), $[Bi_2WO_6]_0$ (b), and $[Norfloxacin]_0$ (c).

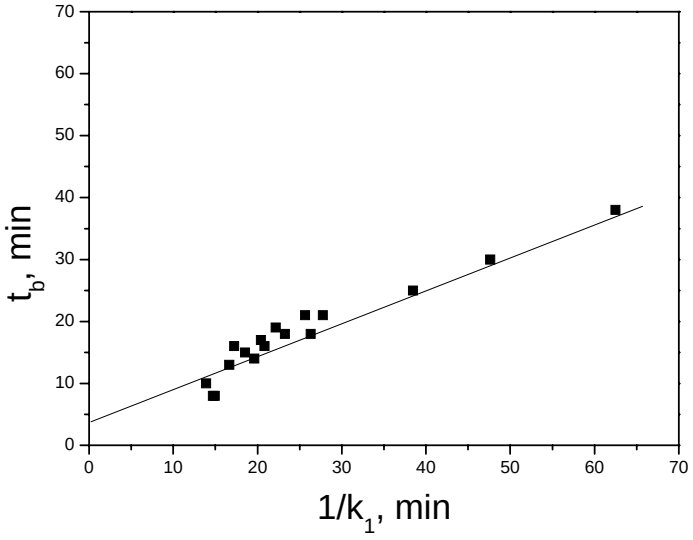

Figure 7-6. The linear relation between C_t and $1/k_1$.

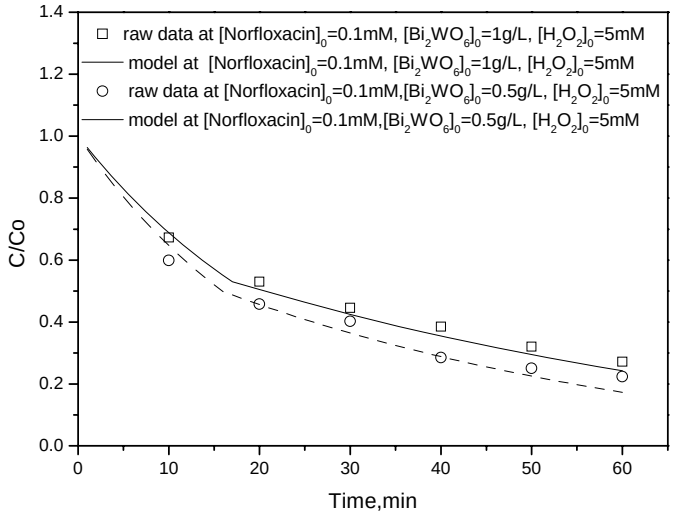

Figure 7-7. Comparison between the experimental data and the predicted results.

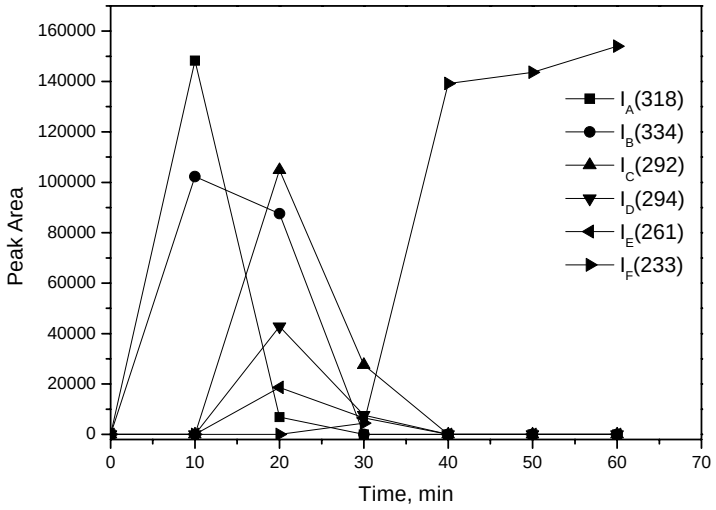

Figure 7-8. The evolution profiles of major intermediates.

Experiment condition: $[H_2O_2]_0$ = 10 mM, $[Bi_2WO_6]_0$ = 2g/L, $[Norfloxacin]_0$ = 0.1 mM

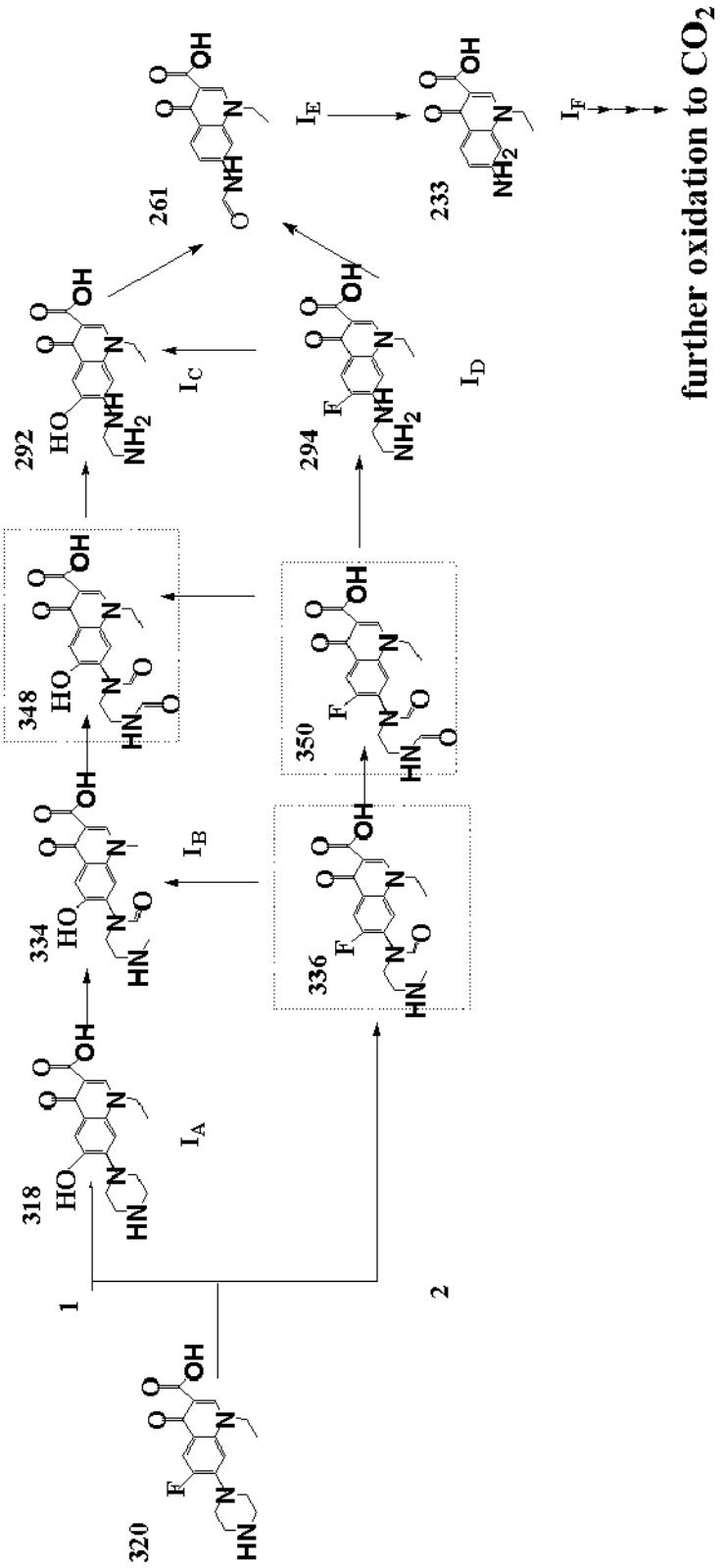

Figure 7-9. Proposed norfloxacin decay pathways in the SSL/Bi_2WO_6/H_2O_2 process.

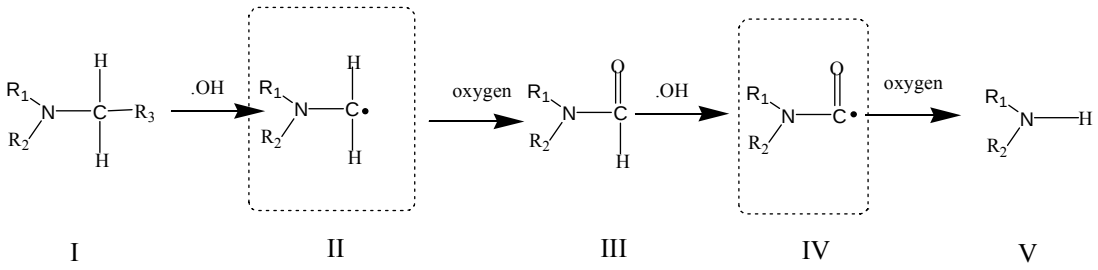

where R_1 and R_2 can each represent H or organic side-chain, respectively.

Scheme 7-1. Proposed reaction pathway on piperazine.

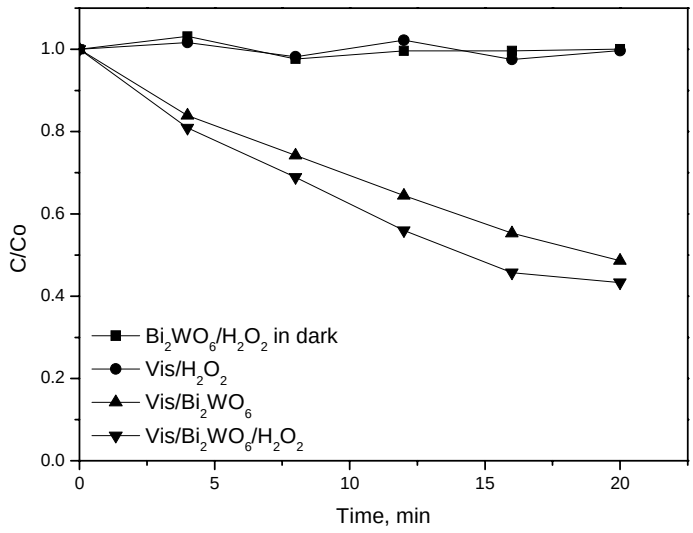

Figure 7-S1. Degradation of norfloxacin under visible light irradiation or in dark. Experiment conditions: $[\text{Norfloxacin}]_0 = 0.0313$ mM, $[Bi_2WO_6]_0 = 0.5$g/L, $[H_2O_2]_0 = 10$ mM

Chapter 8 Degradation of Antibiotic Norfloxacin in Aqueous Solution by Visible Light Mediated C-TiO_2 Photocatalysis

8.1 Introduction

The release of antibiotics into aquaculture has increased significantly in recent years (Giraldo et al. 2010). Norfloxacin belongs to fluoroquinolone antibiotics, which has been used to treat common and complicated urinary tract infections. It was frequently detected in sewage and the concentration reached up to 3.54 μg L^{-1} (Leung et al. 2011). Because the inefficient removal ability of antibiotics in traditional sewage plants (Batt et al. 2006), pollution of these chemicals has been observed in various water sources, including sewage treatment plant effluents (Lindberg et al. 2005), surface water (Cha et al. 2005), seawater (Xu et al. 2007), groundwater (Batt and Aga 2005) and drinking water (Watkinson et al. 2009). The norfloxacin in aqueous system leads to adverse environmental effects (Lee et al. 2008), including development of antibiotic resistance in aquatic bacteria (Phan et al. 2011), direct toxicity to microorganism and possible risks to human health through drinking water and/or food-chain (Phan et al. 2011).

In the past decade, efforts have been made on the removing of norfloxacin. Among the studies, adsorption is found to be a useful method, since norfloxacin can be adsorbed by activated sludge (Li and Zhang 2010), activated carbon (Wang et al. 2010e), carbon nantubes (Wang et al. 2010e), and silica/alumina (Lorphensri et al. 2006). However, the

"removed" norfloxacin only physically resides in sorbent and brings a risk of being released into aquatic environment if the used sorbent is improperly disposed. Therefore, methods resulting in direct or full decomposition are required.

Photocatalysis technique has received intensive attention with key advantages of low cost and enduring stability (Coleman et al. 2007). However, the popularly used photocatalyst, namely TiO_2, can only be excited by UV light with the irradiation wavelength less than 380 nm, which significantly limits its application. To broaden the utilizable range of light, the investigation on visible-light-driven photocatalysts has become one of the most active research areas. Therefore, various photocatalysts responding to visible light have been developed, including TiO2 based catalyst comprised by doping element or composing with other substances (Chen et al. 2005; Gombac et al. 2007; Liu et al. 2009; Nah et al. 2010). Carbon-doped TiO_2 (C-TiO_2) has attracted considerable attention due to its high efficiency and long-term stability. Most previous studies focus on the improvement of C-TiO_2 morphology to enhance the performance on pollutants decomposition. However, investigates on the degradation performance considering the environmental parameters effect is limited.

In this chapter, a visible light sensitive C-TiO_2 was employed to degrade antibiotic norfloxacin. To our best knowledge, this is the first time to employ Vis/C-TiO_2 process in the norfloxacin decay. Environmental parameters, including C-TiO_2 dosage,

norfloxacin initial concentration, and pH levels were investigated and optimized. To elucidate the reaction principle of this Vis/TiO_2 process, an original schematic diagram was built and selected inorganic ions was added into the process to verify the model. Meanwhile, the involved radical was confirmed. Furthermore, to evaluate the potential use of this process for real application, the reuse ability and settling properties of C-TiO_2 were carried out as well.

8.2 Results and Discussion

8.2.1 Effect of C-TiO_2 dosage and norfloxacin initial concentration

It was found that the probe norfloxacin is inert to sole visible light (Figure 8-1), while in the presence of C-TiO_2, 78% of norfloxacin was removed in 70 min and the decay curve showed a pseudo first-order kinetics. In contrast, the decay of norfloxacin in pure TiO_2 and was 25% (data not shown) under other identical conditions, indicating that the Vis/C-TiO_2 process is much effective than Vis/TiO_2 process. In Figure 8-1, the norfloxacin decay was investigated as the C-TiO_2 dosage, [C-TiO_2], varying from 0 to 3.0 g/L. It was found that all decay curves followed pseudo first-order kinetics and the rate constant increased with the increment of catalyst dosage from 0 to 2.0 g/L. The optimal dosage was observed at 2.0 g/L in this process, in which 99% of norfloxacin was removed in 20 min. However, a significant drop was observed when the dosage further increased to 3.0 g/l, which needed 40 min for norfloxacin thoroughly

decomposition. This retardation might be ascribed to the reduction in the light penetration resulting from the abundance of C-TiO_2 particles. Therefore, an unlimited increase in C-TiO_2 dosage is not always favorable in real operation. It is also interesting to note that there is a linear correlation between k and C-TiO_2 dosage in the range of 0 to 2.0 g/L.

To elucidate the effect of probe concentration, the Vis/C-TiO_2 process was examined with different initial norfloxacin concentrations, $[Norfloxacin]_0$. (Figure 8-2) It can be observed that lower initial concentration leads to higher removal efficiency of norfloxacin, i.e. when the $[Norfloxacin]_0$ increased from 0.0094 to 0.0939 mM, the final degradation of norfloxacin decreased from 100 to 37%. Again, a linear correlation between decay rate constant (k) and the reciprocal of $[Norfloxacin]_0$ can be established as shown in the insert of Figure 8-2.

By using multiple regression, the observed pseudo first-order rate constant (k, min^{-1}) becomes predictable in terms of $[Norfloxacin]_0$, mM, and [C-TiO_2], g/L as shown below:

$$k = 5.44 \times 10^{-4}[Norfloxacin]_0^{-1} + 0.10[C - TiO_2] - 1.99 \times 10^{-2} \quad R^2=0.998 \qquad (8\text{-}1)$$

In addition, the Langmuir-Hinshelwood (LH) model was used to evaluate heterogeneous reaction if the solid-liquid interface is the location dominating the process. The LH model is shown as follows (Al-Ekabi and Serpone 1988; Keane et al. 2011):

$$\frac{1}{k} = \frac{1}{k_{LH}}[\text{Norfloxacin}]_0 + \frac{1}{k_{LH}K_L} \quad (8\text{-}2)$$

where k_{LH} is the apparent rate constant of the reaction occurring on the catalyst surface ($mM \cdot min^{-1}$), k is the observed pseudo first-order rate constant (min^{-1}), and K_L is the equilibrium adsorption constant of norfloxacin on C-TiO_2 surface (mM^{-1}). The experimental results fit well with a r^2 of 0.996, which suggests the heterogeneous reaction occurs on the catalyst surface is the dominant process.

The K_L was determined to be 2.37×10^3 mM^{-1} from the original data. By combining above Eqs. 8-1 and 8-2, a general form of the apparent rate constant of the reaction occurring on the catalyst surface (k_{LH}) can be predicted as Eq. 8-3.

$$k_{LH} = 0.10[C - TiO_2][\text{Norfloxacin}]_0 - 1.99 \times 10^{-2}[\text{Norfloxacin}]_0 + 2.30 \times 10^{-7}[\text{Norfloxacin}]_0^{-1} + 4.22 \times 10^{-5}[C - TiO_2] + 5.44 \times 10^{-4} \quad (8\text{-}3)$$

Within the test range of this study, the 3rd and 4th terms on the right-hand side are about 2 to 3 log lower than the others, and can be neglected. The k_{LH} therefore is abbreviated to be as follows,

$$k_{LH} = 0.10[C - TiO_2][\text{Norfloxacin}]_0 - 1.99 \times 10^{-2}[\text{Norfloxacin}]_0 + 5.44 \times 10^{-4}$$

(8-4)

8.2.2 Effect of pH level

The influence of pH levels on norfloxacin decay was showed in Figure 8-3 (a). The pH values were measured by the initial norfloxacin solution in the absence of C-TiO_2. It was obvious that the pH level strongly affects the performance of norfloxacin degradation, where the decay is much faster in weak basic pH (9.2) than those of acidic (2.5, 3.4 and 4.5), neutral (7.1) or alkaline (10.1 and 11.8) conditions. Besides, the pH variation during adsorption (X axis from -10 to 0) and photocatalytic reaction (x axis from 0 to 70) was also examined as shown in Figure 8-3 (b). It was noted that a significant pH drop occurred at adsorption, especially when the pH level is 9.2 and 10.1. It suggests the surface of C-TiO_2 is of acid property, thereby, it favors OH^- anions and will leads to a redistribution/adsorption of OH^- anion from solution to the surface of C-TiO_2, as illuminated in scheme 8-1. It is deserved to note the pH variation during the photocatalytic reaction as initial pH of 7.1 (neutral, without pH adjustment), where a gradually pH drop was found. It implies that the continuous consumption and redistribution/adsorption of OH^- occurs in the Vis/TiO_2 process as well, where the imperceptible pH variation under other pH conditions might be ascribed to their buffer capacity.

At weak alkaline condition, the addition of OH^- into the process leads to the increase of its adsorbed amount (see Figure 8-3 (b)), resulting in a larger amount of hydroxyl radicals (Linsebigler et al. 1995). Thereby, the performance at pH of 9.2 is superior to that of 7.1. However, as the pH further increased to the 10.1 or 11.8, a repulsive force between C-TiO_2 and norfloxacin quickly builds up due to their like surface charges. To verify this, the point of zero charge (pzc) of C-TiO_2 was determined to be around pH 5.5 (as indicated in Table 1), while norfloxacin has two acid dissociation constants pK_{a1} and pK_{a2} at 6.24 and 8.75, respectively (Hyoung-Ryun Park 2000). The negative charge on both sides (i.e. the repulsive force) restrains the norfloxacin approaching to the surface of C-TiO_2, leading to the suppression of norfloxacin degradation. At acidic condition, similar charge repulsion (both at positive charges) occurs. In summary, the Vis/C-TiO_2 process performed well at weak basic pH, especially when moderate OH^- ion present in the suspension.

It is interesting to note that the degradation performance at extreme acidic pH follows the order of $k_{pH2.5} > k_{pH3.4} > k_{pH4.5.}$ The faster rate at extreme acidic condition is likely due to the effective particle size of C-TiO_2, as shown in Table 8-1, where the smaller size of C-TiO_2 at lower pH offers larger surface area and provides more opportunities to contact with norfloxacin molecules and absorb the visible light.

8.2.3 Principle study of the Vis/C-TiO_2 process

In photocatalytic reaction, it is compulsory to illumine semiconductor catalyst with sufficient light energy. The effective incidence light wave (λ) can be calculated according to the following Eq. 8-5 (Arancibia-Bulnes and Cuevas 2004):

$$\lambda = hc/E_{bg} \quad (8\text{-}5)$$

where E_{bg} is the band gap of semiconductor catalyst (e.g. C-TiO_2 of 2.64 eV(Huang et al. 2008b)); h is Plank's constant, 4.14×10^{-15} eV; and c is the light speed, 3×10^{10} cm/s.

As a result, λ is calculated to be 480 nm, which indicates that light with irradiation wavelength less than 480 nm has the potential to participate in a photocatalytic reaction. In this study, the irradiation wavelength selected was 420 nm from low-pressure mercury lamps (Rao and Chu 2010). Obviously, these low pressure lamps are proven useful to activate C-TiO_2 and generate electron (e^-) and hole (h^+) pairs.

Subsequently, the h^+ reacts with surface OH^- to produce ·OH radicals via following Eq. 8-6 (Linsebigler et al. 1995):

$$OH^- + h^+ \rightarrow \cdot OH \quad (8\text{-}6)$$

To verify the involvement of ·OH radicals in our Vis/C-TiO_2 process, methanol was added as a hydroxyl radical quencher due to its high reaction rate constant with the ·OH radical of 1.01×10^{-12}mL·molecule^{-1}·S^{-1} (Chin et al. 2004). As indicated in Figure 8-4(a),

in the presence of 1.2 M methanol, the retardation was found. Therefore, the generation of hydroxyl radicals is confirmed in the Vis/C-TiO_2 process. From Eq. 8-2 and scheme 8-1, more hydroxyl radicals will be produced as the increase of OH^- anions on the C-TiO_2 surface. As a result, higher norfloxacin decay rate was observed in weak alkali.

On the other hand, photo-generated electrons migrate to the surface of catalyst, then react with dissolved oxygen in aqueous solution to produce peroxide radicals (Linsebigler et al. 1995):

$$O_2 + e^- \rightarrow O_2{\cdot}^- \qquad (8\text{-}7)$$

where peroxide radical is also an effective radical for pollutants decay, despite its redox potential is smaller than hydroxyl radial (DeWitte et al. 2008).

To verify the presence of the above electron mechanism, an electron acceptor KIO_3 was added to the reaction, and the degradation of norfloxacin was improved as illuminated in Figure 8-4(a). It is because the involvement of KIO_3 terminates the recombination of e^- and h^+ (Choy and Chu 2008) through the capture of electrons ejected from C-TiO_2 surface by following Eq. 8-8:

$$IO_3^- + 6\,H^+ + 6e^- \rightarrow I^- + 3H_2O \qquad (8\text{-}8)$$

As a result, the number of separated h^+ is increased which will be beneficial to the generation of hydroxyl radicals.

However, It should be noted that the further increment of KIO_3 from 0.01 M to 0.1 M will reduce the decay rates as shown in Figure 8-4(b). It might partly be due to the generation of I^- from Eq. 8-8, which was reported as an effective hole scavenger to react with photogenerated h^+, resulting in the reduction of hydroxyl radicals from Eq. 8-6 (Scot et al., 1995). In addition, it was known that the KIO_3 can be oxidized by Cl_2 and generate IO_6^{5-} (a weaker oxidant than KIO_3) as shown in Eq. 8-9

$$KIO_3 + Cl_2 + 6KOH \rightarrow K_5IO_6 + 3H_2O + 2KCl \quad (8\text{-}9)$$

The above reaction occurs at basic condition, while the OH^- is likely to accumulate and be concentrated at the surface of C-TiO_2 (Scheme 8-1), which makes the hydroxyl radicals (also generated at C-TiO_2 surface) have a very good chance to perform a similar oxidation process due to its much higher reduction potential (2.0-2.8) than Cl_2 (1.36). The possible consumption of valuable ·OH therefore resulted in a slower rate of the norfloxacin's decay as KIO_3 was overdosed.

8.2.4 Effect of inorganic ions

In Figure 8-5(a), norfloxacin decay in the Vis/TiO_2 process was investigated in the presence of various inorganic ions. In view of nitrogen and fluoride are elements of norfloxacin, the effect of inorganic ion containing these ions, such as NH_4^+, NO_3^- and F^-, was investigated. Previous studies showed that NH_4^+ ion is a scavenger for

photo-generated holes in photocatalytic process (Chenthamarakshan et al. 2000; Zhu et al. 2005):

$NH_4^+ + 8h^+ + 3H_2O \rightarrow NO_3^- + 10H^+$ (8-10)

However, an imperceptible effect was found with the addition of 0.10 M NH_4^+ ions. The positive charge on NH_4^+ ions apparently make them difficult to approach to the holes as negatively-charged groups (i.e. $-OH^-$) have formed a barrier on the surface and trap the NH_4^+. As a result, the Eq. 8-10 is invalid or minor in this process and the structure of catalyst as shown in Scheme 8-1 is reconfirmed. Besides, there was no apparent effect in the addition of [NO_3^-] ions to the process, this is because the oxidation state of NO_3^- is already high, the further oxidation of it is difficult and no radical or hole consumption was observed.

In the presence of 0.10 M F^- anions, the norfloxacin decay was suppressed. Additional tests with various [F^-] were conducted to verify this, and the results were shown in Figure 8-5(b), which indicated that the reaction rate progressively decreased with the increment of fluoride concentration. Parallel tests to examine the adsorption of norfloxacin by C-TiO_2 showed that, almost no norfloxacin was adsorbed onto C-TiO_2 at 0.20 M [F^-], while 2.3, 5.4 and 5.6% of norfloxacin were adsorbed at 0.10, 0.01 and 0 M [F^-], respectively. This observation suggests that fluoride ions may restrain the norfloxacin approaching to C-TiO2 surface, leading to the retardation of the heterogeneous reaction. However, it is interesting to note that the chloride ions (0.10 M),

which possess similar chemical property to fluoride ions, did not show an appreciable effect on norfloxacin decay. Therefore, the repressive effect of F^- ions might be ascribed to the exclusive hydrogen bond (O—H···F), which most likely formed around the C-TiO_2 surface (as shown in Scheme 8-1). This additional bonding kindly ties up the hydroxyl ions so that the surface property of C-TiO_2 was changed, and then the norfloxacin approaching was restrained. In addition, the transformation of hydroxyl radicals could be hindered as the hydroxyl ions were bided.

8.2.5 Reuse of C-TiO_2 catalyst

In real applications, it is necessary to demonstrate whether, after photocatalysis and liquid/solid separation, the reuse of catalyst is feasible. To find out the reuse possibility of C-TiO_2, the efficiency of the process by using recycled catalyst was studied, in which 0.2 g of C-TiO_2 was dispersed into 100 mL of 0.0313 mM norfloxacin solution. After 70 min of photocatalytic reaction, the C-TiO_2 was centrifugal separated (4000 rpm) and washed with DI water twice, then dried in an oven at 80^{o}C. Very little weight loss was observed during the separation and wash process (less than 5%). For a fair test, the weight difference was made up by adding fresh catalyst into the next run to reach the same weight. The removal efficiency of each trial (one fresh and four reuses), was 41.23, 40.73, 40.36, 40.87 and 40.99 in sequence. No obvious efficiency degrade was observed with using the same batch of catalyst. This demonstrates that the chemical stability of

the synthesized C-TiO_2 is excellent and the C-TiO_2 catalyst has good potential to be used in water/wastewater treatment.

8.2.6 Sedimentation property of C-TiO_2 catalyst

The sedimentation property of suspended photocatalyst is of importance in water treatment, since most photocatalysts possessing fine particle, e.g. Degussa P25 of average particle size of 25-30 nm, are difficult to be separated from water once enter into aquatic phase (Ding et al. 2000). Thereby, a high operating cost is needed for their separation (Le-Clech et al. 2006). The sedimentation study was carried out on dispersions of the C-TiO_2 and Degussa P25 in norfloxacin solution. The profile of turbidity versus settling time was shown in Figure 8-6. It can be noted that most of C-TiO_2 can be easily settled from the suspension in a short time, around 85% of C-TiO_2 was removed/recycled in 1 h, while it took 6 hr for the P-25 to reach the same removal performance. Because the settling time is reasonably fitted into the scale of a conventional sedimentation tank in water/wastewater treatment process, the fast settling property C-TiO_2 becomes an advantage in real application.

8.3 Summary

In this chapter, a visible light mediated C-TiO_2 process was employed to degrade antibiotic norfloxacin. The influence of C-TiO_2 dosage, norfloxacin initial concentration

and solution pH were investigated. The norfloxacin decay was found to follow a pseudo first order kinetics and the observed rate constant (k, min^{-1}) can be simply expressed by one equation related to $[Norfloxacin]_0$ and $[C\text{-}TiO_2]$. The reaction rational of the Vis/C-TiO_2 was proposed to dominating occur on the C-TiO_2 surface. Hydroxyl radicals were confirmed to play a major role in the Vis/C-TiO_2 process. It was also found that the addition of slight OH^- anions into the system could accelerate the reaction with producing more hydroxyl radicals. Besides, the process was benefited from a small suspension particle of C-TiO_2, which offers larger surface area for reaction. The optimal pH level was found at weak alkali condition. An original schematic diagram for deciphering the surface property of C-TiO_2 was built from the observation of redistribution/adsorption of OH^- in the treatment process. Furthermore, the model was confirmed by various tests, in which, the hole scavenger of NH_4^+ cation showed an inappreciable effect because OH^- on C-TiO_2 surface formed a barrier for NH_4^+ ion to approach the holes, and the F^- anion presented a significant suppression due to the formation of hydrogen bond. Besides, the recycling and sedimentation tests justified that the Vis/C-TiO_2 process is a cost-effective and feasible way for water treatment.

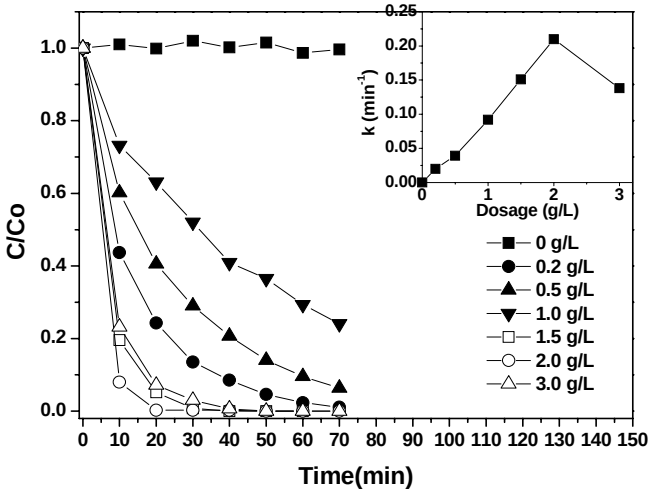

Figure 8-1. Effect of catalyst dosage.

Experiment conditions: $[Norfloxacin]_0$ = 0.0313 mM

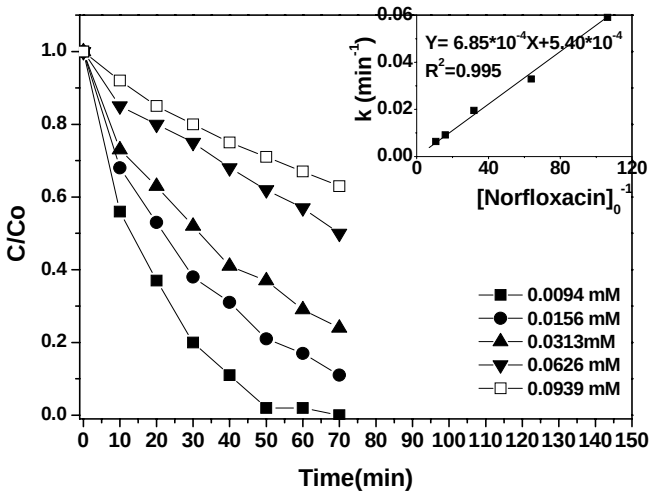

Figure 8-2. Effect of norfloxacin initial concentration.

Experiment conditions: $[C\text{-}TiO_2]$ = 0.2 g/L

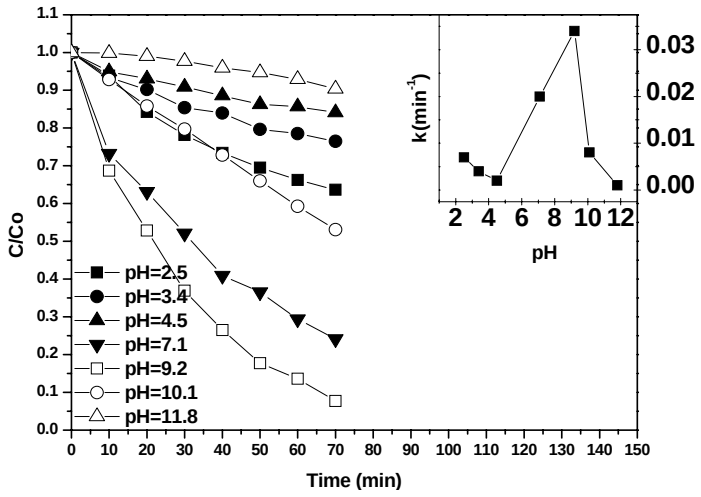

Figure 8-3(a). Effect of pH level.

Experiment conditions: [C-TiO_2] = 0.2 g/L, $[Norfloxacin]_0$ = 0.0313 mM

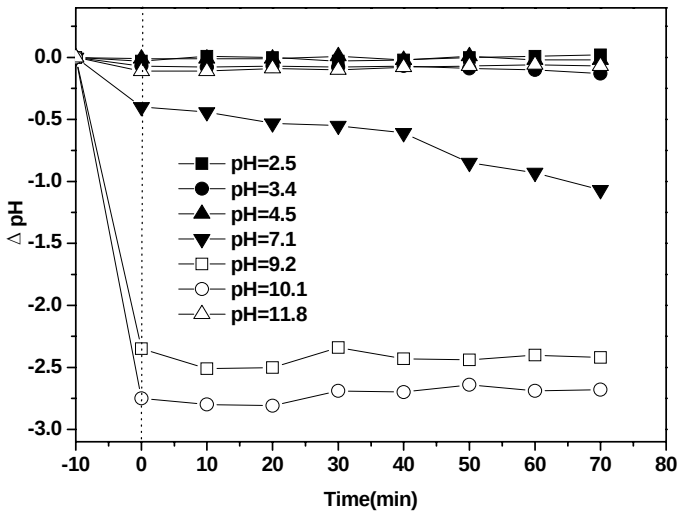

Figure 8-3(b). pH variation during reaction

Experiment conditions: [C-TiO_2] = 0.2 g/L, $[Norfloxacin]_0$ = 0.0313 mM

Notes: $\triangle pH = pH_t - pH_{initial}$, e.g. $\triangle pH_{-10} = pH_{initial} - pH_{initial}$, and $\triangle pH_0 = pH_{equilibrium} - pH_{initial}$.

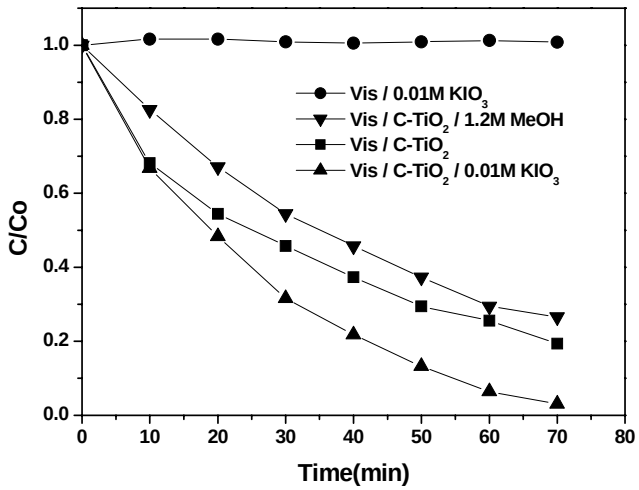

Figure 8-4(a). Effect of methanol and KIO_3.

(Experiment conditions: [C-TiO_2] = 0.2 g/L, [Norfloxacin]$_0$ = 0.0313 mM

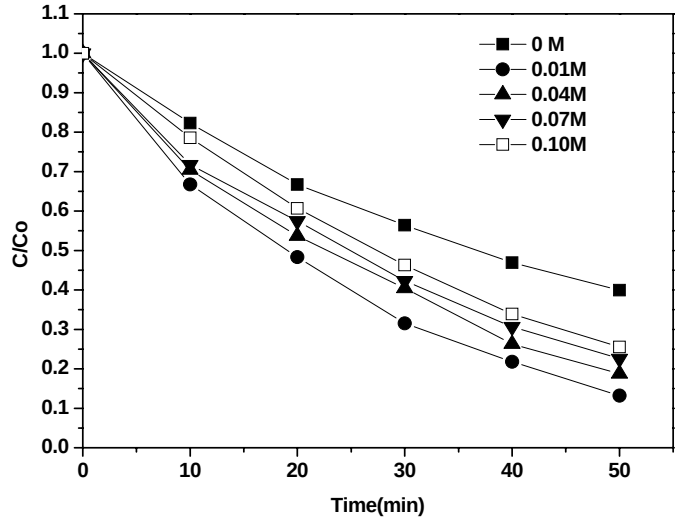

Figure 8-4(b). Effect of KIO_3 dosage.

Experiment conditions: [C-TiO_2] = 0.2 g/L, [Norfloxacin]$_0$ = 0.0313 mM

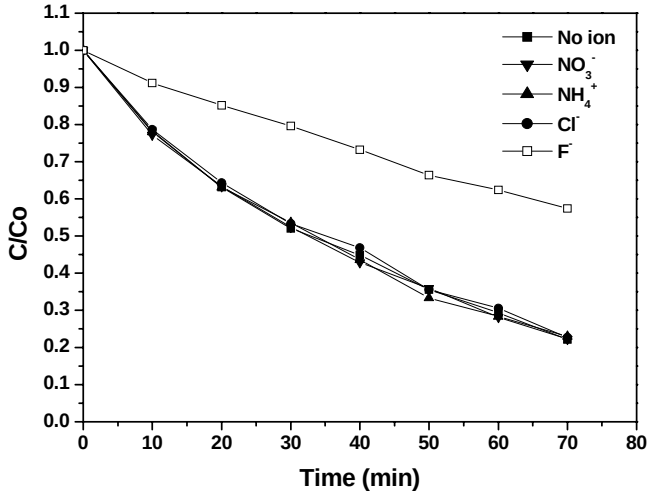

Figure 8-5(a). Effect of inorganic ions (all 0.10 M).

Experiment conditions: [C-TiO_2] = 0.2 g/L, $[Norfloxacin]_0$ = 0.0313 mM

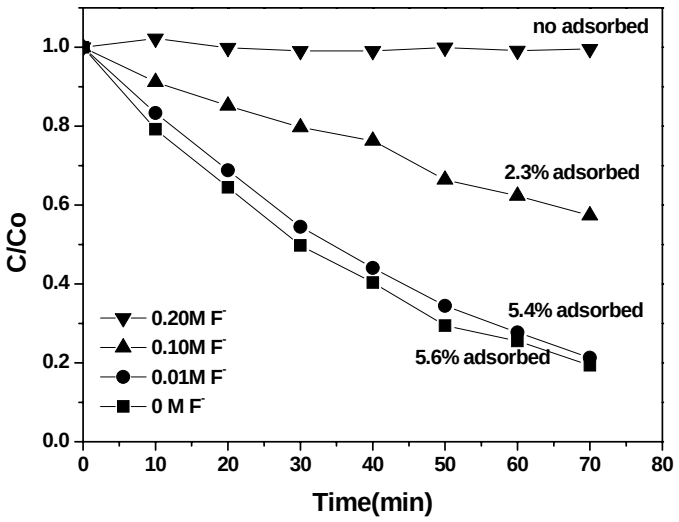

Figure 8-5(b). Effect of fluoride ions dosage.

Experiment conditions: [C-TiO_2] = 0.2 g/L, $[Norfloxacin]_0$ = 0.0313 mM

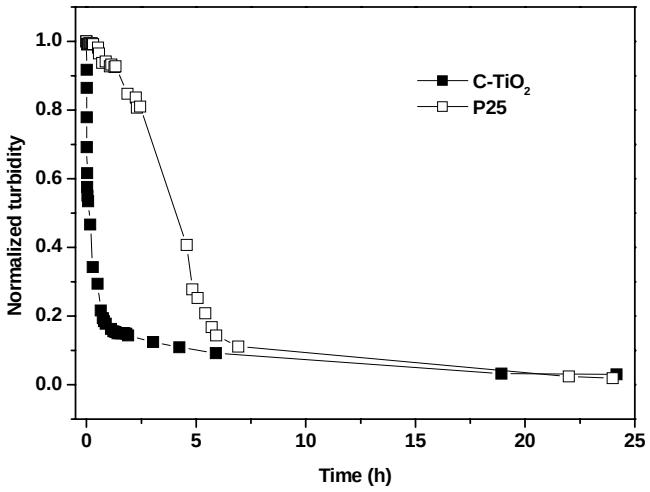

Figure 8-6. Turbidity variation by gravity settling of C-TiO_2 (a), and Degussa P25 (b). Experiment conditions: catalyst dosage = 0.2 g/L, $[Norfloxacin]_0$ = 0.0313 mM

Table 8-1. Effective particle diameter of C-TiO_2 at different pH levels

pH	2.5	3.4	4.5	5.5	7.1	9.2	10.1	11.8
Effective Diameter* (nm)	300	467	498	894	583	283	258	338

*The effective diameter is the biggest at pH of point of zero charge. It is because the like charges of C-TiO_2 particles repelled each other at pH away from pzc, as a result, the C-TiO_2 presented a small effective particle size in aqueous solution.

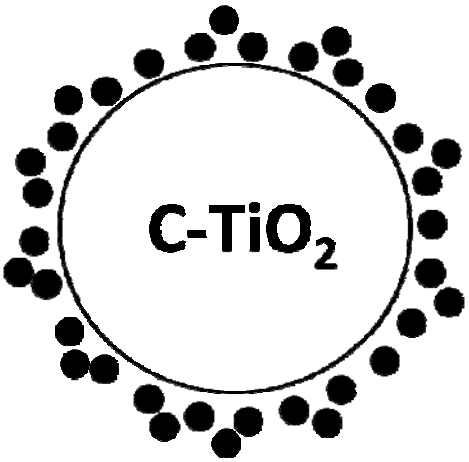

Scheme 8-1. Interface model of C-TiO_2 in the reaction process

○ represents C-TiO2, and ● represents OH- anion.

Chapter 9 Conclusions and Recommendations

9.1 Conslusions

This thesis focused on the investigation of reliable wastewater treatment technologies. Firstly, a simulated solar light mediated Bi_2WO_6 (SSL/Bi_2WO_6) photocatalytic process was explored with the aim to utilize the free sunlight in wastewater treatment. The study showed that the SSL/Bi_2WO_6 process was effective in the elimination of norfloxacin antibiotics. To overcome the drawback of the requirement of moderate pH conditions existing in the SSL/Bi_2WO_6 process, hybrid system of SSL/Fe^{3+}/Bi_2WO_6 and SSL/Bi_2WO_6/buffer was introduced at acidic and basic conditions respectively. Further development has been conducted to accelerate norfloxacin removal based on SSL/Bi_2WO_6 process. Therefore, a more efficient SSL/Bi_2WO_6/H_2O_2 process combing the advantages of SSL/Bi_2WO_6 and H_2O_2 photolysis was proposed. Besides, the process of Vis/C-TiO_2 was investigated to enrich the feasible system for norfloxacin elimination.

The SSL/Bi_2WO_6 process showed an excellent performance in norfloxacin decay, where the decay could be ascribed to the contributions of the sole-SSL, UV/Bi_2WO_6, and Vis/Bi_2WO_6, which was quantified as 21%, 24%, and 55%, respectively. The norfloxacin decay in the SSL/Bi_2WO_6 process was found to follow pseudo first-order kinetics. The effect of Bi_2WO_6 dosage, norfloxacin initial concentration and pH level

were investigated. The experiment results showed that the decay rates: (1) increased linearly at lower Bi_2WO_6 dosage then leveled off after a breakpoint (optimal) dosage of 2 g/L; (2) continuously decreased with the increment of norfloxacin initial concentration; and (3) increased with the increment of pH, and reached an optimal at pH of 10.5 (before Bi_2WO_6 dosing), then it decreased again at extreme basic conditions. The norfloxacin decay was found to fit the LH model perfectly, indicating the reaction was initialed by a rapid norfloxacin adsorption, and followed by a slower degradation reaction on the Bi_2WO_6 surface. After the treatment by the SSL/Bi_2WO_6 process, the norfloxacin was deeply decomposed associated with defluorination and denitrogenation because fluoride and ammonium were gradually accumulated in the process. Moreover, toxicity examination in vitro E.coli bioassays suggested that the antibiotic activity of norfloxacin could be efficiently removed via the treatment of SSL/Bi_2WO_6 process since norfloxacin and its germicidal intermediates were degraded to an ineffective level.

On the active species investigations, the superoxide radical ($O_2^{\cdot-}$) originated from photogenerated electrons was proved to be a useless oxidant in norfloxacin decay in the SSL/Bi_2WO_6 process. Therefore, the norfloxacin decay in the SSL/Bi_2WO_6 process should be completely ascribed to the photogenerated holes, where 87.8% of holes have been translated into hydroxyl radicals, and the leaving holes react with organics directly. The overall norfloxacin decay in the SSL/Bi_2WO_6 process can be characterized into photolysis, photocatalysis-via hydroxyl radical, and photocatalysis-via direct hole

oxidation, of which their contributions were 29.7, 65.5, and 4.8%, respectively. This finding demonstrated that the ·OH radicals played a major role in the SSL/Bi_2WO_6 process for norfloxacin decay. It was further confirmed by the observations in the presence of inorganic ions of SO_4^-, HCO_3^-, Fe^{3+} and Fe^{2+}. Fourteen intermediates were identified by LC/MS analysis. The norfloxacin decay was proposed to involve in include defluorination, decarboxyl acid, and piperazine ring transformation, where the piperazine ring transformation was major and processed first by ring cleavage, followed by loss of the 4'- amine nitrogen, then the 1'- amine nitrogen. The possible decay pathway of norfloxacin was proposed accordingly.

The pH level has been demonstrated to have a great influence on the norfloxacin decay in SSL/Bi_2WO_6 process. In general, the SSL/Bi_2WO_6 process showed a good performance only at a narrow pH range (from 5.0 to 9.0). In order to overcome this disadvantage, modification of SSL/Bi_2WO_6 process has been carried out to broaden the sensitive pH range. The buffer system (SSL/Bi_2WO_6/Buffer) established at extremely basic pH condition significantly improved the norfloxacin decay because it can continuously supply higher dosage of hydroxyl ion and thereby facilitates the generation of hydroxyl radicals. At the extremely acidic pH condition, the norfloxacin decay was accelerated obviously through dosing ferric salts into the SSL/Bi_2WO_6 process (forming the SSL/Bi_2WO_6/Fe^{3+} system), in which a homogeneous photo-sensitization mechanism offered by SSL/Fe^{3+} was triggered. Based on the experimental results, the interfacial

property of Bi_2WO_6 was described in models, i.e. OH^- enriched Bi_2WO_6 model with a negative charged surface in the SSL/Bi_2WO_6/Buffer system, and $Fe^{III}OH^{2+}$ enriched model with a positive charged surface in the SSL/Bi_2WO_6/Fe^{3+} system.

To further impove the norfloxacin decay, a combined process of SSL/Bi_2WO_6 and H_2O_2 photolysis (SSL/Bi_2WO_6/H_2O_2) was proposed by simple dosing H_2O_2 into the SSL/Bi_2WO_6 system. This process was effective in terms of its superior performance over the processes of SSL/Bi_2WO_6 and H_2O_2 photolysis. The effect of operational parameters was examined and optimized. In the selected tests, the best H_2O_2 and Bi_2WO_6 dosage is found to be 10 mM and 2 g/L respectively, which illuminates that an uncontrolled increment of H_2O_2 and/or Bi_2WO_6 is unfavorable to the SSL/Bi_2WO_6/H_2O_2 process. For the effect of norfloxacin concentration, the norfloxacin decay became slower with the increase of $[norfloxacin]_0$. The reaction kinetics of the norfloxacin decay via the SSL/Bi_2WO_6/H_2O_2 process followed a two-stage pseudo first-order reaction kinetics, which was started by a fast initial decay (k_1) then followed by slow second-stage decay (k_2). From the design point, the values of $1/k_1$ and $1/k_2$ were linearly correlated to $[H_2O_2]_0$, $[Bi_2WO_6]_0$ and $[Norfloxacin]_0$, and the break time was strongly correlated to $1/k_1$. Therefore, the norfloxacin decay via the SSL/Bi_2WO_6/H_2O_2 process became predictable and relative equations were established. The fine distinction between experimental data and modeling curves indicated that the proposed equations successfully predicted the norfloxacin decay in the SSL/Bi_2WO_6/H_2O_2 process within

the tested conditions. Furthermore, six intermediates were identified by using LC/MS analysis, based on which a possible decay pathway of norfloxacin was proposed.

The norfloxacin decay was carried out by using C-TiO_2 catalyst and visible light irradiation (420 nm lamps are used as light source). This C-TiO_2 process showed a high removal efficiency of 78% within 70 min. The experimental parameters including C-TiO_2 dosage, initial norfloxacin concentration and solution pH level were all found to be relevant to the norfloxacin decay performance. Based on the experimental results, an original model was proposed for deciphering the surface property of the catalyst. The hydroxyl radical was confirmed to be the main active species and the electron acceptor KIO_3 improved the norfloxacin decay because it increases the number of separated hole and further benefits the generation of hydroxyl radicals. However, inorganic hole scavenger NH_4^+ did not show an appreciable influence on the norfloxacin decay because they were trapped by OH^- groups on C-TiO_2 surface. The negative effect of fluoride validated the proposed model because H-bond (O - H…F) is likely formed on the C-TiO_2 surface and hinder the formation of hydroxyl radicals. The recycling and sedimentation tests recommended that Vis/C-TiO_2 is a cost-effective and feasible way for water treatment.

9.2 Recommendations for further works

Based on the results presented in this thesis, the investigated SSL/Bi_2WO_6 and

Vis/C-TiO_2 process were shown to effectively degrade and removal antibiotic norfloxacin. However, each process presented in this thesis could lead to various further investigative paths. Some recommendations on the improvements of these processes and on the further research directions of the issues are detailed as following.

In this study, all the reactions were conducted in a lab-scale batch reactor with the aim of destroying norfloxacin in aqueous solution. For practical applications, further research work may be extended to develop corresponding continuous pilot scale reactors for these processes.

The use of powder Bi_2WO_6 and C-TiO_2 results in disadvantages of stirring during the reaction and of separation after the reaction. To overcome these disadvantages and to extend the industrial application, preparation of the catalysts coated as thin films will be more convenient in further application. Fortunately, it is easy to prepare films using our sol-gel method.

The processes used in this study are low cost because they use of free and abundance solar light, and the lifetime of the catalysts is longer enough. However, their real cost in application should be estimated and compared with other AOPs.

REFERENCES

Ai, Z., Huang, Y., Lee, S. and Zhang, L., 2011. Monoclinic α-Bi2O3 photocatalyst for efficient removal of gaseous NO and HCHO under visible light irradiation. Journal of Alloys and Compounds 509(5), 2044-2049.

Al-Ekabi, H. and Serpone, N., 1988. Kinetics studies in heterogeneous photocatalysis. I. Photocatalytic degradation of chlorinated phenols in aerated aqueous solutions over titania supported on a glass matrix. The Journal of Physical Chemistry 92(20), 5726-5731.

Albini, A. and Monti, S., 2003. Photophysics and photochemistry of fluoroquinolones. Chemical Society Reviews 32(4), 238-250.

An, T., Yang, H., Song, W., Li, G., Luo, H. and Cooper, W.J., 2010a. Mechanistic Considerations for the Advanced Oxidation Treatment of Fluoroquinolone Pharmaceutical Compounds using TiO2 Heterogeneous Catalysis. The Journal of Physical Chemistry A 114(7), 2569-2575.

An, T.C., Yang, H., Song, W.H., Li, G.Y., Luo, H.Y. and Cooper, W.J., 2010b. Mechanistic Considerations for the Advanced Oxidation Treatment of Fluoroquinolone Pharmaceutical Compounds using TiO(2) Heterogeneous Catalysis. Journal of Physical Chemistry A 114(7), 2569-2575.

Andersson, D.I. and Hughes, D., 2010. Antibiotic resistance and its cost: Is it possible to

reverse resistance? Nature Reviews Microbiology 8(4), 260-271.

Arancibia-Bulnes, C.A. and Cuevas, S.A., 2004. Modeling of the radiation field in a parabolic trough solar photocatalytic reactor. Solar Energy 76(5), 615-622.

Arslan-Alaton, I. and Gurses, F., 2004. Photo-Fenton-like and photo-fenton-like oxidation of Procaine Penicillin G formulation effluent. Journal of Photochemistry and Photobiology a-Chemistry 165(1-3), 165-175.

Asahi, R., Morikawa, T., Ohwaki, T., Aoki, K. and Taga, Y., 2001. Visible-light photocatalysis in nitrogen-doped titanium oxides. Science 293(5528), 269-271.

Babic, S., Perisa, M. and Skoric, I., 2013. Photolytic degradation of norfloxacin, enrofloxacin and ciprofloxacin in various aqueous media. Chemosphere 91(11), 1635-1642.

Babuponnusami, A. and Muthukumar, K., 2012. Advanced oxidation of phenol: A comparison between Fenton, electro-Fenton, sono-electro-Fenton and photo-electro-Fenton processes. Chemical Engineering Journal 183, 1-9.

Bamwenda, G.R., Uesigi, T., Abe, Y., Sayama, K. and Arakawa, H., 2001. The photocatalytic oxidation of water to O2 over pure CeO2, WO3, and TiO2 using Fe3+ and Ce4+ as electron acceptors. Applied Catalysis A: General 205(1–2), 117-128.

Bansal, P., Singh, D. and Sud, D., 2010. Photocatalytic degradation of azo dye in aqueous TiO2 suspension: Reaction pathway and identification of intermediates products by LC/MS. Separation and Purification Technology 72(3), 357-365.

Batt, A.L. and Aga, D.S., 2005. Simultaneous Analysis of Multiple Classes of Antibiotics by Ion Trap LC/MS/MS for Assessing Surface Water and Groundwater Contamination. Analytical Chemistry 77(9), 2940-2947.

Batt, A.L., Bruce, I.B. and Aga, D.S., 2006. Evaluating the vulnerability of surface waters to antibiotic contamination from varying wastewater treatment plant discharges. Environmental Pollution 142(2), 295-302.

Bond, T., Goslan, E.H., Jefferson, B., Roddick, F., Fan, L. and Parsons, S.A., 2009. Chemical and biological oxidation of NOM surrogates and effect on HAA formation. Water Research 43(10), 2615-2622.

Budai, M., Gróf, P., Zimmer, A., Pápai, K., Klebovich, I. and Ludányi, K., 2008. UV light induced photodegradation of liposome encapsulated fluoroquinolones: An MS study. Journal of Photochemistry and Photobiology A: Chemistry 198(2–3), 268-273.

Burbano, A.A., Dionysiou, D.D., Suidan, M.T. and Richardson, T.L., 2005. Oxidation kinetics and effect of pH on the degradation of MTBE with Fenton reagent. Water Research 39(1), 107-118.

Buxton, G.V. and Elliot, A.J., 1986. Rate constant for reaction of hydroxyl radicals with bicarbonate ions. International Journal of Radiation Applications and Instrumentation. Part C. Radiation Physics and Chemistry 27(3), 241-243.

Cai, Y.J., Lin, L.N., Xia, D.S., Zeng, Q.F. and Zhu, H.L., 2011. Degradation of Reactive Brilliant Red X-3B Dye by Microwave Electrodeless UV Irradiation. Clean-Soil

Air Water 39(1), 68-73.

Cao, Y.S., Chen, J.X., Huang, L., Wang, Y.L., Hou, Y. and Lu, Y.T., 2005. Photocatalytic degradation of chlorfenapyr in aqueous suspension of TiO2. Journal of Molecular Catalysis a-Chemical 233(1-2), 61-66.

Cao, Z.N., Liu, X.Y., Zhang, X.Y., Chen, L.S., Liu, S.S. and Hu, Y., 2012. Short-term effects of diesel fuel on rhizosphere microbial community structure of native plants in Yangtze estuarine wetland. Environmental Science and Pollution Research 19(6), 2179-2185.

Castiglioni, S., Bagnati, R., Fanelli, R., Pomati, F., Calamari, D. and Zuccato, E., 2006. Removal of pharmaceuticals in sewage treatment plants in Italy. Environmental Science and Technology 40(1), 357-363.

Cha, J.M., Yang, S. and Carlson, K.H., 2005. Rapid analysis of trace levels of antibiotic polyether ionophores in surface water by solid-phase extraction and liquid chromatography with ion trap tandem mass spectrometric detection. Journal of Chromatography A 1065(2), 187-198.

Chang, C.C., Chiu, C.Y., Chang, C.Y., Chang, C.F., Chen, Y.H., Ji, D.R., Yu, Y.H. and Chiang, P.C., 2009. Combined photolysis and catalytic ozonation of dimethyl phthalate in a high-gravity rotating packed bed. Journal of Hazardous Materials 161(1), 287-293.

Chang, E.E., Liu, T.Y., Huang, C.P., Liang, C.H. and Chiang, P.C., 2012. Degradation of mefenamic acid from aqueous solutions by the ozonation and O-3/UV processes.

Separation and Purification Technology 98, 123-129.

Chang, X.S., Meyer, M.T., Liu, X.Y., Zhao, Q., Chen, H., Chen, J.A., Qiu, Z.Q., Yang, L., Cao, J. and Shu, W.Q., 2010. Determination of antibiotics in sewage from hospitals, nursery and slaughter house, wastewater treatment plant and source water in Chongqing region of Three Gorge Reservoir in China. Environmental Pollution 158(5), 1444-1450.

Chen, D.L., Yin, L., Ge, L.F., Fan, B.B., Zhang, R., Sun, J. and Shao, G.S., 2013. Low-temperature and highly selective NO-sensing performance of WO3 nanoplates decorated with silver nanoparticles. Sensors and Actuators B-Chemical 185, 445-455.

Chen, L., Zhou, H.-y. and Deng, Q.-y., 2007. Photolysis of nonylphenol ethoxylates: The determination of the degradation kinetics and the intermediate products. Chemosphere 68(2), 354-359.

Chen, M. and Chu, W., 2012a. Degradation of antibiotic norfloxacin in aqueous solution by visible-light-mediated C-TiO2 photocatalysis. Journal of Hazardous Materials 219–220(0), 183-189.

Chen, M. and Chu, W., 2012b. Efficient Degradation of an Antibiotic Norfloxacin in Aqueous Solution via a Simulated Solar-Light-Mediated Bi2WO6 Process. Industrial & Engineering Chemistry Research 51(13), 4887-4893.

Chen, P., Zhu, L., Fang, S., Wang, C. and Shan, G., 2012. Photocatalytic Degradation Efficiency and Mechanism of Microcystin-RR by Mesoporous Bi2WO6 under

Near Ultraviolet Light. Environmental Science & Technology 46(4), 2345-2351.

Chen, X.B., Lou, Y.B., Dayal, S., Qiu, X.F., Krolicki, R., Burda, C., Zhao, C.F. and Becker, J., 2005. Doped semiconductor nanomaterials. Journal of Nanoscience and Nanotechnology 5(9), 1408-1420.

Chen, Y.H., Franzreb, M., Lin, R.H., Chen, L.L., Chang, C.Y., Yu, Y.H. and Chiang, P.C., 2009. Platinum-Doped TiO2/Magnetic Poly(methyl methacrylate) Microspheres as a Novel Photocatalyst. Industrial & Engineering Chemistry Research 48(16), 7616-7623.

Chenthamarakshan, C.R., Rajeshwar, K. and Wolfrum, E.J., 2000. Heterogeneous Photocatalytic Reduction of Cr(VI) in UV-Irradiated Titania Suspensions:鈥?Effect of Protons, Ammonium Ions, and Other Interfacial Aspects. Langmuir 16(6), 2715-2721.

Childs, S.J., 2000. Safety of the fluoroquinolone antibiotics: Focus on molecular structure. Infections in Urology 13(1), 3-10.

Chin, Y.-P., Miller, P.L., Zeng, L., Cawley, K. and Weavers, L.K., 2004. Photosensitized Degradation of Bisphenol A by Dissolved Organic Matter†. Environmental Science & Technology 38(22), 5888-5894.

Cho, M., Chung, H., Choi, W. and Yoon, J., 2004. Linear correlation between inactivation of E. coli and OH radical concentration in TiO2 photocatalytic disinfection. Water Research 38(4), 1069-1077.

Chong, M.N., Jin, B., Chow, C.W.K. and Saint, C., 2010. Recent developments in

photocatalytic water treatment technology: A review. Water Research 44(10), 2997-3027.

Choy, W.K. and Chu, W., 2008. Photo-oxidation of o-chloroaniline in the presence of TiO2 and IO3−: A study of photo-intermediates and successive IO3− dose. Chemical Engineering Journal 136(2-3), 180-187.

Chu, W., Choy, W.K. and So, T.Y., 2007. The effect of solution pH and peroxide in the TiO2-induced photocatalysis of chlorinated aniline. Journal of Hazardous Materials 141(1), 86-91.

Chu, W., Jafvert, C.T., Diehl, C.A., Marley, K. and Larson, R.A., 1998. Phototransformations of Polychlorobiphenyls in Brij 58 Micellar Solutions. Environmental Science & Technology 32(13), 1989-1993.

Coleman, H.M., Vimonses, V., Leslie, G. and Amal, R., 2007. Degradation of 1,4-dioxane in water using TiO2 based photocatalytic and H2O2/UV processes. Journal of Hazardous Materials 146(3), 496-501.

D'Andrea, G. and Di Nicolantonio, G., 2002. A Graphical Approach to Determine the Isoelectric Point and Charge of Small Peptides from pH 0 to 14. Journal of Chemical Education 79(8), 972-null.

Daniel, L.S., Nagai, H. and Sato, M., 2013. Absorption spectra and photocurrent densities of Ag nanoparticle/TiO2 composite thin films with various amounts of Ag. Journal of Materials Science 48(20), 7162-7170.

de Jongh, C.M., Kooij, P.J.F., de Voogt, P. and ter Laak, T.L., 2012. Screening and

human health risk assessment of pharmaceuticals and their transformation products in Dutch surface waters and drinking water. Science of the Total Environment 427, 70-77.

De Witte, B., Van Langenhove, H., Demeestere, K., Saerens, K., De Wispelaere, P. and Dewulf, J., 2010. Ciprofloxacin ozonation in hospital wastewater treatment plant effluent: Effect of pH and H2O2. Chemosphere 78(9), 1142-1147.

Deng, Y. and Ezyske, C.M., 2011. Sulfate radical-advanced oxidation process (SR-AOP) for simultaneous removal of refractory organic contaminants and ammonia in landfill leachate. Water Research 45(18), 6189-6194.

Devi, L.G., Munikrishnappa, C., Nagaraj, B. and Rajashekhar, K.E., 2013. Effect of chloride and sulfate ions on the advanced photo Fenton and modified photo Fenton degradation process of Alizarin Red S. Journal of Molecular Catalysis a-Chemical 374, 125-131.

DeWitte, B., Dewulf, J., Demeestere, K., Van De Vyvere, V., De Wispelaere, P. and Van Langenhove, H., 2008. Ozonation of Ciprofloxacin in Water: HRMS Identification of Reaction Products and Pathways. Environmental Science & Technology 42(13), 4889-4895.

Dieckmann, M.S. and Gray, K.A., 1996. A comparison of the degradation of 4-nitrophenol via direct and sensitized photocatalysis in TiO2 slurries. Water Research 30(5), 1169-1183.

Ding, Z., Hu, X., Lu, G.Q., Yue, P.-L. and Greenfield, P.F., 2000. Novel Silica Gel

Supported TiO2 Photocatalyst Synthesized by CVD Method. Langmuir 16(15), 6216-6222.

Dobrović, S., Juretić, H. and Ružinski, N., 2007. Photodegradation of natural organic matter in water with UV irradiation at 185 and 254nm: Importance of hydrodynamic conditions on the decomposition rate. Separation Science and Technology 42(7), 1421-1432.

Drillia, P., Stamatelatou, K. and Lyberatos, G., 2005. Fate and mobility of pharmaceuticals in solid matrices. Chemosphere 60(8), 1034-1044.

Duong, H.A., Pham, N.H., Nguyen, H.T., Hoang, T.T., Pham, H.V., Pham, V.C., Berg, M., Giger, W. and Alder, A.C., 2008. Occurrence, fate and antibiotic resistance of fluoroquinolone antibacterials in hospital wastewaters in Hanoi, Vietnam. Chemosphere 72(6), 968-973.

Emeline, A.V., Ryabchuk, V.K. and Serpone, N., 2005. Dogmas and Misconceptions in Heterogeneous Photocatalysis. Some Enlightened Reflections. The Journal of Physical Chemistry B 109(39), 18515-18521.

Ensing, B., Buda, F. and Baerends, E.J., 2003. Fenton-like Chemistry in Water: Oxidation Catalysis by Fe(III) and H2O2. The Journal of Physical Chemistry A 107(30), 5722-5731.

Fick, J., Soederstrom, H., Lindberg, R.H., Phan, C., Tysklind, M. and Larsson, D.G.J., 2009. CONTAMINATION OF SURFACE, GROUND, AND DRINKING WATER FROM PHARMACEUTICAL PRODUCTION. Environmental Toxicology and

Chemistry 28(12), 2522-2527.

Finlayson, A.P., Tsaneva, V.N., Lyons, L., Clark, M. and Glowacki, B.A., 2006. Evaluation of Bi-W-oxides for visible light photocatalysis. Physica Status Solidi (A) Applications and Materials Science 203(2), 327-335.

Flynn, C.M., 1984. Hydrolysis of inorganic iron(III) salts. Chemical Reviews 84(1), 31-41.

Fox, M.A. and Dulay, M.T., 1993. Heterogeneous photocatalysis. Chemical Reviews 93(1), 341-357.

Frimmel, F.H., 1998. Impact of light on the properties of aquatic natural organic matter. Environment International 24(5-6), 559-571.

Fu, Y., Chang, C., Chen, P., Chu, X. and Zhu, L., 2013a. Enhanced photocatalytic performance of boron doped Bi2WO6 nanosheets under simulated solar light irradiation. Journal of Hazardous Materials 254, 185-192.

Fu, Y., Chang, C., Chen, P., Chu, X. and Zhu, L., 2013b. Enhanced photocatalytic performance of boron doped Bi2WO6 nanosheets under simulated solar light irradiation. Journal of Hazardous Materials 254–255(0), 185-192.

Giraldo, A.L., Peñuela, G.A., Torres-Palma, R.A., Pino, N.J., Palominos, R.A. and Mansilla, H.D., 2010. Degradation of the antibiotic oxolinic acid by photocatalysis with TiO2 in suspension. Water Research 44(18), 5158-5167.

Goldstein, S., Behar, D. and Rabani, J., 2008. Mechanism of visible light photocatalytic oxidation of methanol in aerated aqueous suspensions of carbon-doped TiO2.

Journal of Physical Chemistry C 112(39), 15134-15139.

Golet, E.M., Alder, A.C. and Giger, W., 2002. Environmental exposure and risk assessment of fluoroquinolone antibacterial agents in wastewater and river water of the Glatt Valley watershed, Switzerland. Environmental Science and Technology 36(17), 3645-3651.

Golet, E.M., Alder, A.C., Hartmann, A., Ternes, T.A. and Giger, W., 2001. Trace Determination of Fluoroquinolone Antibacterial Agents in Urban Wastewater by Solid-Phase Extraction and Liquid Chromatography with Fluorescence Detection. Analytical Chemistry 73(15), 3632-3638.

Gombac, V., De Rogatis, L., Gasparotto, A., Vicario, G., Montini, T., Barreca, D., Balducci, G., Fornasiero, P., Tondello, E. and Graziani, M., 2007. TiO2 nanopowders doped with boron and nitrogen for photocatalytic applications. Chemical Physics 339(1-3), 111-123.

Goslan, E.H., Gurses, F., Banks, J. and Parsons, S.A., 2006. An investigation into reservoir NOM reduction by UV photolysis and advanced oxidation processes. Chemosphere 65(7), 1113-1119.

Gros, M., Petrović, M., Ginebreda, A. and Barceló, D., 2010. Removal of pharmaceuticals during wastewater treatment and environmental risk assessment using hazard indexes. Environment International 36(1), 15-26.

Guillard, C., Lachheb, H., Houas, A., Ksibi, M., Elaloui, E. and Herrmann, J.-M., 2003. Influence of chemical structure of dyes, of pH and of inorganic salts on their

photocatalytic degradation by TiO2 comparison of the efficiency of powder and supported TiO2. Journal of Photochemistry and Photobiology A: Chemistry 158(1), 27-36.

Gulkowska, A., Leung, H.W., So, M.K., Taniyasu, S., Yamashita, N., Yeung, L.W.Y., Richardson, B.J., Lei, A.P., Giesy, J.P. and Lam, P.K.S., 2008. Removal of antibiotics from wastewater by sewage treatment facilities in Hong Kong and Shenzhen, China. Water Research 42(1-2), 395-403.

Hao, J., Wuyundalai, Liu, H.J., Chen, T.P., Zhou, Y.X., Su, Y.C. and Li, L.T., 2011. Reduction of Pesticide Residues on Fresh Vegetables with Electrolyzed Water Treatment. Journal of Food Science 76(4), C520-C524.

Hazime, R., Nguyen, Q.H., Ferronato, C., Huynh, T.K.X., Jaber, F. and Chovelon, J.M., 2013. Optimization of imazalil removal in the system UV/TiO2/K2S2O8 using a response surface methodology (RSM). Applied Catalysis B-Environmental 132, 519-526.

Heberer, T., Massmann, G., Fanck, B., Taute, T. and Dunnbier, U., 2008. Behaviour and redox sensitivity of antimicrobial residues during bank filtration. Chemosphere 73(4), 451-460.

Herrmann, J.M., 1999. Heterogeneous photocatalysis: Fundamentals and applications to the removal of various types of aqueous pollutants. Catalysis Today 53(1), 115-129.

Hu, X.L., Wang, X.F., Ban, Y.X. and Ren, B.Z., 2011. A comparative study of

UV-Fenton, UV-H2O2 and Fenton reaction treatment of landfill leachate. Environmental Technology 32(9), 945-951.

Huang, X., Leal, M. and Li, Q., 2008a. Degradation of natural organic matter by TiO2 photocatalytic oxidation and its effect on fouling of low-pressure membranes. Water Research 42(4-5), 1142-1150.

Huang, Y., Ai, Z., Ho, W., Chen, M. and Lee, S., 2010. Ultrasonic Spray Pyrolysis Synthesis of Porous Bi2WO6 Microspheres and Their Visible-Light-Induced Photocatalytic Removal of NO. The Journal of Physical Chemistry C 114(14), 6342-6349.

Huang, Y., Ho, W.K., Lee, S.C., Zhang, L.Z., Li, G.S. and Yu, J.C., 2008b. Effect of carbon doping on the mesoporous structure of nanocrystalline titanium dioxide and its solar-light-driven photocatalytic degradation of NOx. Langmuir 24(7), 3510-3516.

Hubicka, U., Zmudzki, P., Talik, P., Zuromska-Witek, B. and Krzek, J., 2013. Photodegradation assessment of ciprofloxacin, moxifloxacin, norfloxacin and ofloxacin in the presence of excipients from tablets by UPLC-MS/MS and DSC. Chemistry Central Journal 7.

Hyoung-Ryun Park, K.-Y.C., Hyong-Chul Lee, Jin-Ki Lee, and Ki-Min Bark, 2000. Ionization and divalent cation complexation of quinolone antibiotics in aqueous solution. Bulletin of the Korean Chemical Society 21(9), 849.

Javier Rivas, F., Beltran, F.J. and Encinas, A., 2012. Removal of emergent contaminants:

Integration of ozone and photocatalysis. Journal of Environmental Management 100, 10-15.

Jia, A., Wan, Y., Xiao, Y. and Hu, J., 2012. Occurrence and fate of quinolone and fluoroquinolone antibiotics in a municipal sewage treatment plant. Water Research 46(2), 387-394.

Jiang, H.Y., Dai, H.X., Meng, X., Ji, K.M., Zhang, L. and Deng, J.G., 2011. Porous olive-like BiVO(4): Alcoho-hydrothermal preparation and excellent visible-light-driven photocatalytic performance for the degradation of phenol. Applied Catalysis B-Environmental 105(3-4), 326-334.

Jiang, Z.P., Wang, H.Y., Huang, H. and Cao, C.C., 2004. Photocatalysis enhancement by electric field: TiO2 thin film for degradation of dye X-3B. Chemosphere 56(5), 503-508.

Kümmerer, K., 2009. Antibiotics in the aquatic environment – A review – Part I. Chemosphere 75(4), 417-434.

Keane, D., Basha, S., Nolan, K., Morrissey, A., Oelgemöller, M. and Tobin, J., 2011. Photodegradation of Famotidine by Integrated Photocatalytic Adsorbent (IPCA) and Kinetic Study. Catalysis Letters 141(2), 300-308.

Kim, D., Kim, S., Yeo, M.-K., Jung, I.-G. and Kang, M., 2009. Synthesis of nanometer sized Bi_2WO_6s by a hydrothermal method and their conductivities. Korean Journal of Chemical Engineering 26(1), 261-264.

Kim, S.-D., Choe, W.-G. and Jeong, J.-R., 2013. Environmentally friendly electroless

plating for Ag/TiO2-coated core-shell magnetic particles using ultrasonic treatment. Ultrasonics Sonochemistry 20(6), 1456-1462.

Kim, S. and Aga, D.S., 2007. Potential ecological and human health impacts of antibiotics and antibiotic-resistant bacteria from wastewater treatment plants. Journal of Toxicology and Environmental Health - Part B: Critical Reviews 10(8), 559-573.

Kleiser, G. and Frimmel, F.H., 2000. Removal of precursors for disinfection by-products (DBPs) — differences between ozone- and OH-radical-induced oxidation. Science of The Total Environment 256(1), 1-9.

Koker, E.B., Bilski, P.J., Motten, A.G., Zhao, B., Chignell, C.F. and He, Y.-Y., 2010. Real-time Visualization of Photochemically Induced Fluorescence of 8-Halogenated Quinolones: Lomefloxacin, Clinafloxacin and Bay3118 in Live Human HaCaT Keratinocytes dagger. Photochemistry and Photobiology 86(4), 792-797.

Kotzerke, A., Sharma, S., Schauss, K., Heuer, H., Thiele-Bruhn, S., Smalla, K., Wilke, B.M. and Schloter, M., 2008. Alterations in soil microbial activity and N-transformation processes due to sulfadiazine loads in pig-manure. Environmental Pollution 153(2), 315-322.

Kubacka, A., Fernández-García, M. and Colón, G., 2012. Advanced nanoarchitectures for solar photocatalytic applications. Chemical Reviews 112(3), 1555-1614.

Kuo, Y.-L., Chen, H.-W. and Ku, Y., 2007. Analysis of silver particles incorporated on

TiO2 coatings for the photodecomposition of o-cresol. Thin Solid Films 515(7-8), 3461-3468.

Lam, F.L.Y. and Hu, X.J., 2013. pH-Insensitive Bimetallic Catalyst for the Abatement of Dye Pollutants by Photo-Fenton Oxidation. Industrial & Engineering Chemistry Research 52(20), 6639-6646.

Lanao, M., Ormad, M.P., Ibarz, C., Miguel, N. and Ovelleiro, J.L., 2008. Bactericidal Effectiveness of O3, O3/H2O2 and O3/TiO2 on Clostridium perfringens. Ozone-Science & Engineering 30(6), 431-438.

Larsson, D.G.J., de Pedro, C. and Paxeus, N., 2007. Effluent from drug manufactures contains extremely high levels of pharmaceuticals. Journal of Hazardous Materials 148(3), 751-755.

Le-Clech, P., Lee, E.-K. and Chen, V., 2006. Hybrid photocatalysis/membrane treatment for surface waters containing low concentrations of natural organic matters. Water Research 40(2), 323-330.

Lee, Y.-J., Lee, S.-E., Lee, D.S. and Kim, Y.-H., 2008. Risk assessment of human antibiotics in Korean aquatic environment. Environmental Toxicology and Pharmacology 26(2), 216-221.

Legrini, O., Oliveros, E. and Braun, A.M., 1993. Photochemical processes for water treatment. Chemical Reviews 93(2), 671-698.

Leung, H.W., Minh, T.B., Murphy, M.B., Lam, J.C.W., So, M.K., Martin, M., Lam, P.K.S. and Richardson, B.J., 2011. Distribution, fate and risk assessment of

antibiotics in sewage treatment plants in Hong Kong, South China. Environment International (0).

Levy, S.B., 2001. Antibiotic resistance: Consequences of inaction. Clinical Infectious Diseases 33(SUPPL. 3), S124-S129.

Li, B. and Zhang, T., 2010. Biodegradation and Adsorption of Antibiotics in the Activated Sludge Process. Environmental Science & Technology 44(9), 3468-3473.

Li, B. and Zhang, T., 2013. Different removal behaviours of multiple trace antibiotics in municipal wastewater chlorination. Water Research 47(9), 2970-2982.

Li, G.S., Zhang, D.Q., Yu, J.C. and Leung, M.K.H., 2010. An Efficient Bismuth Tungstate Visible-Light-Driven Photocatalyst for Breaking Down Nitric Oxide. Environmental Science & Technology 44(11), 4276-4281.

Li, K., Chen, T., Yan, L., Dai, Y., Huang, Z., Guo, H., Jiang, L., Gao, X., Xiong, J. and Song, D., 2012a. Synthesis of mesoporous graphene and tourmaline co-doped titania composites and their photocatalytic activity towards organic pollutant degradation and eutrophic water treatment. Catalysis Communications 28, 196-201.

Li, Q., Guo, B., Yu, J., Ran, J., Zhang, B., Yan, H. and Gong, J.R., 2011. Highly efficient visible-light-driven photocatalytic hydrogen production of CdS-cluster-decorated graphene nanosheets. Journal of the American Chemical Society 133(28), 10878-10884.

Li, W., Guo, C., Su, B. and Xu, J., 2012b. Photodegradation of four fluoroquinolone compounds by titanium dioxide under simulated solar light irradiation. Journal of Chemical Technology and Biotechnology 87(5), 643-650.

Lin, Y.-C. and Lee, H.-S., 2010. Effects of TiO2 coating dosage and operational parameters on a TiO2/Ag photocatalysis system for decolorizing Procion red MX-5B. Journal of Hazardous Materials 179(1-3), 462-470.

Lindberg, R., Jarnheimer, P.Å., Olsen, B., Johansson, M. and Tysklind, M., 2004. Determination of antibiotic substances in hospital sewage water using solid phase extraction and liquid chromatography/mass spectrometry and group analogue internal standards. Chemosphere 57(10), 1479-1488.

Lindberg, R.H., Wennberg, P., Johansson, M.I., Tysklind, M. and Andersson, B.A.V., 2005. Screening of Human Antibiotic Substances and Determination of Weekly Mass Flows in Five Sewage Treatment Plants in Sweden. Environmental Science & Technology 39(10), 3421-3429.

Lindsey, M.E. and Tarr, M.A., 2000. Quantitation of hydroxyl radical during Fenton oxidation following a single addition of iron and peroxide. Chemosphere 41(3), 409-417.

Ling, Z.H., Guo, H., Zheng, J.Y., Louie, P.K.K., Cheng, H.R., Jiang, F., Cheung, K., Wong, L.C. and Feng, X.Q., 2012. Establishing a conceptual model for photochemical ozone pollution in subtropical Hong Kong. Atmospheric Environment (0).

Linsebigler, A.L., Lu, G. and Yates, J.T., 1995. Photocatalysis on TiO2 Surfaces: Principles, Mechanisms, and Selected Results. Chemical Reviews 95(3), 735-758.

Liu, C., Nanaboina, V., Korshin, G.V. and Jiang, W., 2012. Spectroscopic study of degradation products of ciprofloxacin, norfloxacin and lomefloxacin formed in ozonated wastewater. Water Research 46(16), 5235-5246.

Liu, G., Wang, L.Z., Sun, C.H., Yan, X.X., Wang, X.W., Chen, Z.G., Smith, S.C., Cheng, H.M. and Lu, G.Q., 2009. Band-to-Band Visible-Light Photon Excitation and Photoactivity Induced by Homogeneous Nitrogen Doping in Layered Titanates. Chemistry of Materials 21(7), 1266-1274.

Liu, J.L. and Li, X.Y., 2010. Biodegradation and biotransformation of wastewater organics as precursors of disinfection byproducts in water. Chemosphere 81(9), 1075-1083.

Liu, S.Q., Chen, Z., Zhang, N., Tang, Z.R. and Xu, Y.J., 2013. An Efficient Self-Assembly of CdS Nanowires-Reduced Graphene Oxide Nanocomposites for Selective Reduction of Nitro Organics under Visible Light Irradiation. Journal of Physical Chemistry C 117(16), 8251-8261.

Liu, W., Zhang, J., Zhang, C. and Ren, L., 2011a. Sorption of norfloxacin by lotus stalk-based activated carbon and iron-doped activated alumina: Mechanisms, isotherms and kinetics. Chemical Engineering Journal 171(2), 431-438.

Liu, Y., Wang, W., Fu, Z., Wang, H., Wang, Y. and Zhang, J., 2011b. Nest-like structures of Sr doped Bi2WO6: Synthesis and enhanced photocatalytic properties. Materials

Science and Engineering B-Advanced Functional Solid-State Materials 176(16), 1264-1270.

Lorphensri, O., Intravijit, J., Sabatini, D.A., Kibbey, T.C.G., Osathaphan, K. and Saiwan, C., 2006. Sorption of acetaminophen, 17 alpha-ethynyl estradiol, nalidixic acid, and norfloxacin to silica, alumina, and a hydrophobic medium. Water Research 40(7), 1481-1491.

Mahmoodi, N.M., Arami, M., Limaee, N.Y. and Tabrizi, N.S., 2006. Kinetics of heterogeneous photocatalytic degradation of reactive dyes in an immobilized TiO2 photocatalytic reactor. Journal of Colloid and Interface Science 295(1), 159-164.

Malato, S., Fernández-Ibáñez, P., Maldonado, M.I., Blanco, J. and Gernjak, W., 2009. Decontamination and disinfection of water by solar photocatalysis: Recent overview and trends. Catalysis Today 147(1), 1-59.

Martin, R.L., Hay, P.J. and Pratt, L.R., 1998. Hydrolysis of Ferric Ion in Water and Conformational Equilibrium. The Journal of Physical Chemistry A 102(20), 3565-3573.

Matilainen, A. and Sillanpää, M., 2010. Removal of natural organic matter from drinking water by advanced oxidation processes. Chemosphere 80(4), 351-365.

Měšťánková, H., Mailhot, G., Jirkovský, J., Krýsa, J. and Bolte, M., 2009. Effect of iron speciation on the photodegradation of Monuron in combined photocatalytic systems with immobilized or suspended TiO<sub>2</sub&gt. Environmental Chemistry Letters 7(2), 127-132.

Mestankova, H., Mailhot, G., Jirkovsky, J., Krysa, J. and Bolte, M., 2009. Effect of iron speciation on the photodegradation of Monuron in combined photocatalytic systems with immobilized or suspended TiO(2). Environmental Chemistry Letters 7(2), 127-132.

Miao, X.S., Bishay, F., Chen, M. and Metcalfe, C.D., 2004. Occurrence of antimicrobials in the final effluents of wastewater treatment plants in Canada. Environmental Science and Technology 38(13), 3533-3541.

Molinari, R., Pirillo, F., Loddo, V. and Palmisano, L., 2006. Heterogeneous photocatalytic degradation of pharmaceuticals in water by using polycrystalline TiO2 and a nanofiltration membrane reactor. Catalysis Today 118(1–2), 205-213.

Nah, Y.C., Paramasivam, I. and Schmuki, P., 2010. Doped TiO2 and TiO2 Nanotubes: Synthesis and Applications. Chemphyschem 11(13), 2698-2713.

Naik, P.N., Chimatadar, S.A. and Nandibewoor, S.T., 2009. Kinetics and Oxidation of Fluoroquinoline Antibacterial Agent, Norfloxacin, by Alkaline Permanganate: A Mechanistic Study. Industrial & Engineering Chemistry Research 48(5), 2548-2555.

Nakamura, R., Tanaka, T. and Nakato, Y., 2004. Mechanism for visible light responses in anodic photocurrents at N-doped TiO2 film electrodes. Journal of Physical Chemistry B 108(30), 10617-10620.

Namasivayam, C. and Sangreetha, D., 2006. Recycling of agricultural solid waste, coir pith: Removal of anions, heavy metals, organics and dyes from water by adsorption

onto ZnCl2 activated coir pith carbon. Journal of Hazardous Materials 135(1-3), 449-452.

Neta, P., Huie, R.E. and Ross, A.B., 1988. J. Phys. Chem. 17.

Neugebauer, U., Szeghalmi, A., Schmitt, M., Kiefer, W., Popp, J. and Holzgrabe, U., 2005. Vibrational spectroscopic characterization of fluoroquinolones. Spectrochimica Acta Part A: Molecular and Biomolecular Spectroscopy 61(7), 1505-1517.

Neyens, E. and Baeyens, J., 2003. A review of classic Fenton's peroxidation as an advanced oxidation technique. Journal of Hazardous Materials 98(1-3), 33-50.

Niu, H., Dizhang, Meng, Z. and Cai, Y., 2012a. Fast defluorination and removal of norfloxacin by alginate/Fe@Fe3O4 core/shell structured nanoparticles. Journal of Hazardous Materials 227, 195-203.

Niu, H., Dizhang, Meng, Z. and Cai, Y., 2012b. Fast defluorination and removal of norfloxacin by alginate/Fe@Fe3O4 core/shell structured nanoparticles. Journal of Hazardous Materials 227–228(0), 195-203.

Oberlé, K., Capdeville, M.J., Berthe, T., Budzinski, H. and Petit, F., 2012. Evidence for a complex relationship between antibiotics and antibiotic-resistant escherichia coli: From medical center patients to a receiving environment. Environmental Science and Technology 46(3), 1859-1868.

Palominos, R., Freer, J., Mondaca, M.A. and Mansilla, H.D., 2008. Evidence for hole participation during the photocatalytic oxidation of the antibiotic flumequine.

Journal of Photochemistry and Photobiology A: Chemistry 193(2–3), 139-145.

Paton, J.H. and Reeves, D.S., 1991. CLINICAL-FEATURES AND MANAGEMENT OF ADVERSE-EFFECTS OF QUINOLONE ANTIBACTERIALS. Drug Safety 6(1), 8-27.

Pei, Z.-G., Shan, X.-Q., Zhang, S.-Z., Kong, J.-J., Wen, B., Zhang, J., Zheng, L.-R., Xie, Y.-N. and Janssens, K., 2011. Insight to ternary complexes of co-adsorption of norfloxacin and Cu(II) onto montmorillonite at different pH using EXAFS. Journal of Hazardous Materials 186(1), 842-848.

Pelaez, M., Falaras, P., Likodimos, V., Kontos, A.G., de la Cruz, A.A., O'Shea, K. and Dionysiou, D.D., 2010. Synthesis, structural characterization and evaluation of sol–gel-based NF-TiO2 films with visible light-photoactivation for the removal of microcystin-LR. Applied Catalysis B: Environmental 99(3–4), 378-387.

Peng, H., Feng, S., Zhang, X., Li, Y. and Zhang, X., 2012a. Adsorption of norfloxacin onto titanium oxide: Effect of drug carrier and dissolved humic acid. Science of the Total Environment 438, 66-71.

Peng, H., Pan, B., Wu, M., Liu, Y., Zhang, D. and Xing, B., 2012b. Adsorption of ofloxacin and norfloxacin on carbon nanotubes: Hydrophobicity- and structure-controlled process. Journal of Hazardous Materials 233, 89-96.

Phan, T.P.H., Managaki, S., Nakada, N., Takada, H., Shimizu, A., Anh, D.H., Viet, P.H. and Suzuki, S., 2011. Antibiotic contamination and occurrence of antibiotic-resistant bacteria in aquatic environments of northern Vietnam. Science

of The Total Environment 409(15), 2894-2901.

Pophali, G.R., Hedau, S., Gedam, N., Rao, N.N. and Nandy, T., 2011. Treatment of refractory organics from membrane rejects using ozonation. Journal of Hazardous Materials 189(1-2), 273-277.

Rao, Y.F. and Chu, W., 2010. Linuron decomposition in aqueous semiconductor suspension under visible light irradiation with and without H2O2. Chemical Engineering Journal 158(2), 181-187.

Rao, Y.F. and Chu, W., 2009. Reaction Mechanism of Linuron Degradation in TiO2 Suspension under Visible Light Irradiation with the Assistance of H2O2. Environmental Science & Technology 43(16), 6183-6189.

Renew, J.E. and Huang, C.-H., 2004. Simultaneous determination of fluoroquinolone, sulfonamide, and trimethoprim antibiotics in wastewater using tandem solid phase extraction and liquid chromatography–electrospray mass spectrometry. Journal of Chromatography A 1042(1–2), 113-121.

Rigos, G., Nengas, I., Alexis, M. and Troisi, G.M., 2004. Potential drug (oxytetracycline and oxolinic acid) pollution from Mediterranean sparid fish farms. Aquatic Toxicology 69(3), 281-288.

Rivas, J., Encinas, A., Beltran, F. and Graham, N., 2011. Application of advanced oxidation processes to doxycycline and norfloxacin removal from water. Journal of Environmental Science and Health Part a-Toxic/Hazardous Substances & Environmental Engineering 46(9), 944-951.

Ruppert, G., Bauer, R. and Heisler, G., 1994. UV-O3, UV-H2O2, UV-TIO2 AND THE PHOTO-FENTON REACTION - COMPARISON OF ADVANCED OXIDATION PROCESSES FOR WASTE-WATER TREATMENT. Chemosphere 28(8), 1447-1454.

Sökmen, M. and Özkan, A., 2002. Decolourising textile wastewater with modified titania: the effects of inorganic anions on the photocatalysis. Journal of Photochemistry and Photobiology A: Chemistry 147(1), 77-81.

Saison, T., Chemin, N., Chaneac, C., Durupthy, O., Ruaux, V., Mariey, L., Mauge, F., Beaunier, P. and Jolivet, J.P., 2011. Bi(2)O(3), BiVO(4), and Bi(2)WO(6): Impact of Surface Properties on Photocatalytic Activity under Visible Light. Journal of Physical Chemistry C 115(13), 5657-5666.

Santos, L.H.M.L.M., Araújo, A.N., Fachini, A., Pena, A., Delerue-Matos, C. and Montenegro, M.C.B.S.M., 2010. Ecotoxicological aspects related to the presence of pharmaceuticals in the aquatic environment. Journal of Hazardous Materials 175(1–3), 45-95.

Sarathy, S. and Mohseni, M., 2010. Effects of UV/H2O2 advanced oxidation on chemical characteristics and chlorine reactivity of surface water natural organic matter. Water Research 44(14), 4087-4096.

Sarathy, S. and Mohseni, M., 2009. The fate of natural organic matter during UV/H2O2 advanced oxidation of drinking water. Canadian Journal of Civil Engineering 36(1), 160-169.

Schwitzgebel, J., Ekerdt, J.G., Gerischer, H. and Heller, A., 1995. Role of the Oxygen Molecule and of the Photogenerated Electron in TiO2-Photocatalyzed Air Oxidation Reactions. The Journal of Physical Chemistry 99(15), 5633-5638.

Scialdone, O., Galia, A. and Randazzo, S., 2012. Electrochemical treatment of aqueous solutions containing one or many organic pollutants at boron doped diamond anodes. Theoretical modeling and experimental data. Chemical Engineering Journal 183, 124-134.

Selvam, K., Muruganandham, M., Muthuvel, I. and Swaminathan, M., 2007. The influence of inorganic oxidants and metal ions on semiconductor sensitized photodegradation of 4-fluorophenol. Chemical Engineering Journal 128(1), 51-57.

Senthilnathan, J. and Philip, L., 2010. Photocatalytic degradation of lindane under UV and visible light using N-doped TiO2. Chemical Engineering Journal 161(1-2), 83-92.

Shang, M., Wang, W.Z., Sun, S.M., Zhou, L. and Zhang, L., 2008. Bi2WO6 nanocrystals with high photocatalytic activities under visible light. Journal of Physical Chemistry C 112(28), 10407-10411.

Son, H.S., Ko, G. and Zoh, K.D., 2009. Kinetics and mechanism of photolysis and TiO2 photocatalysis of triclosan. Journal of Hazardous Materials 166(2-3), 954-960.

Song, W., Ma, J., Ma, W., Chen, C. and Zhao, J., 2006. Photochemical production or depletion of hydrogen peroxide controlled by different electron transfer pathways in methyl viologen intercalated clays. Journal of Photochemistry and Photobiology

a-Chemistry 183(1-2), 31-34.

Stahlmann, R. and Lode, H., 2010. Safety Considerations of Fluoroquinolones in the Elderly An Update. Drugs & Aging 27(3), 193-209.

Sturini, M., Speltini, A., Maraschi, F., Profumo, A., Pretali, L., Fasani, E. and Albini, A., 2010. Photochemical Degradation of Marbofloxacin and Enrofloxacin in Natural Waters. Environmental Science & Technology 44(12), 4564-4569.

Sturini, M., Speltini, A., Maraschi, F., Profumo, A., Pretali, L., Irastorza, E.A., Fasani, E. and Albini, A., 2012. Photolytic and photocatalytic degradation of fluoroquinolones in untreated river water under natural sunlight. Applied Catalysis B: Environmental 119–120(0), 32-39.

Sui, M., Zhou, Y., Sheng, L. and Duan, B., 2012. Adsorption of norfloxacin in aqueous solution by Mg-Al layered double hydroxides with variable metal composition and interlayer anions. Chemical Engineering Journal 210, 451-460.

Sun, L. and Bolton, J.R., 1996. Determination of the Quantum Yield for the Photochemical Generation of Hydroxyl Radicals in TiO2 Suspensions. The Journal of Physical Chemistry 100(10), 4127-4134.

Szilagyi, I.M., Forizs, B., Rosseler, O., Szegedi, A., Nemeth, P., Kiraly, P., Tarkanyi, G., Vajna, B., Varga-Josepovits, K., Laszlo, K., Toth, A.L., Baranyai, P. and Leskela, M., 2012. WO3 photocatalysts: Influence of structure and composition. Journal of Catalysis 294, 119-127.

Tan, F., Sun, D., Gao, J., Zhao, Q., Wang, X., Teng, F., Quan, X. and Chen, J., 2013.

Preparation of molecularly imprinted polymer nanoparticles for selective removal of fluoroquinolone antibiotics in aqueous solution. Journal of Hazardous Materials 244, 750-757.

Tang, J., Zou, Z. and Ye, J., 2004. Efficient photocatalytic decomposition of organic contaminants over CaBi2O4 under visible-light irradiation. Angewandte Chemie - International Edition 43(34), 4463-4466.

Thiele-Bruhn, S., 2003. Pharmaceutical antibiotic compounds in soils – a review. Journal of Plant Nutrition and Soil Science 166(2), 145-167.

Thomson, J., Roddick, F.A. and Drikas, M., 2004. Vacuum ultraviolet irradiation for natural organic matter removal. Journal of Water Supply: Research and Technology - AQUA 53(4), 193-206.

Tokura, Y., Iwamoto, Y., Mizutani, K. and Takigawa, M., 1996. Sparfloxacin phototoxicity: Potential photoaugmentation by ultraviolet A and B sources. Archives of Dermatological Research 288(1), 45-50.

Toor, R. and Mohseni, M., 2007. UV-H2O2 based AOP and its integration with biological activated carbon treatment for DBP reduction in drinking water. Chemosphere 66(11), 2087-2095.

Vedrenne, M., Vasquez-Medrano, R., Prato-Garcia, D., Frontana-Uribe, B.A., Hernandez-Esparza, M. and de Andres, J.M., 2012. A ferrous oxalate mediated photo-Fenton system: Toward an increased biodegradability of indigo dyed wastewaters. Journal of Hazardous Materials 243, 292-301.

Verlicchi, P., Galletti, A., Petrovic, M. and Barceló, D., 2010. Hospital effluents as a source of emerging pollutants: An overview of micropollutants and sustainable treatment options. Journal of Hydrology 389(3–4), 416-428.

Vieno, N., Tuhkanen, T. and Kronberg, L., 2007. Elimination of pharmaceuticals in sewage treatment plants in Finland. Water Research 41(5), 1001-1012.

Wadworth, A.N. and Goa, K.L., 1991. LOMEFLOXACIN - A REVIEW OF ITS ANTIBACTERIAL ACTIVITY, PHARMACOKINETIC PROPERTIES AND THERAPEUTIC USE. Drugs 42(6), 1018-1060.

Wammer, K.H., Korte, A.R., Lundeen, R.A., Sundberg, J.E., McNeill, K. and Arnold, W.A., 2013. Direct photochemistry of three fluoroquinolone antibacterials: Norfloxacin, ofloxacin, and enrofloxacin. Water Research 47(1), 439-448.

Wang, C., Zhang, H., Li, F. and Zhu, L., 2010a. Degradation and Mineralization of Bisphenol A by Mesoporous Bi2WO6 under Simulated Solar Light Irradiation. Environmental Science & Technology 44(17), 6843-6848.

Wang, C.Y., Zhu, L.Y., Song, C., Shan, G.Q. and Chen, P., 2011. Characterization of photocatalyst Bi(3.84)W(0.16)O(6.24) and its photodegradation on bisphenol A under simulated solar light irradiation. Applied Catalysis B-Environmental 105(1-2), 229-236.

Wang, H., Maiyalagan, T. and Wang, X., 2012. Review on recent progress in nitrogen-doped graphene: Synthesis, characterization, and its potential applications. ACS Catalysis 2(5), 781-794.

Wang, K.-H., Hsieh, Y.-H., Wu, C.-H. and Chang, C.-Y., 2000. The pH and anion effects on the heterogeneous photocatalytic degradation of o-methylbenzoic acid in TiO2 aqueous suspension. Chemosphere 40(4), 389-394.

Wang, P., He, Y.-L. and Huang, C.-H., 2010b. Oxidation of fluoroquinolone antibiotics and structurally related amines by chlorine dioxide: Reaction kinetics, product and pathway evaluation. Water Research 44(20), 5989-5998.

Wang, P., He, Y.L. and Huang, C.H., 2010c. Oxidation of fluoroquinolone antibiotics and structurally related amines by chlorine dioxide: Reaction kinetics, product and pathway evaluation. Water Research 44(20), 5989-5998.

Wang, Y.B. and Hong, C.S., 1999. Effect of hydrogen peroxide, periodate and persulfate on photocatalysis of 2-chlorobiphenyl in aqueous TiO2 suspensions. Water Research 33(9), 2031-2036.

Wang, Y.R. and Chu, W., 2012. Photo-assisted degradation of 2,4,5-trichlorophenoxyacetic acid by Fe(II)-catalyzed activation of Oxone process: The role of UV irradiation, reaction mechanism and mineralization. Applied Catalysis B: Environmental 123–124(0), 151-161.

Wang, Z., Yu, X., Pan, B. and Xing, B., 2010d. Norfloxacin Sorption and Its Thermodynamics on Surface-Modified Carbon Nanotubes. Environmental Science & Technology 44(3), 978-984.

Wang, Z.Y., Yu, X.D., Pan, B. and Xing, B.S., 2010e. Norfloxacin Sorption and Its Thermodynamics on Surface-Modified Carbon Nanotubes. Environmental Science

& Technology 44(3), 978-984.

Watkinson, A.J., Murby, E.J. and Costanzo, S.D., 2007. Removal of antibiotics in conventional and advanced wastewater treatment: Implications for environmental discharge and wastewater recycling. Water Research 41(18), 4164-4176.

Watkinson, A.J., Murby, E.J., Kolpin, D.W. and Costanzo, S.D., 2009. The occurrence of antibiotics in an urban watershed: From wastewater to drinking water. Science of The Total Environment 407(8), 2711-2723.

Wu, C.H., 2009. Photodegradation of CI Reactive Red 2 in UV/TiO2-based systems: Effects of ultrasound irradiation. Journal of Hazardous Materials 167(1-3), 434-439.

Xu, W.-h., Zhang, G., Zou, S.-c., Li, X.-d. and Liu, Y.-c., 2007. Determination of selected antibiotics in the Victoria Harbour and the Pearl River, South China using high-performance liquid chromatography-electrospray ionization tandem mass spectrometry. Environmental Pollution 145(3), 672-679.

Xu, X.R., Li, X.Y., Li, X.Z. and Li, H.B., 2009. Degradation of melatonin by UV, UV/H2O2, Fe2+/H2O2 and UV/Fe2+/H2O2 processes. Separation and Purification Technology 68(2), 261-266.

Xu, Y., 2001. Comparative studies of the Fe3+/2+–UV, H2O2–UV, TiO2–UV/vis systems for the decolorization of a textile dye X-3B in water. Chemosphere 43(8), 1103-1107.

Yang, J.-F., Ying, G.-G., Liu, S., Zhou, L.-J., Zhao, J.-L., Tao, R. and Peng, P.-A., 2012a.

Biological degradation and microbial function effect of norfloxacin in a soil under different conditions. Journal of Environmental Science and Health Part B-Pesticides Food Contaminants and Agricultural Wastes 47(4), 288-295.

Yang, L.-H., Ying, G.-G., Su, H.-C., Stauber, J.L., Adams, M.S. and Binet, M.T., 2008. Growth-inhibiting effects of 12 antibacterial agents and their mixtures on the freshwater microalga Pseudokirchneriella subcapitata. Environmental Toxicology and Chemistry 27(5), 1201-1208.

Yang, W., Lu, Y., Zheng, F., Xue, X., Li, N. and Liu, D., 2012b. Adsorption behavior and mechanisms of norfloxacin onto porous resins and carbon nanotube. Chemical Engineering Journal 179(0), 112-118.

Yang, W., Lu, Y., Zheng, F., Xue, X., Li, N. and Liu, D., 2012c. Adsorption behavior and mechanisms of norfloxacin onto porous resins and carbon nanotube. Chemical Engineering Journal 179, 112-118.

Yao, J.M., Lee, C.K., Yang, S.J. and Hwang, C.S., 2009. Characterization of nano-InVO(4) powders synthesized by the hydrothermal process on various In/V molar ratio and soaking conditions. Journal of Alloys and Compounds 481(1-2), 740-745.

Yu, J.C., Ho, W.K., Yu, J.G., Yip, H., Wong, P.K. and Zhao, J.C., 2005. Efficient visible-light-induced photocatalytic disinfection on sulfur-doped nanocrystalline titania. Environmental Science & Technology 39(4), 1175-1179.

Yu, J.C., Yu, J.G., Ho, W.K., Jiang, Z.T. and Zhang, L.Z., 2002. Effects of F- doping on

the photocatalytic activity and microstructures of nanocrystalline TiO2 powders. Chemistry of Materials 14(9), 3808-3816.

Yu, J.C., Zhang, L.Z., Zheng, Z. and Zhao, J.C., 2003a. Synthesis and characterization of phosphated mesoporous titanium dioxide with high photocatalytic activity. Chemistry of Materials 15(11), 2280-2286.

Yu, J.G., Yu, J.C., Leung, M.K.P., Ho, W.K., Cheng, B., Zhao, X.J. and Zhao, J.C., 2003b. Effects of acidic and basic hydrolysis catalysts on the photocatalytic activity and microstructures of bimodal mesoporous titania. Journal of Catalysis 217(1), 69-78.

Zhang, J.-q. and Dong, Y.-h., 2007. Influence of strength and species of cation on adsorption of norfloxacin in typical soils of China. Huanjing Kexue 28(10), 2383-2388.

Zhang, J., Fu, D. and Wu, J., 2012a. Photodegradation of Norfloxacin in aqueous solution containing algae. Journal of Environmental Sciences-China 24(4), 743-749.

Zhang, L.-S., Wong, K.-H., Yip, H.-Y., Hu, C., Yu, J.C., Chan, C.-Y. and Wong, P.-K., 2010. Effective Photocatalytic Disinfection of E. coli K-12 Using AgBr-Ag-Bi2WO6 Nanojunction System Irradiated by Visible Light: The Role of Diffusing Hydroxyl Radicals. Environmental Science & Technology 44(4), 1392-1398.

Zhang, L., Wang, H., Chen, Z., Wong, P.K. and Liu, J., 2011. Bi2WO6

micro/nano-structures: Synthesis, modifications and visible-light-driven photocatalytic applications. Applied Catalysis B-Environmental 106(1-2), 1-13.

Zhang, L., Wang, W., Chen, Z., Zhou, L., Xu, H. and Zhu, W., 2007. Fabrication of flower-like Bi2WO6 superstructures as high performance visible-light driven photocatalysts. Journal of Materials Chemistry 17(24), 2526-2532.

Zhang, Q., Li, C. and Li, T., 2013. Rapid photocatalytic decolorization of methylene blue using high photon flux UV/TiO2/H2O2 process. Chemical Engineering Journal 217, 407-413.

Zhang, Y., Zhang, P., Huo, Y., Zhang, D., Li, G. and Li, H., 2012b. Ethanol supercritical route for fabricating bimodal carbon modified mesoporous TiO2 with enhanced photocatalytic capability in degrading phenol. Applied Catalysis B: Environmental 115–116(0), 236-244.

Zhao, H., Wang, Y., Wang, Y., Cao, T. and Zhao, G., 2012. Electro-Fenton oxidation of pesticides with a novel Fe3O4@Fe2O3/activated carbon aerogel cathode: High activity, wide pH range and catalytic mechanism. Applied Catalysis B: Environmental 125(0), 120-127.

Zheng, H.L., Pan, Y.X. and Xiang, X.Y., 2007. Oxidation of acidic dye Eosin Y by the solar photo-Fenton processes. Journal of Hazardous Materials 141(3), 457-464.

Zhong, W.J., Wang, D.H. and Xu, X.W., 2012. Phenol removal efficiencies of sewage treatment processes and ecological risks associated with phenols in effluents. Journal of Hazardous Materials 217, 286-292.

Zhu, K.J., Zhang, W.C., Wang, H.F. and Xiao, Z.L., 2008. Electro-catalytic degradation of phenol organics with SnO2-Sb2O3/Ti electrodes. Clean-Soil Air Water 36(1), 97-102.

Zhu, S., Xu, T., Fu, H., Zhao, J. and Zhu, Y., 2007. Synergetic Effect of Bi2WO6 Photocatalyst with C60 and Enhanced Photoactivity under Visible Irradiation. Environmental Science & Technology 41(17), 6234-6239.

Zhu, X., Castleberry, S.R., Nanny, M.A. and Butler, E.C., 2005. Effects of pH and Catalyst Concentration on Photocatalytic Oxidation of Aqueous Ammonia and Nitrite in Titanium Dioxide Suspensions. Environmental Science & Technology 39(10), 3784-3791.

Zhu, Z., Yu, H. and Li, J., 2012. Nest-like Bi2WO6 Self-assembled Microspheres Synthesized Via One Step Template-Free Hydrothermal Process. Journal of Nano Research 17, 1-12.

Appendix 1: Characterization of Bi_2WO_6

The phase structure of as-prepared Bi_2WO_6 was investigated by a Philips Xpert X-ray Diffraction (XRD) instrument with Cu Kα radiation (λ= 1.54178Å) at a scan rate of 0.06° 2Θ/s. The accelerating voltage and the applied current were 40 kv and 30 mA, respectively. A Varian Cary 100 scan UV-visible system equipped with a Labsphere diffuse reflectance accessory was used to evaluate the reflectance spectra.

The phase of obtained product is evaluated by XRD patterns as shown in Figure A1-1. All diffraction peaks can be indexed to the pure orthorhoibic Bi_2WO_6 (JCPDF No. 39-256). UV-vis diffuse reflectance spectroscopy was also used to characterize the optical absorption of the as prepared Bi_2WO_6 (Figure A1-2). An obvious visible light absorption appears for the synthesized Bi_2WO_6 with a band extension from ultraviolet to about 450 nm.

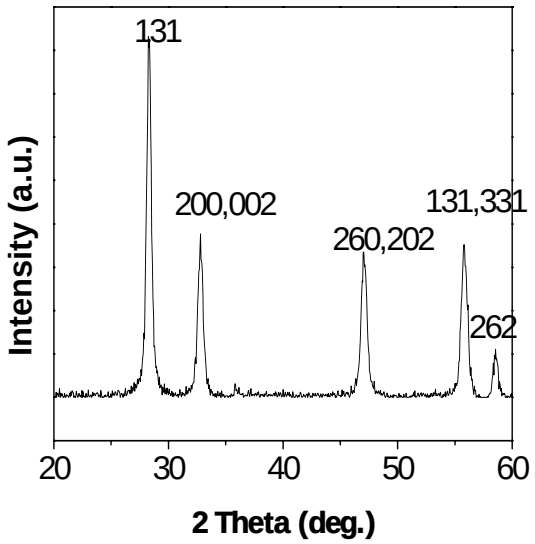

Figure A1-1. XRD pattern of Bi_2WO_6

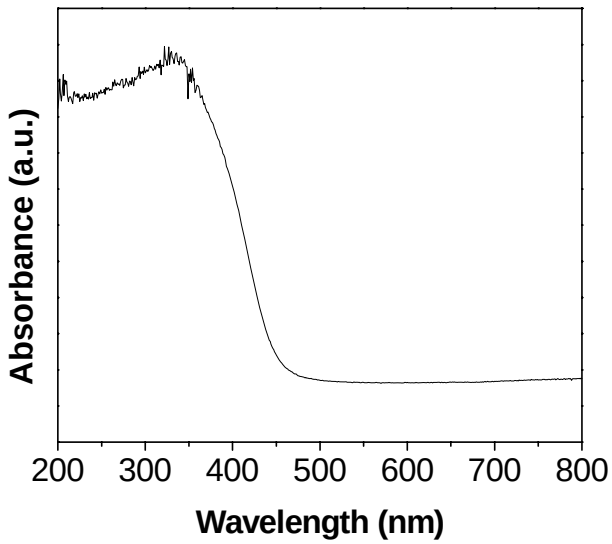

Figure A1-2. UV-vis absorption spectra of Bi_2WO_6

Appendix 2: Characterization of C-TiO_2

Figure A2-1 and A2-2 showed the XRD patterns and UV-vis absorption spectra for C-TiO_2 and pure TiO_2, respectively. The characterization method is the same to that of Bi_2WO_6. In the XRD patterns, it is clear that the diffraction peaks of carbon-doped samples shifted to higher diffraction angles compared with that of pure TiO_2. The results imply that an oxygen atom in the TiO_2 lattice is substituted by a carbon atom. Both anatase (JCPDS, file No. 84-1285) and rutile (JCPDS, file No. 77-442) phases were found in the samples. As shown in Figure A2-2, a strong absorption in the ultraviolet region ascribed to the band−band transition can be observed clearly in both C-TiO_2 and pure TiO_2. However, comparing to the pure TiO_2, the C-doped TiO_2 crystallites showed typical absorption in the visible light region from 400 to 550 nm. As a result, the carbon content in the carbon-modified TiO_2 showed red shift effect on light absorption.

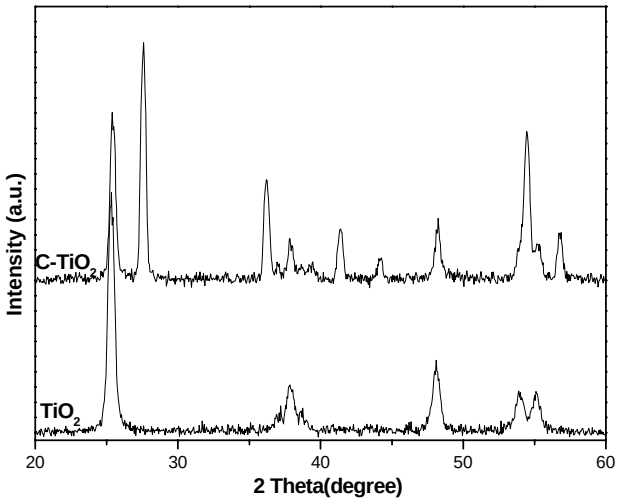

Figure A2-1. XRD patterns of C-TiO_2 and pure TiO_2.

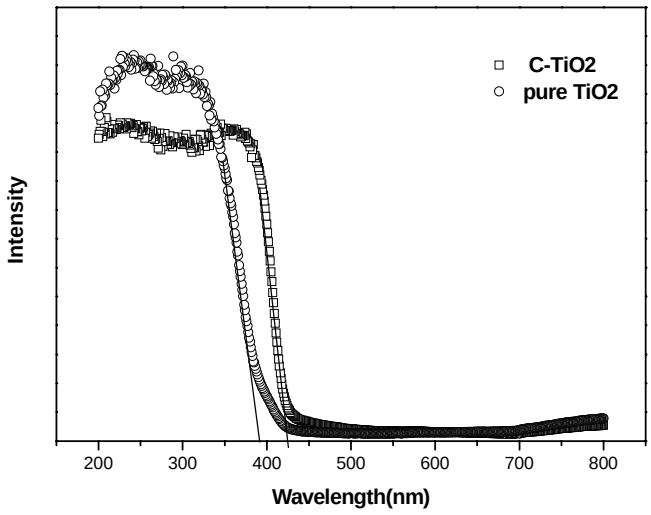

Figure A2-2. UV-vis absorption spectra of C-TiO_2 and pure TiO_2.